GOBIERNO DE ESPAÑA
MINISTERIO DE TRANSPORTES Y MOVILIDAD SOSTENIBLE
VICEPRESIDENCIA TERCERA DEL GOBIERNO
MINISTERIO PARA LA TRANSICIÓN ECOLÓGICA Y EL RETO DEMOGRÁFICO
CEDEX CENTRO DE ESTUDIOS Y EXPERIMENTACIÓN DE OBRAS PÚBLICAS

INFORME TÉCNICO

para

PROYECTO GEOLAB

European Union Horizon 2020 Research and Innovation Programme
Grant agreement No. 101006512

PEDLER PROJECT

INFORME FINAL
TOMO ÚNICO

Laboratorio de Geotecnia

Clave CEDEX:89-421-0-004

Madrid, abril 2026

GOBIERNO DE ESPAÑA
MINISTERIO DE TRANSPORTES Y MOVILIDAD SOSTENIBLE
VICEPRESIDENCIA TERCERA DEL GOBIERNO
MINISTERIO PARA LA TRANSICIÓN ECOLÓGICA Y EL RETO DEMOGRÁFICO
CEDEX CENTRO DE ESTUDIOS Y EXPERIMENTACIÓN DE OBRAS PÚBLICAS

TÍTULO:

PEDLER PROJECT

INFORME FINAL

CLIENTE:

PROYECTO GEOLAB

EL PRESENTE INFORME CONSTITUYE UN DOCUMENTO OFICIAL DE ESTE TRABAJO Y, DE ACUERDO CON LAS NORMAS GENERALES DEL ORGANISMO, SU ENTREGA SUPONE EL CUMPLIMIENTO DE LAS ACTUACIONES TÉCNICAS DEL MISMO REFERENTES A LA MATERIA OBJETO DEL INFORME.

V A L I D E Z O F I C I A L

VISTO EL CONTENIDO DEL INFORME SE PROPONE AUTORIZAR SU EMISIÓN.

EL DIRECTOR DEL
LABORATORIO DE GEOTECNIA

Firmado por ESTAIRE GEPP JOSE - DNI ***1934** el día 14/04/2026 con un certificado emitido por AC Sector Público

Fdo. José Estaire Gepp

AUTORIZA LA EMISIÓN DEL INFORME:

A la fecha de la firma electrónica

LA DIRECTORA DEL CEDEX

Firmado por PERUCHO MARTINEZ AUREA - DNI ***1291** el día 21/04/2026 con un certificado emitido por AC Sector Público

Fdo. Áurea Perucho Martínez

SÓLO SON INFORMES OFICIALES DEL CENTRO DE ESTUDIOS Y EXPERIMENTACIÓN DE OBRAS PÚBLICAS (CEDEX) LOS REFRENDADOS POR SU DIRECCIÓN.

TABLE OF CONTENTS

LIST OF FIGURES

LIST OF TABLES

1. BACKGROUND

In February 2020, CEDEX signed up to participate in the European GEOLAB project.

GEOLAB - Science for enhancing Europe's Critical Infrastructure - is a four-year Horizon 2020 project (2021-2025) funded by the European Union's H2020 Research and Innovation Programme. This project has received funding from the European Union's Horizon 2020 Research and Innovation Programme under grant agreement No. 101006512 (more information at https://project-geolab.eu/).

The GEOLAB project aims to strengthen the resilience of Europe's Critical Infrastructure (water, energy, transport, and urban systems) against challenges such as climate change, extreme events, ageing, and increased demand. It integrates 11 unique research facilities across Europe dedicated to studying subsurface behaviour and its interaction with infrastructure and the environment. In the case of CEDEX, the unique facility participating in the GEOLAB project is the CEDEX Track Box (CTB), which is part of the Geotechnical Laboratory.

GEOLAB serves as a leading platform for advanced research and innovation through three core activities:

- Joint Research Activities (JRA): enhancing laboratory capabilities in physical modelling, 3D-4D measurement, new materials and sensors, and data management.
- Transnational Access (TA): enabling external researchers, infrastructure managers, and industry to perform pioneering experiments and validate innovative solutions.
- Networking Activities (NA): building a strong scientific and industrial community through workshops, outreach, and SME engagement.

The outcomes will support decision-making, foster construction industry innovation, and boost Europe's competitiveness. The consortium, coordinated by Deltares (Netherlands), includes leading institutions such as CEDEX (Spain), NGI (Norway), the University of Cambridge, TU Delft, ETH Zürich, the University Gustave Eiffel, Deltares, and the University of Maribor.

In this division of labour, the TAs primarily focus on conducting tests at the facilities associated with the GEOLAB project.

The tasks assigned are various and numerous. To ensure their proper execution, they have been grouped into different work packages. This report will only address work package 17 (WP17). This work package relates to the TA to be developed in the CEDEX Track Box.

This report begins with the Background section, which outlines the study context and objectives. Section 2 presents the Transnational Access (TA) activities, including a general description of the TA framework and the specific scope of the PEDLER project. Section 3 provides a detailed description of the CEDEX Track Box facility, followed in Section 4 by a comprehensive explanation of the test section, covering its cross-section and all structural layers, from the embankments to the track components. Section 5 describes the construction stages of the test section, including dismantling the previous configuration, constructing each layer, and installing instrumentation. Section 6 outlines the testing program, detailing the static, dynamic, and fatigue tests carried out, along with the analysis methodologies applied to each parameter measured. Section 7

presents a comparative analysis between the results obtained in this study and those from other sections previously tested at the CTB. Finally, Section 8 summarises the main conclusions derived from the experimental campaign.

2. TRANSNATIONAL ACCESS (TA) ACTIVITIES

2.1 TA DESCRIPTION

Transnational Access (TA) in GEOLAB aimed to provide leading researchers across Europe with unique research facilities available only in a few institutions. Through three thematic rounds, access was granted to 11 installations, enabling User Groups to conduct advanced research and innovation. Proposals were evaluated using a common User Selection Procedure (USP), established by the participating infrastructures.

The selection process prioritised scientific merit, while also considering the potential contribution to the resilience of Europe's Critical Infrastructures, the experience of the User Group, gender balance, and the involvement of Early-Stage Researchers. Selected groups received infrastructural, technical, and scientific support from the host facilities. Access was monitored through project reports and user statistics, ensuring both the quality of the research and the diversity of participation.

Work package WP2 focuses on the administrative aspects of the TAs. The objectives are illustrated in Figure 1.

Work package number [9]	WP2	**Lead beneficiary** [10]	3 - ETHZ
Work package title	NA1: Outreach to new users and development procedure TA		
Start month	2	**End month**	48

Objectives
Objectives The aim of this work package are as follows: • Reach out to potential new users of TA facilities, ensuring that the largest possible number of people have the opportunity to bid for TA • Develop the Access Policy for use of the GEOLAB research infrastructures • Provide access and support to the TA users

Figure 1.- Objectives for WP2 (from Grant Agreement)

The GEOLAB project issued three calls for proposals aimed at the European scientific and business community. It invites participants to submit project proposals that can be carried out at one of the various facilities associated with GEOLAB. The description of Work Package 2 (WP 2) clearly outlines the data that will be required from the working group submitting a Project:

1. The scientific context of the study, scientific need to use a specific installation, methodology and proposed analysis of the results.

2. Publication plan and data storage plan that especially focused on the dissemination of knowledge and making the experiment results available to the stakeholders.

3. Exposition of how their research will use the envisaged advances of the GEOLAB research infrastructure under our JRAs.

After each call for proposals, the committee selected the projects that were the most promising. To achieve this, a group of experts was formed to analyse all the information and evaluate various aspects:

- *Fitment to the purpose of the installation.*
- *Relevance of the possible outcome of the project (utility of the possible outcome, extent of results of the project, relevance with respect to the theme)*
- *Scientific merits of the proposal (content of the proposal, the need to use the specific installation, effectiveness of the research approach, technical feasibility, experience in other (small-scale) installations or in field experiments, competence of the team, scientific interaction with the local research team)*
- *Conformity with the objectives of the EC (training of researchers in the use of the installation, stimulating collaboration, priority to users who normally do not have access to similar installations, percentage of female users in the group, number of first-time users in the group).*
- *Amount of access required for the Project.*

The three call for proposal submission deadlines were in October 2021, 2022, and 2023, respectively.

In the specific case of CEDEX, the CTB participated in two calls for proposals. In the first call, two proposals were submitted, and the project named PEDLER, presented by LECA, was selected, which will be described later.

In the second call for proposals, there were also two proposals to conduct tests at the CTB. After being reviewed by experts during the annual project meeting held in Zurich, the DegTrez project was selected, whose aim was to study the long-term degradation in railway transition zones.

Unfortunately, CTB was unable to participate in the third call for proposals due to various issues encountered during the installation process. Additionally, CTB even had to abandon the second project. All relevant information regarding the problems and the attempts to resolve them was communicated to the other GEOLAB project partners, the European Commission, and the user group that proposed the test (LECA).

2.2 PEDLER PROJECT

The key general aspects of the PEDLER project are listed below.

- **PEDLER**: **PE**rformance and **D**urability of **LECA** [lightweight expanded clay] filling in **R**ailway embankments.
- The main objective of the project is to analyse the performance of LECA material when used as part of the embankment, beneath the track bed layers (ballast and sub-ballast), and subjected to railway traffic loads from passenger and freight trains.
- The use of LECA as part of the embankment material is intended for situations where the railway section must be constructed over soils with low bearing capacity or where suitable conventional materials for embankment construction are scarce or unavailable.

- This project has been proposed by the company LECA, in collaboration with a research team from LNEC (Laboratório Nacional de Engenharia Civil).
- The use of LECA is common in the construction of sections used by trams or light trains. However, experience with the performance of this material on high-speed rail tracks is very limited. This test allows for the verification of durability and impact on the behaviour of the rail section under high-speed trains. Furthermore, the experience with the use of CTB in this type of transport allows for comparison with the material commonly used.

The tests conducted at the CTB can be categorised into three main types:

1. Static Tests: These tests assess the stiffness of the railway track section, providing a semi-quantitative measure of the section's condition or degradation.
2. Dynamic Tests: During these tests, the pass-by of a standard train is simulated at various speeds. The resulting displacements, loads, speeds, and accelerations of the different track components are measured.
3. Fatigue Tests: These involve simulating the passage of a great number of axles (around one million) from both passenger and freight standard trains passing at specified speeds, while measuring the same parameters as in the dynamic tests and the permanent settlement of the different layers.

The project began with the dismantling of the previous section present in the CEDEX Track BOX (CTB). This process was carried out with special care to recover as much material as possible, which must be relocated after the test, as well as to remove the instrumentation placed in the previous test. Next, the test railway track section was constructed, consisting, from bottom to top, of 1.1 m of LECA material, 30 cm of granular material for the form layer, 30 cm of granular material for the sub-ballast layer and 35 cm of ballast. Finally, the sleepers and rails were laid (Figure 2).

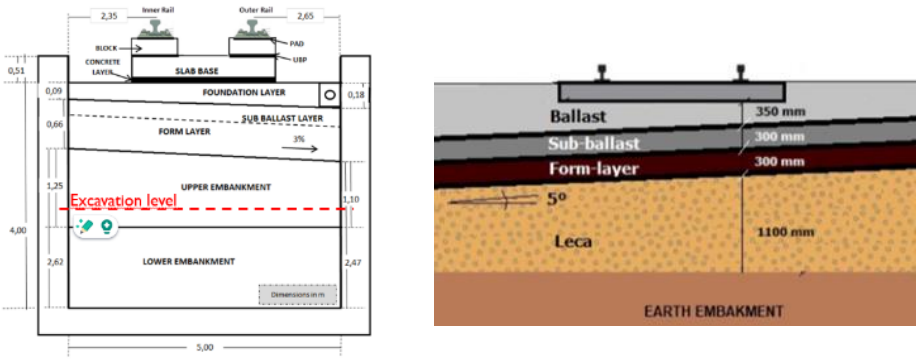

Figure 2.- Left: previous model at test section. Right: Schematic PEDLER railway track test section

The construction of the embankment with LECA-type material was carried out under the supervision of the LECA Portugal staff. Given the special characteristics of the installation, the material was compacted using machinery different from that normally used on construction sites. Furthermore, compaction control could not be carried out using standard soil mechanics

methods, so a new methodology was implemented: PANDA-type tests and dynamic plates. Given that the main objective of the test is to control both the behaviour of the entire railway track section and that of the embankment made of LECA, extensive instrumentation was installed, most of it in the interfaces of the various railway track layers: linear variable differential transformers (LVDTs), pressure cells and accelerometers. The superstructure elements (sleepers, pads and rails) were also equipped with accelerometers, geophones and laser devices to record their mechanical behaviour during the tests.

Figure 3. Different stages of model construction. Top left: embankment excavation completed. Top right: LECA embankment during compaction. Bottom: PEDLER railway track test section finished.

In this project, the Siemens S-103 passenger train was selected to conduct all tests due to the previous CEDEX knowledge of its performance in CTB. As shown in Figure 4, the train consists of a total of 32 axles arranged in 16 bogies, with a total length of 200.32 m and an average axle load of 142.04 kN. One of its distinctive features is its distributed traction system, whereby traction and auxiliary equipment are distributed along the entire train, eliminating the need for conventional locomotive units.

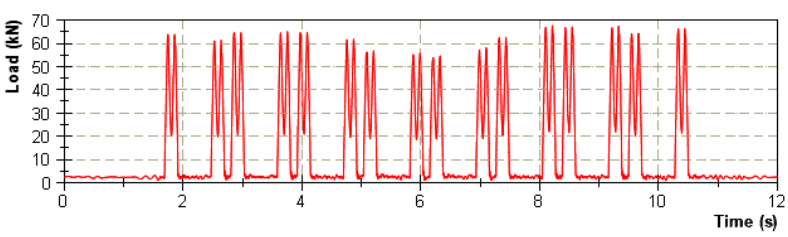

axle	distance (m)	load (t)	axle	distance (m)	load (t)
1	3.51	15.5	17	4.9	13.5
2	2.5	15.5	18	2.5	13.5
3	14.875	15.5	19	14.875	13.5
4	2.5	15.5	20	2.5	13.5
5	4.9	15.5	21	4.9	15.5
6	2.5	15.5	22	2.5	15.5
7	14.875	15.5	23	14.875	15.5
8	2.5	15.5	24	2.5	15.5
9	4.9	15.5	25	4.9	15.5
10	2.5	15.5	26	2.5	15.5
11	14.875	15.5	27	14.875	15.5
12	2.5	15.5	28	2.5	15.5
13	4.9	13.5	29	4.9	15.5
14	2.5	13.5	30	2.5	15.5
15	14.875	13.5	31	14.875	15.5
16	2.5	13.5	32	2.5	15.5
				3.51	
			total	200.32	480.00

Figure 4.- Siemens S-103 train details: aspect and load distribution

The simulation of freight train passage was performed using the Type 7 train specified in the standard EN 1991-2 (Eurocode 1) as the reference loading model. Figure 5 presents the load distribution diagram for this train type. The model consists of one locomotive and ten freight cars, with a total train load of 10,350 kN and an overall length of 196.5 m. The train operates at a maximum speed of 120 km/h, and the corresponding axle load is 225 kN. These parameters were adopted to ensure consistency with standardised loading conditions and to provide a representative dynamic demand for the analyses conducted.

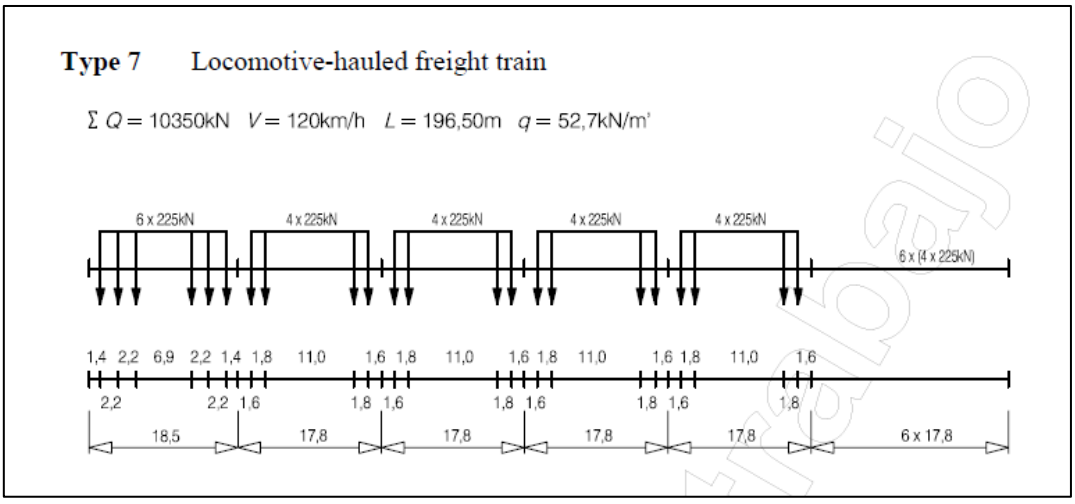

Figure 5.- Freight train used in tests (extracted from EN 1991-2: 2025)

All this information is further elaborated in the sections that follow.

3. CEDEX TRACK BOX. FACILITY DESCRIPTION

CEDEX Track Box (CTB) is a 21 m long, 5 m wide and 4 m deep facility whose main objective is to test, at 1:1 scale, complete railway track sections of conventional and high speed lines for passenger and freight trains, at speeds up to 420 km/h. Figure 6 shows a general view of the testing facility.

The testing facility was designed, built and developed as part of SUPERTRACK ("Sustained Performance of Railway Tracks", 2001-05) and INNOTRACK ("Innovative Track Systems", 2005-2009) projects funded by the European Union Fifth and Sixth Framework Programs, respectively.

Its principal advantage is the possibility of performing fatigue tests in a fast way, as in one working week, the effect of the passing-by of trains during a year in a real section can be modelled.

The reproduction of the effect of the approaching, passing-by and departing of a train in a test cross-section, as it occurs in a real track section, is performed by application of loads, adequately unphased as a function of the train velocity which is being simulated, produced by three pairs of servo-hydraulic actuators, that can apply a maximum load of 250 kN with a maximum frequency of 50 Hz, placed on each rail and 1.5 m longitudinally separated, as seen in Figure 7.

The time-dependent signals applied by each actuator are generated based on a set of calculations that account for the spatial distribution of the simulated train axles, the load associated with each axle, the train speed, and the track stiffness conditions. In this way, the passage of the train over the track is reproduced with a high degree of accuracy.

Furthermore, the reproduction of wheel and track imperfection effects that produce low amplitude high frequency dynamic loads can also be carried out by the use of two piezoelectric actuators, shown in Figure 8, that can apply loads up to 20 kN at 300 Hz.

The railway track response, in terms of displacements, velocities, accelerations and pressures, is collected from a great number of linear variable differential transformers (LVDTs), geophones, accelerometers and pressure cells installed inside both the embankment and the bed layers (ballast, sub-ballast and form layer) of the track.

On the other hand, the railway superstructure response is recorded with mechanical displacement transducers, laser sensors, geophones and accelerometers installed on the different track components (rail, sleeper and railpad), as seen in Figure 9. The acquisition data unit can receive information from 150 sensors at the same time.

For more information (of all facilities in GEOLAB project), please visit https://project-geolab.eu/wp-content/uploads/2021/06/Description-of-Geolab-Research-Infrastructures.pdf

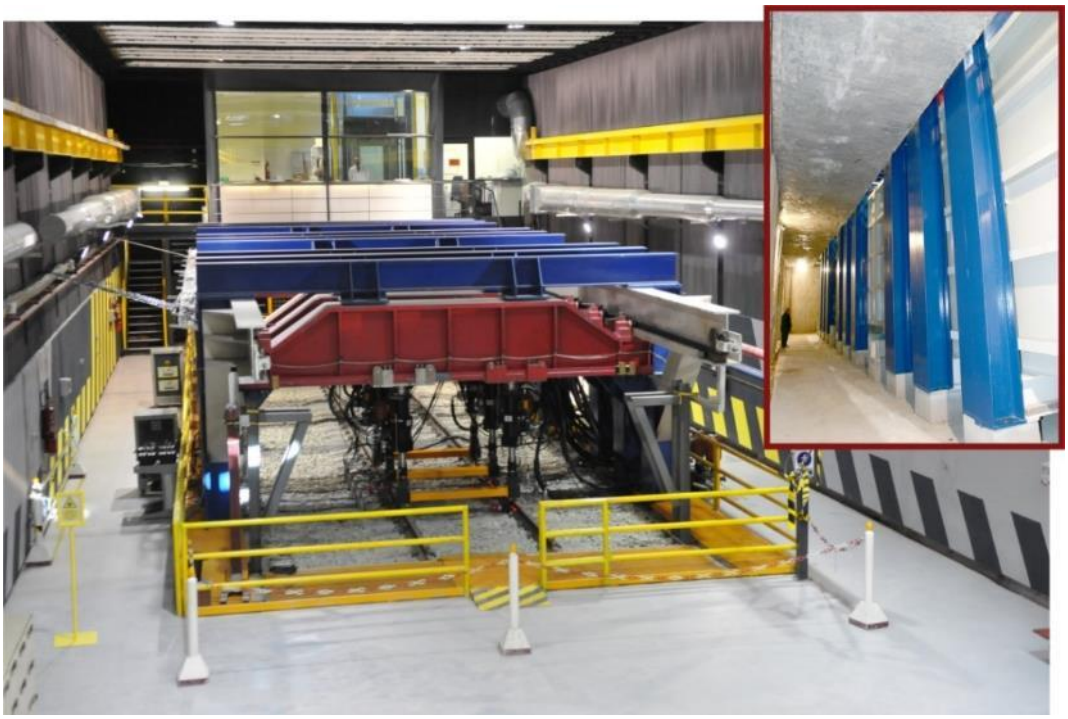

Figure 6.- General view of Cedex track box (CTB) with the control room in the background

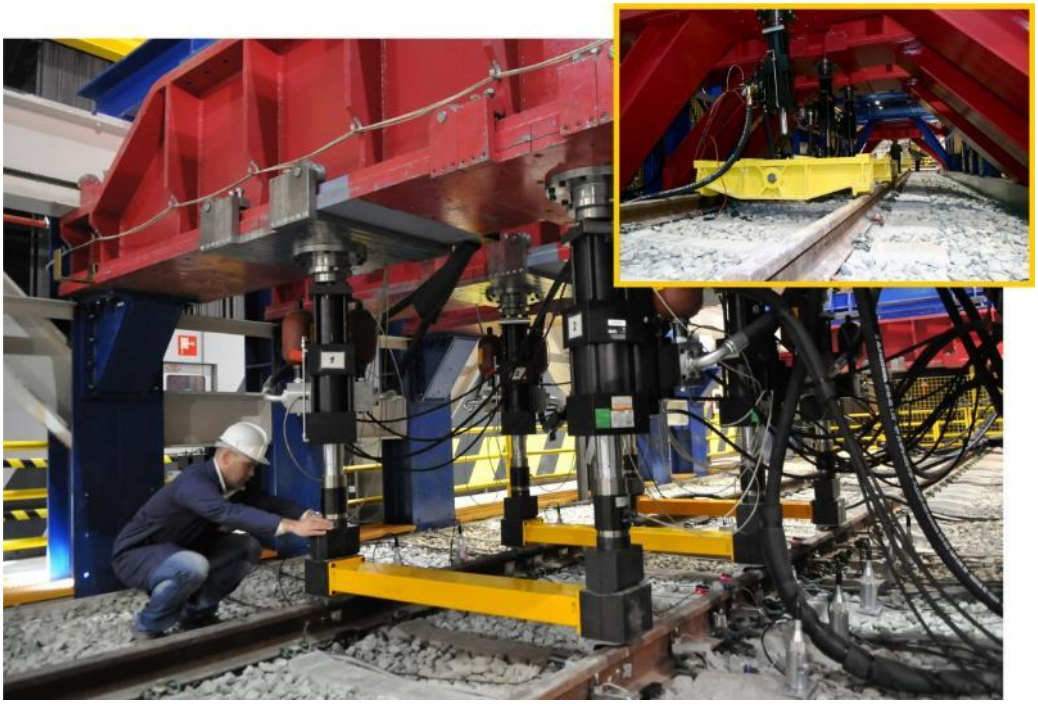

Figure 7.- Loading system formed by three pairs of hydraulic actuators

Figure 8.- Piezoelectric actuators to simulate the effect of track imperfection

Figure 9.- Surface instrumentation installed in one test

The installation spans a length of 21 m, allowing it to be divided into three testing areas. In this instance, the railway track model was constructed in what is referred to as “Test Area 1”, which is the farthest from the control room. Since all the instrumentation is named based on the location of the sleepers, the accompanying figure illustrates the names given to the sleepers. The section in which Sleeper 0 is located will be named “Section 0” in the rest of the document.

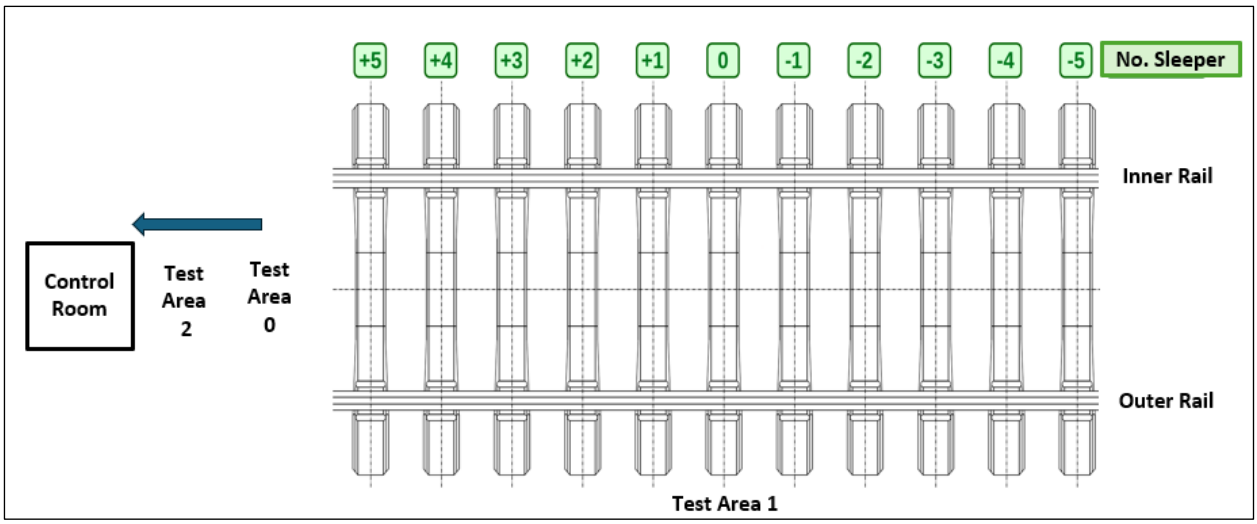

Figure 10.- Plan view of the track section with sleeper numbering at test area 1

4. DESCRIPTION OF THE TEST SECTION

4.1 CROSS-SECTION

The structural section of the CEDEX Track Box is 4 m deep, 5 m wide and 7 m long, being formed by the following elements, listed from bottom to top, as shown in Figure 11.

- Earth embankment
- LECA embankment
- Form layer
- Sub-ballast layer
- Ballast layer
- Sleepers, rails and fastening system

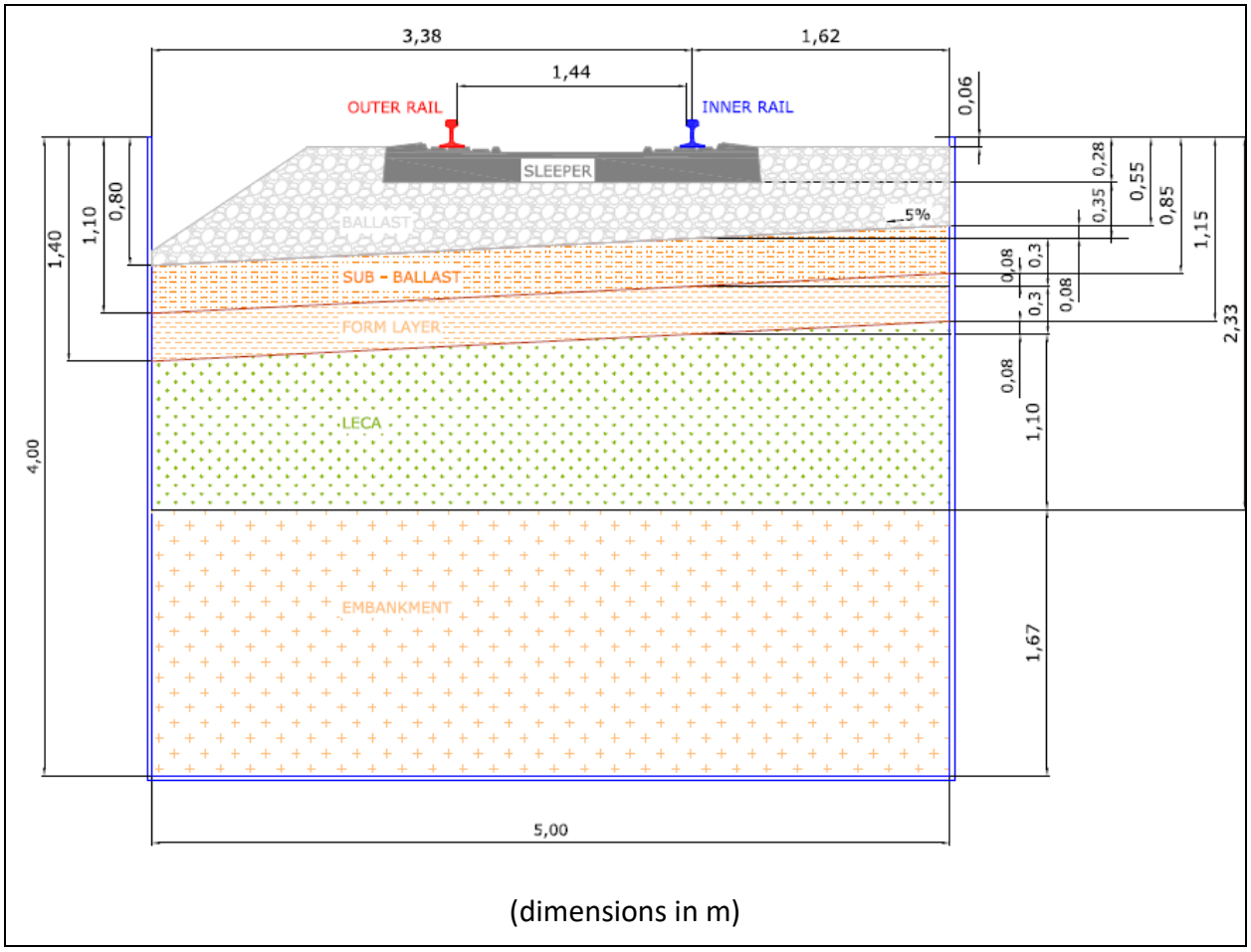

Figure 11.- Schematic diagram of the railway track section used in the test

4.2 EARTH EMBANKMENT

The embankment with a thickness of 1.67 m, as shown in Figure 11, is composed of clayey gravel (GC), low plasticity material with a Liquid Limit of 25% and a Plasticity Index of 7%. It was placed with a dry density of 2.12 g/cm³ and a water content of 2%.

4.3 LECA EMBANKMENT

LECA-type material consists of lightweight expanded clay aggregates, with a particle size between 10 and 20 mm (10/20). The general appearance of the material is illustrated in Figure 12.

Figure 12.- Appearance of LECA material (10/20) used in the railway track section

4.4 FORM LAYER

The form layer has a thickness of 0.30 m and a gradient of 5% from the inner edge of the track to the outer edge. According to its grain size distribution curve, shown in Figure 13, it can be classified as GW (well-graded gravel with sand). Its dry density determined in situ by nuclear methods was 2.20 Mg/m^3 with a moisture content between 5 and 7%.

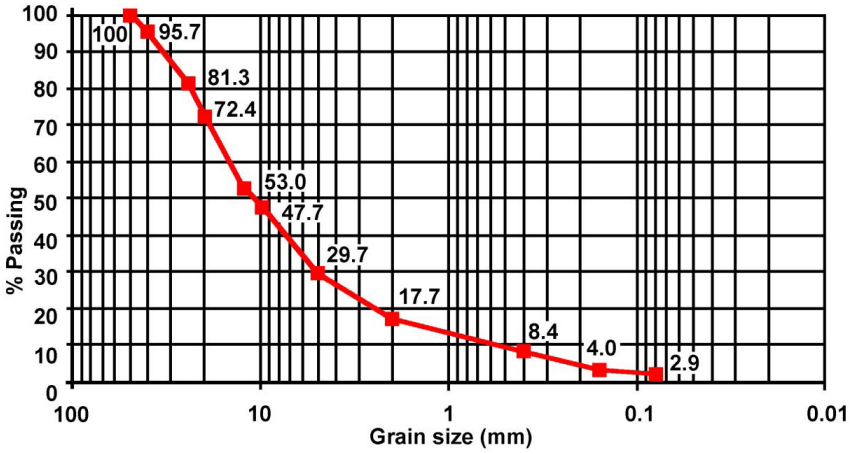

Figure 13.- Form layer grain size distribution curve

4.5 SUB-BALLAST LAYER

The sub-ballast layer used in this test is a granular sub-ballast, as shown in Figure 14. Information about the construction of this layer is provided in Section 5.4 of this document.

Figure 14.- Granular sub-ballast used in the railway track section

4.6 BALLAST LAYER

The railway track section has been finished with a 35 cm thick layer of ballast placed beneath the inner rail. The ballast material is sourced from a quarry approved by ADIF and is commonly used in the CTB. The installation was carried out in two layers, with the shoulder left on the outer track side.

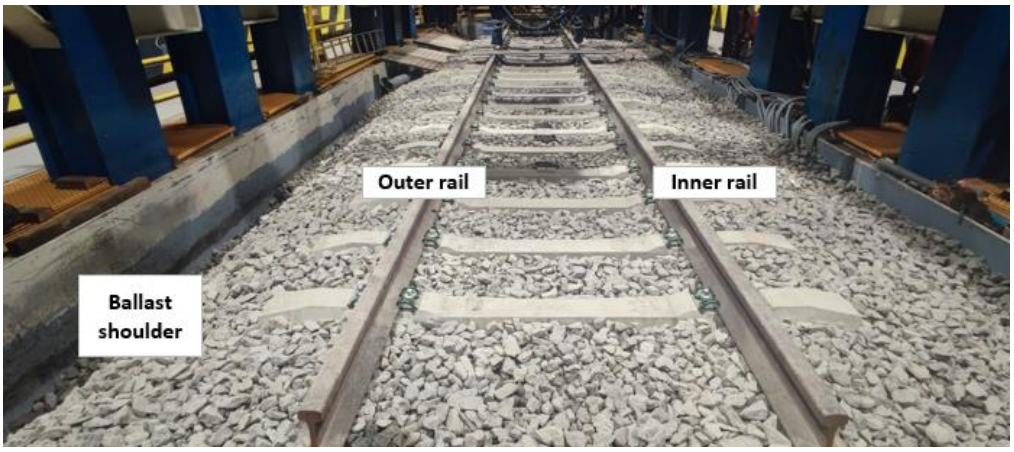

Figure 15.-Ballast layer used in the railway track section

4.7 SLEEPERS, RAILS AND FASTENING SYSTEM

a.- Sleepers: The sleepers are monoblock concrete pre-stressed units of the AI-04 EA type. They are placed every 0.6 meters along the track. Each sleeper has an average mass of 320 kg, a width of 0.22 meters at the centre and 0.30 meters at the edges, as well as a height of 0.21 meters at the centre and 0.23 meters at the edges, as shown in Figure 16.

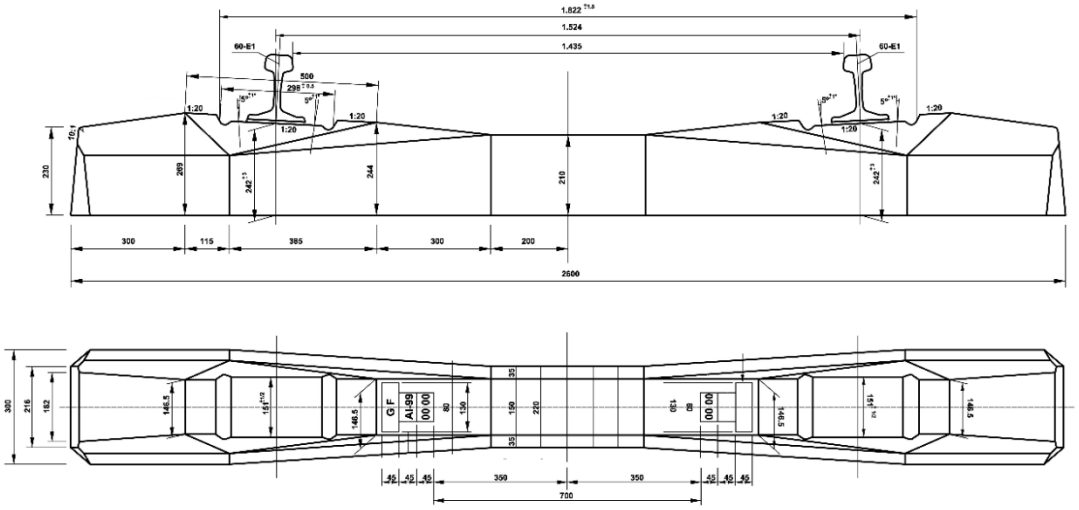

(dimensions in mm)

Figure 16: AI-04 sleeper used in the railway track section

b.- Rails: UIC 60

The model has been constructed using UIC60 rail (60E1 profile), a flat-bottom rail standardised under EN 13674-1, widely applied in mainline railway infrastructure for heavy-haul freight and high-speed passenger traffic. The rail has a nominal weight of approximately 60 kg/m, a height

of 172 mm, a head width of 72 mm, and a base width of 150 mm, providing high structural stability and efficient load distribution (Figure 17).

Figure 17: UIC 60 rail used in railway track section

c.- Fastening system:

The fastening system employed, corresponding to the sleeper type described above, is a VE-type fastening system. For each sleeper unit, the fastening system consists of the following components:

- Under-rail pad: These elastic plates, made of elastomeric material, feature a series of rounded rectangular protrusions on both sides, arranged in rows and columns (see Figure 18 up-left).
- 4 removable anti-rotation sleeves.
- 4 AV-1 lag screws. These steel screws are supplied with a captive washer.
- 4 SKL-1 elastic steel clips (see Figure 18 up-right).
- 4 A2-type angular guide plates. These lightweight components are manufactured from polyamide 66 reinforced with 35% fibreglass (see Figure 18-down).

Figure 18.- Fastening system components:
Up-left: Under-rail pad; Up-right: Screws; Down: Angular guide plate and clip

5. CONSTRUCTION STAGES OF THE TEST SECTION

5.1 DISMANTLING OF THE PREVIOUS SECTION

This section provides a summary of the work involved in dismantling the existing railway track section in the test area where the new section for the PEDLER project was installed within the CEDEX Track Box.

This project has presented a significant challenge for the facility, as routine tests typically do not require dismantling part of the embankment. Figure 19 shows the section to be dismantled and a photo of the track section with the slab track model, previously tested.

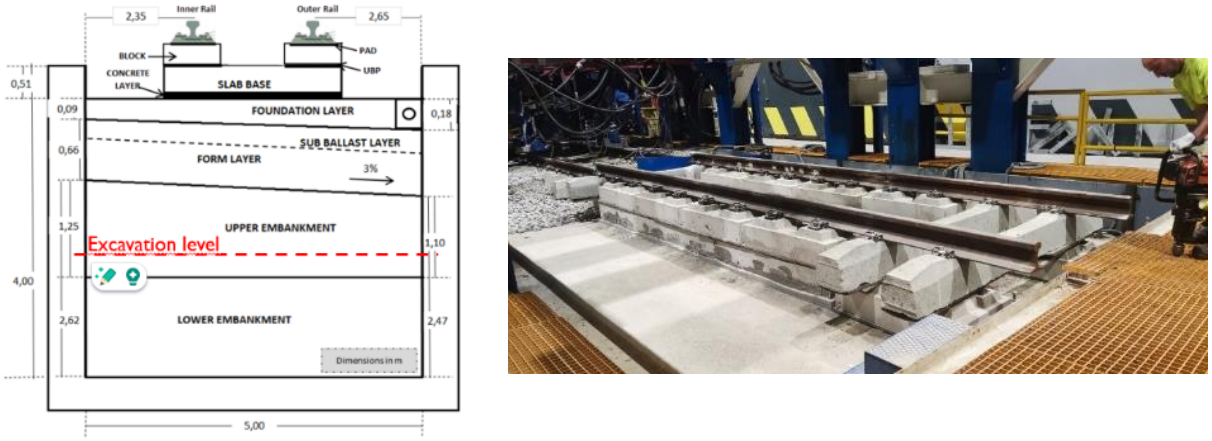

Figure 19.- Diagram of the section to be dismantled (left) and photograph of the slab track model, previously tested (right)

First, the rail fastening system was unscrewed so that it could be dismantled and the clips removed. Next, the entire track slab and foundation layer, consisting mainly of concrete, was broken up, as shown in Figure 20.

Figure 20.- Dismantling the foundation layer of the previous test

After this process, the form layer and sub-ballast layer were exposed. Both were composed of granular material, as shown in Figure 21.

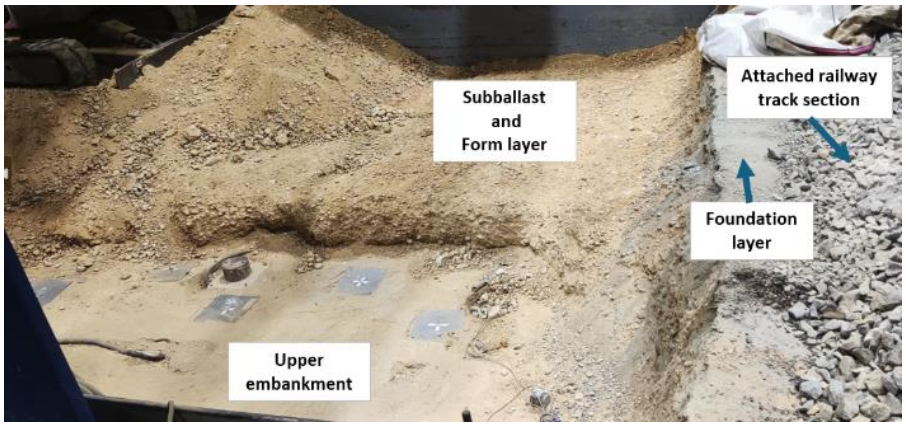

Figure 21.- Dismantling of the sub-ballast layer and form layer

The photograph shows that both layers were made up of granular material. The boundary where the embankment begins, which was composed of smaller granular material, was clearly visible. Additionally, instrumentation located at this boundary can be observed, although it was removed for reuse.

The process concluded by excavating the embankment material to the appropriate level to ensure a 1.1 m thick layer of LECA is placed beneath the inner rail. This excavation was performed using a small excavator, as shown in Figure 22.

Figure 22.- Excavation of the embankment using machinery

Once the excavation level was reached, its top surface was scarified, and a final layer was compacted to create a stable base for the LECA embankment. The planned instrumentation was then installed (as described in Section 5.6). To assess the condition of this stable base, several

tests were conducted using the Panda equipment. The final aspect of the top of the earth embankment is shown in Figure 23.

Figure 23.- Final aspect of test section at the top of the earth embankment

The earth embankment was characterised by means of four Panda-type dynamic penetration tests (Figure 24). The tests were performed in the vicinity of the central sleeper location, with two tests conducted along the inner rail line and two along the outer rail line, in order to ensure a representative assessment of the track cross-section.

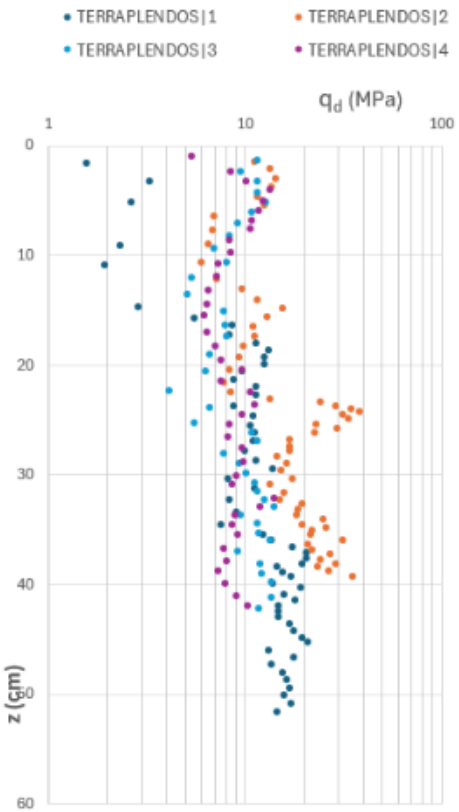

Figure 24.- Panda test results at earth embankment

The measured peak cone resistance values (q_d) ranged between 5 and 35 MPa. For subsequent analyses, a representative value of 18 MPa has been adopted.

5.2 LECA EMBANKMENT

5.2.1 CONSTRUCTION PROCEDURE

The next phase involved constructing the upper part of the embankment using LECA material. To do this, the instructions from the material manufacturers were followed, due to their vast experience in its use.

The first step involved placing a non-woven geotextile covering over the base of the embankment. The LECA material was applied in four sub-layers. The first sub-layer was 30 cm thick; however, due to difficulties with compaction, it was decided that the subsequent sub-layers would have a maximum thickness of 15 cm. Each layer was compacted using a vibrating plate, and the process was found to be more effective when the surface of each sub-layer was lightly moistened with water, as seen in Figure 25.

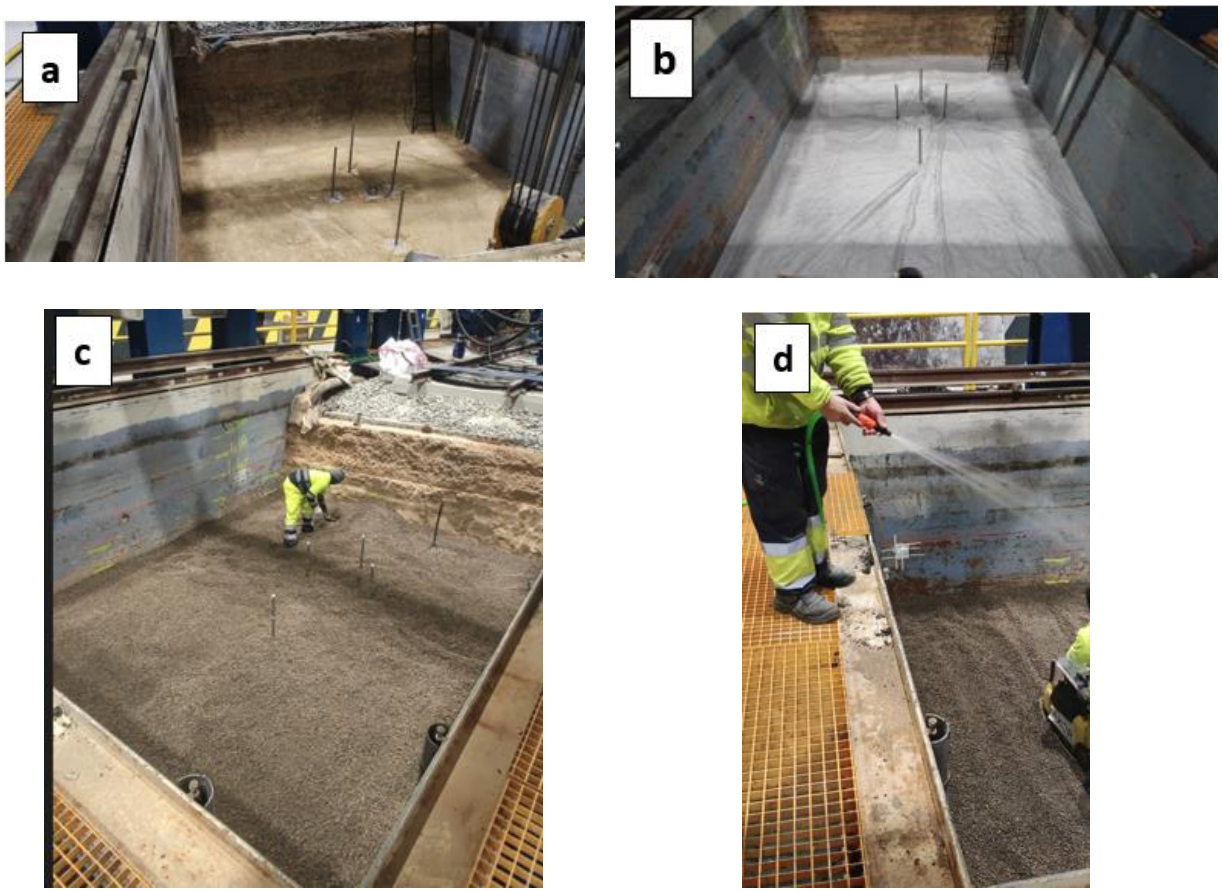

Figure 25.- Different stages of the construction of the LECA embankment. a: base of the embankment with instrumentation, b: placement of geotextile on the base of the embankment, c: spreading of the LECA material, d: watering of the LECA embankment.

5.2.2 PANDA AND DYNAMIC PLATE TESTS

The LECA embankment was tested using Panda penetration tests and dynamic plate load tests at two distinct stages of construction: when approximately 50% of the design thickness had been reached, and after the full layer thickness had been reached. The results corresponding to each construction stage are presented separately.

Eight Panda penetration tests were carried out on the LECA embankment, once it had reached half the thickness of the layer to be laid (55 cm), as seen in Figure 26.

Figure 26.- Left: Aspect of the test section with the half-thickness of LECA embankment, in which some instrumentation was already installed. Right: Execution of Panda test in the half-thickness of LECA embankment. The dynamic load plate is shown in the background

The locations of the Panda tests performed at the half thickness of the LECA embankment are shown in Figure 27 (left), and also the results obtained (right). Most values of resistance to penetration (q_d) are in the range 3 - 10 MPa, with an average value around 6 MPa.

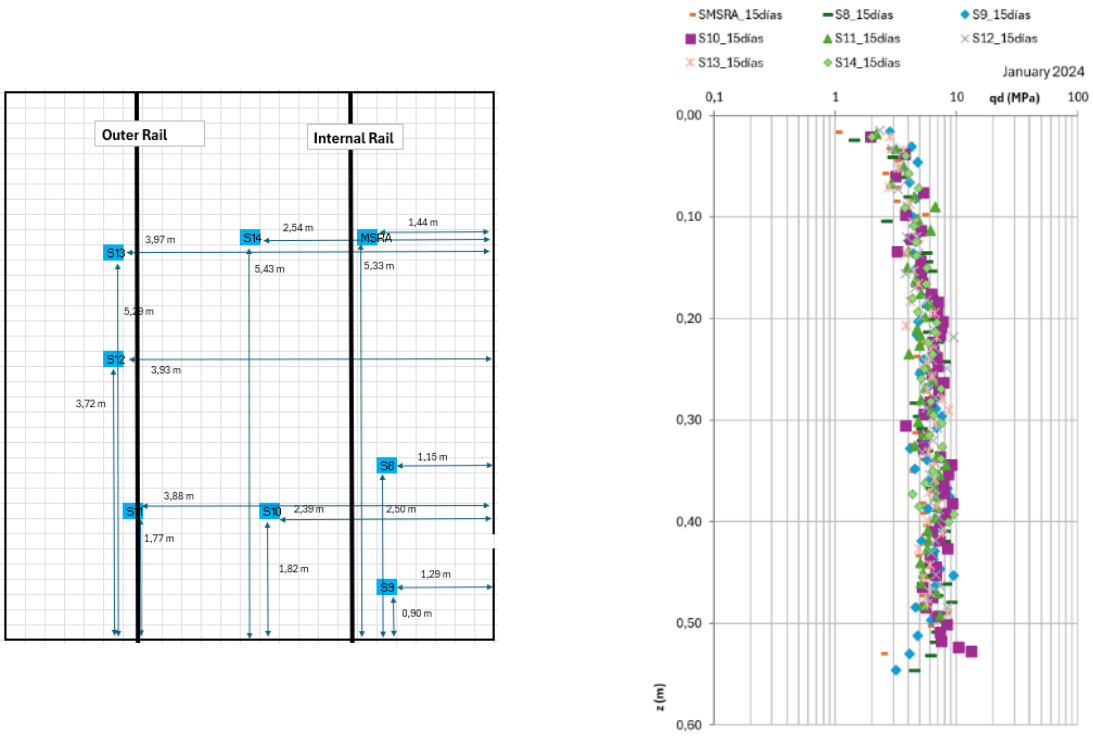

Figure 27.- Scheme of test points performed in the half-thickness of LECA embankment (left) and Panda results (right)

The characterisation was further completed by performing dynamic plate load tests. Figure 28 shows the settlement values (*s*) and the corresponding vertical modulus of deformation (E_{vd}) obtained during the tests and the location of the test points.

As can be seen in Figure 28, most settlement values ranged between 0.8 and 1.5 mm, with an average value of around 1.1 mm. Most values for the vertical deformation modulus (E_{vd}) are between 15 and 27 MPa, with a characteristic value of 21 MPa.

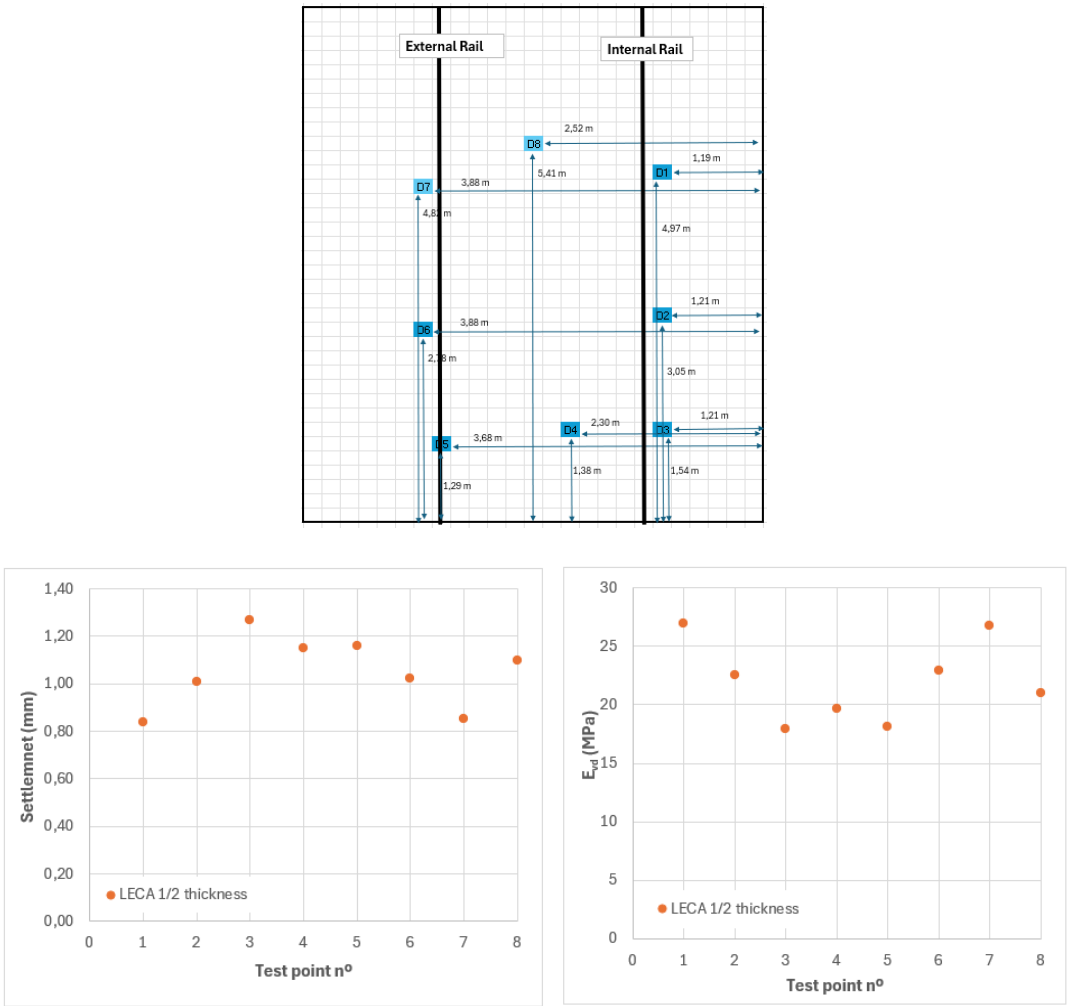

Figure 28.- Location test points (up). Settlement (left) and Modulus of vertical deformation (E_{vd}) (right) obtained in the different test points

Once construction of the entire LECA embankment was completed, testing was repeated. The total thickness of the expanded clay layer, once compacted, is 1.2 m at the inner rail and decreases toward the outer edge with a 5% slope (0.99 m). Figure 29 shows a general view of the test section after the LECA embankment was compacted and finished.

Figure 29 General view of test section with LECA layer once compacted and finished

The locations of the Panda tests performed at the LECA embankment, once the construction ends, are shown in Figure 30 (left), and also the results obtained (right). Most of the values of resistance to penetration (q_d) are in the range between 5.7 and 6.3 MPa, with an average value around 6 MPa. This value is identical to that obtained for the half-thickness LECA embankment.

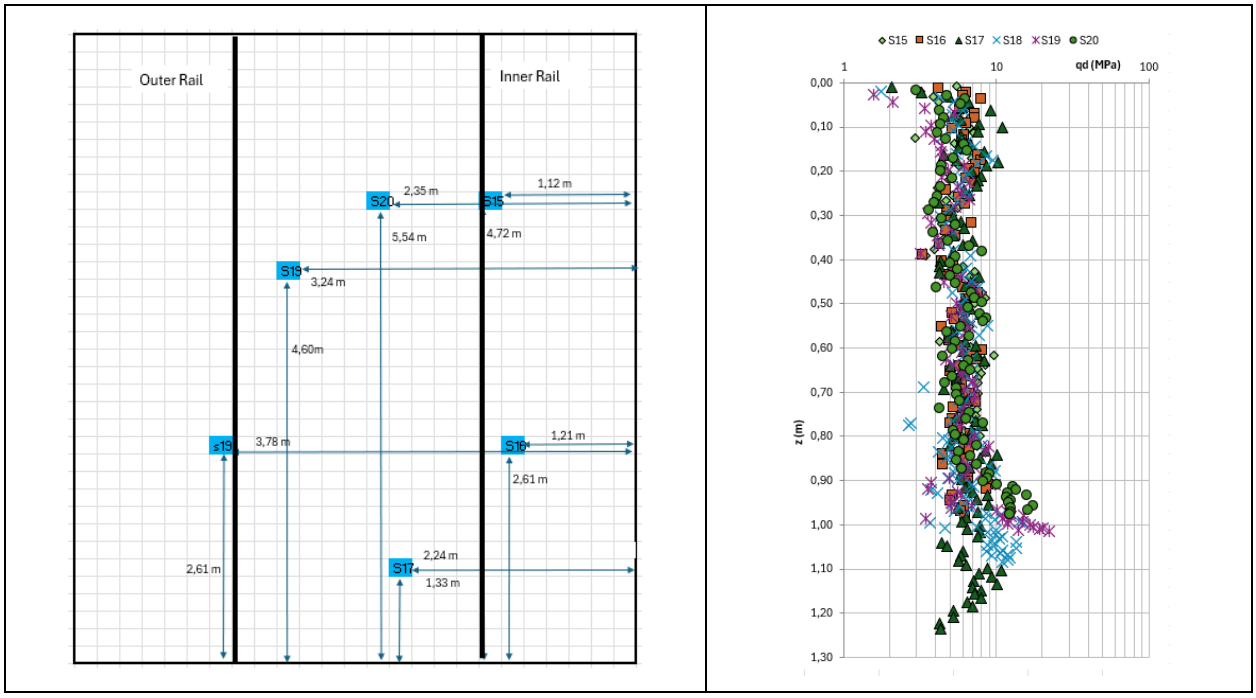

Figure 30.- Scheme of test points performed in LECA embankment (left) and Panda results (right) with the total thickness

At this point, the condition of the LECA embankment was also examined using the dynamic plate. Figure 31 shows the values of settlement and vertical deformation modulus (E_{vd}) obtained at different test points after the LECA embankment construction is complete, and the test point locations.

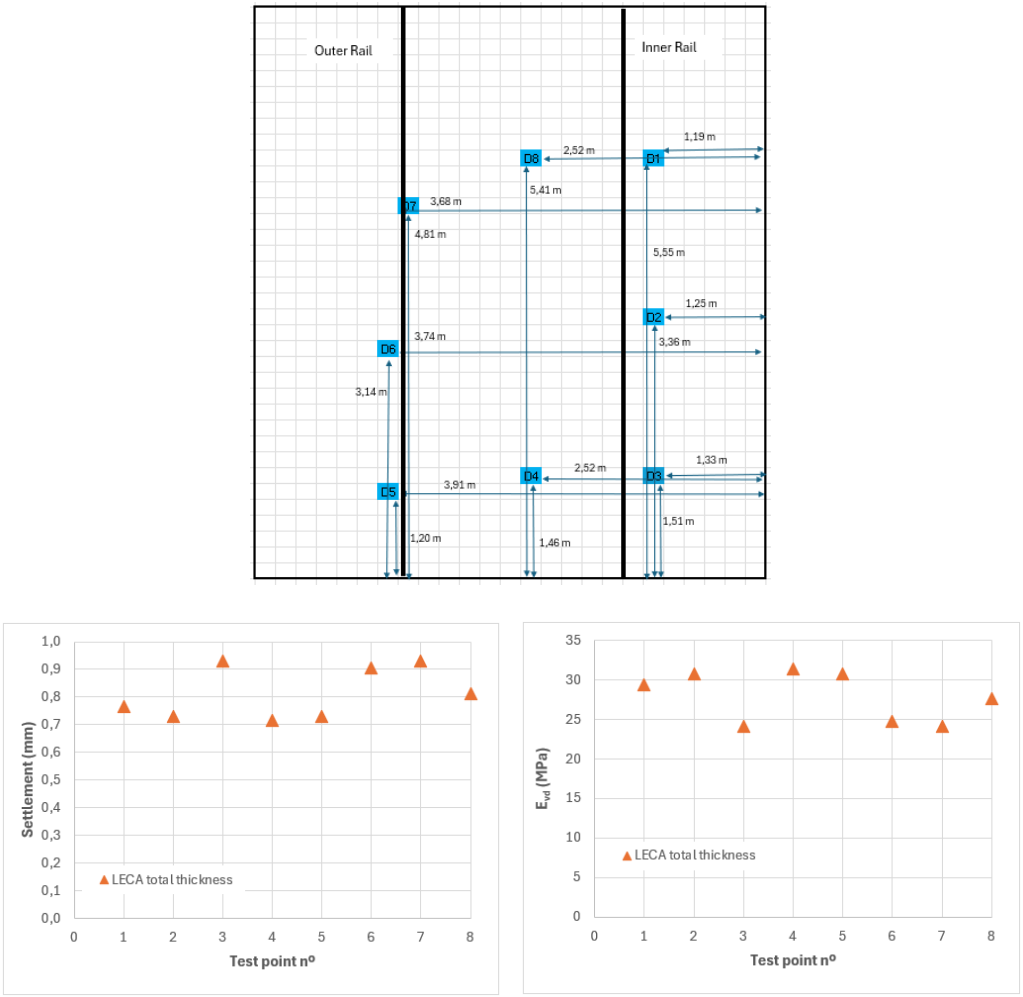

Figure 31.- Test point locations (up). Settlement (left) and Modulus of vertical deformation (E_{vd}) (right) obtained in the different test points in January 2024, once the LECA embankment was completed

The settlement values ranged from 0.7 to 0.9 mm, which are much lower than those obtained in the half thickness of the LECA embankment. The average value for E_{vd} is 28 MPa. It corresponds to the maximum value obtained for the half-thickness tests.

It should be noted that CEDEX has no prior experience assessing the compaction state of LECA using these techniques (PANDA and dynamic plate tests). Given the limited previous experience at CEDEX in assessing LECA compaction using PANDA and dynamic plate tests, the values obtained in this study should be interpreted primarily on a comparative basis within the present test campaign, rather than as absolute acceptance criteria directly equivalent to those commonly

adopted for conventional granular materials. Therefore, the values obtained can be used for comparison with those measured during the dismantling of the railway section.

To visualise the final state of the LECA embankment, several points near the corners of the section were lightly scraped by hand. It was observed that the LECA material appeared somewhat fractured, as shown in Figure 32: the left-hand side presents a photograph of the upper surface of the layer, which shows no visible breakage, while on the right-hand side, the image shows that the material was fractured a few centimetres below the surface.

Figure 32.- Left: LECA material at the top of layer, no breakage. Right: LECA material broken at some centimetres below top surface

Finally, the instrumentation was installed, and a geotextile (identical to that of the lower layer) was placed for protection.

Figure 33.- Left: LECA embankment top with instrumentation. Right: Geotextile over LECA embankment

5.2.3 DETERMINATION OF V_S OF LECA EMBANKMENT

The determination of critical speed requires an accurate shear-wave velocity (V_S) profile for the track layers. In this study, the V_S of the LECA embankment was obtained using the Spectral Analysis of Surface Waves (SASW) technique, which estimates V_S from the dispersion curve of Rayleigh waves generated at the surface. This method is particularly suitable for stratified profiles and provides high-resolution for shallow layers, which is essential for assessing dynamic performance under high-speed conditions.

In this study, tests were conducted with sensors positioned on both sides of the rails at an inter-sensor spacing of 1.97 m (Figure 34 (a)). Only low-frequency accelerometers were employed,

each mounted on spikes driven into the ballast to ensure proper ground coupling (Figure 34 (b)). Signal excitation was applied either directly to the ballast using a sledgehammer or onto a metal plate to achieve a uniform energy distribution and reduce high-frequency content. Impact points were located between 1.5 m and 2 m from the end of the sensor array.

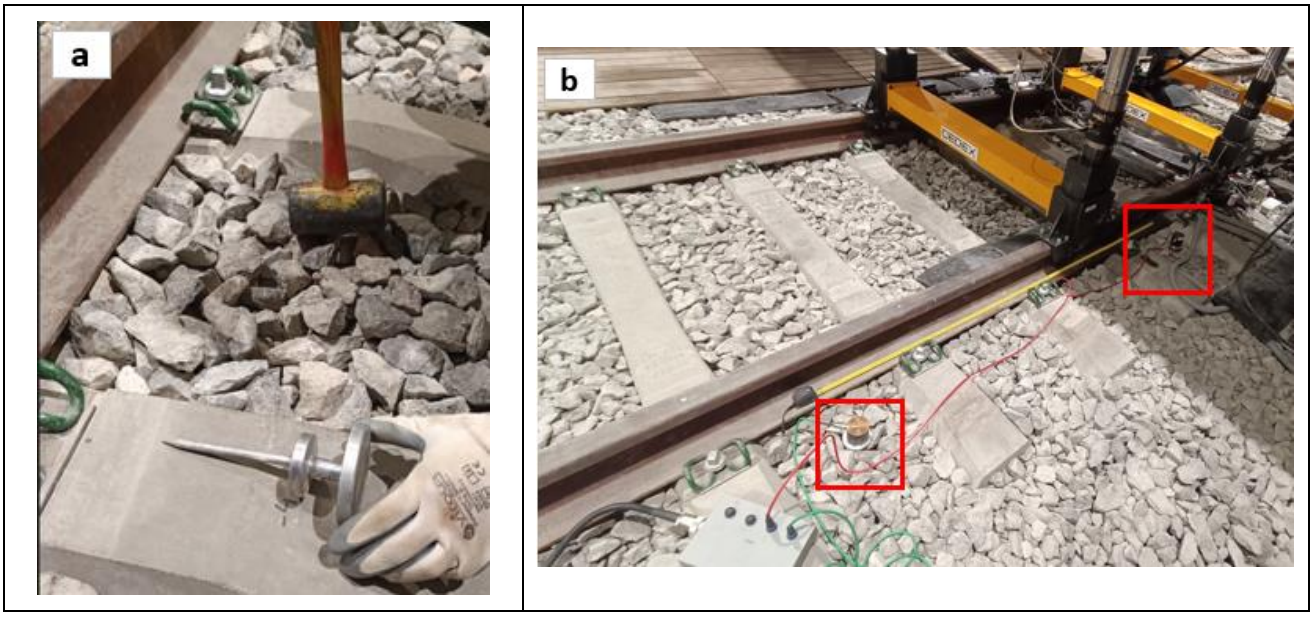

Figure 34.- Detail of spikes used (a) and test conducted at outer rail (b)

The interpretation of SASW measurements involved deriving experimental dispersion curves and comparing them with theoretical curves obtained from the best-fitting layered model (Figure 35). This inversion process enabled the characterisation of the LECA embankment and its interface with the underlying formation. As a result, the shear-wave velocity of the LECA embankment was determined to be 283 m/s, which constitutes a key parameter for evaluating the critical speed of the track system.

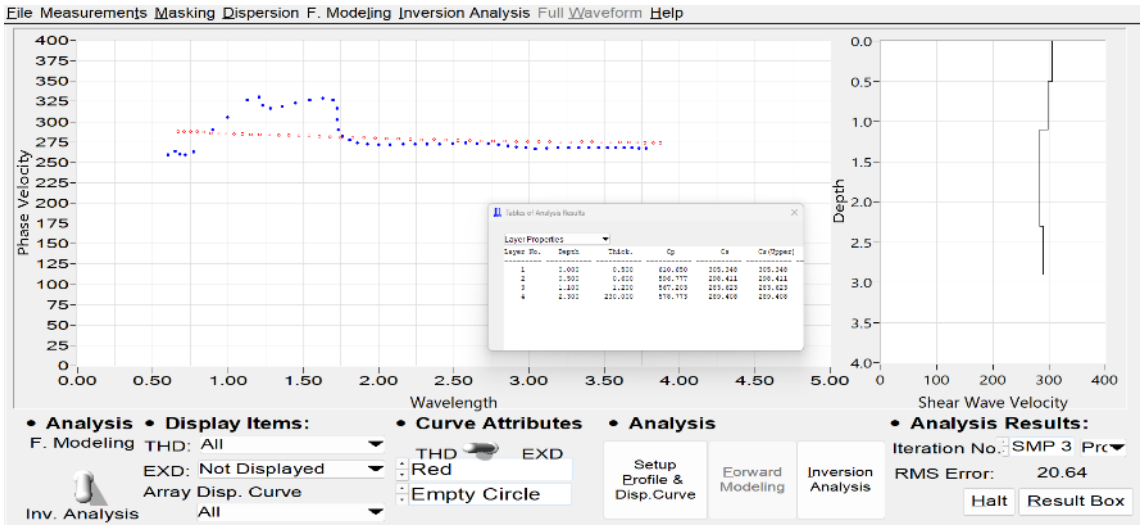

Figure 35.- Layered model compatible with the average dispersion curve, with a shear-wave velocity in the LECA embankment of Vs = 283 m/s.

5.3 FORM LAYER

The form layer was placed on top of the LECA embankment, once covered with a geotextile. The material used for this form layer was the same as that used in the previously dismantled section. The thickness of the form layer was 30 cm and was constructed in two sub-layers, each 15 cm thick. Figure 36 shows the appearance of the form layer after compaction.

Figure 36.- Top of the form layer after construction

The values of maximum density and optimum moisture content obtained in the form layer after compaction were determined using a Troxler equipment. Seven measurements were made, distributed evenly across the entire surface of the form layer. The average value for maximum density obtained was 2.25 Mg/m³ (with a reference laboratory value of 2.30 Mg/m³), while the optimum moisture content was 4.7% (with a reference laboratory value of 5.0 %).

After finishing the construction of this layer, eight Panda tests were conducted along the entire railway track section. The locations and the results of the Panda tests performed are labelled as S21 to S28 in Figure 37.

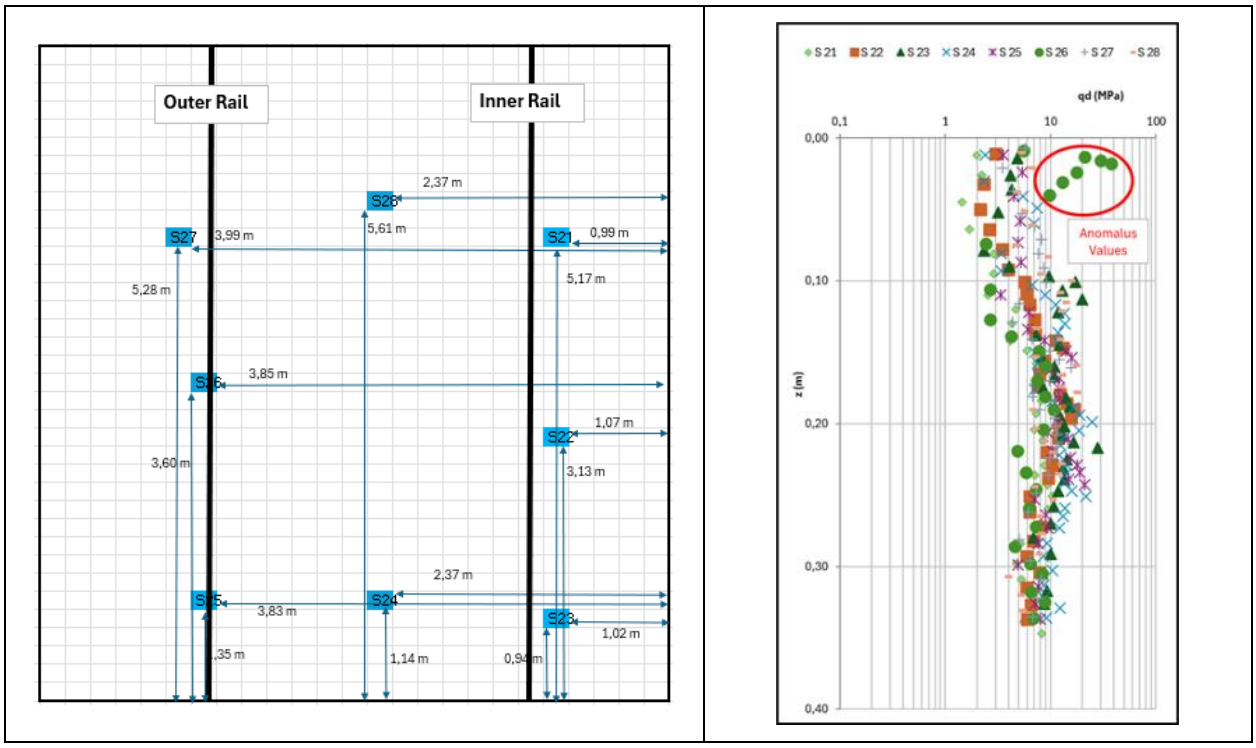

Figure 37.- Left: Location of Panda test on the Form layer. Right: results obtained

As shown in the graphs above, most of the values ranged from 2 to 20 MPa, with an average value of approximately 9.5 MPa.

The study included dynamic load plate tests. Figure 38 displays the values of settlements (s) along with the corresponding vertical modulus of deformation (E_{vd}) obtained during these tests. The test locations are the same as those shown in Figure 37.

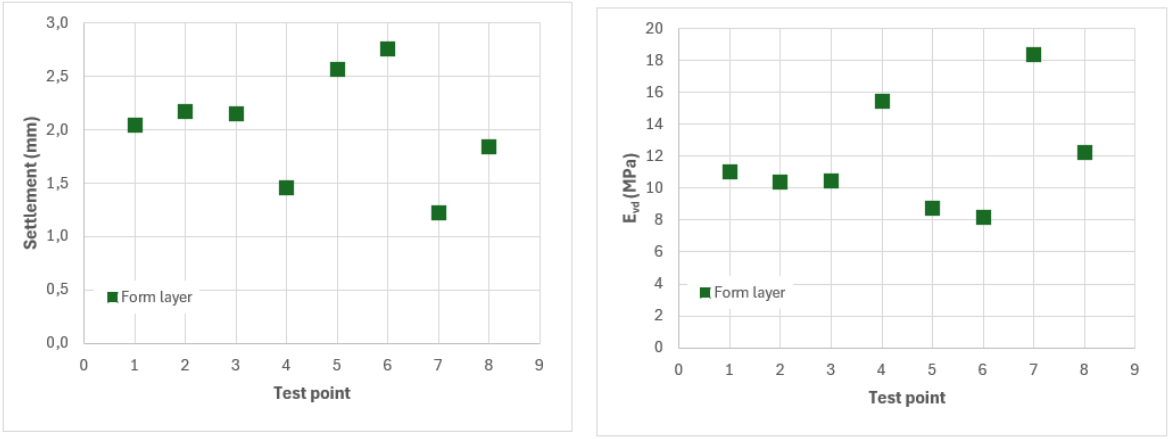

Figure 38.- Settlement (left) and Modulus of vertical deformation (E_{vd}) (right) obtained in the form layer

As can be seen in the graph above, most settlement values ranged between 1.5 and 2.7 mm, with an average value of around 2 mm. Values for vertical deformation modulus (E_{vd}) are between 8 and 18 MPa, while the average value is 12 MPa.

5.4 SUB-BALLAST LAYER

After the form layer, the granular sub-ballast layer was spread. It is 30 cm thick and was compacted with the same equipment as the rest of the layers of the railway track section. The final aspect is shown in Figure 39.

Figure 39.- Sub-ballast layer after its construction

At the end of its compaction (31/1/2024), density and moisture values were determined with Troxler equipment. The result obtained showed that the values of density were around 97% of the values obtained in the laboratory with the Modified Proctor, and the moisture values were in the low range (mean value of 4% instead of 7% that was the optimum). Based on these data, it has been decided to scarify, wet and re-compact the sub-ballast layer.

However, in order to have more data, it was decided to carry out four dynamic load plate tests. Two tests were carried out on the inner rail and two on the outer rail, and approximately around the central sleepers. The average value obtained for the modulus of vertical deformation (E_{vd}) was 46.6 MPa. After re-compaction, the layer was re-tested with the dynamic load plate, and the vertical modulus of deformation was almost identical to the previous one (46.9 MPa).

The moisture and density values obtained with the Troxler did not comply with ADIF specifications in PF7. This document requires that the average of the six density values shall be greater than or equal to 100% of the maximum Modified Proctor density obtained in the tests. Up to two of the six values may give a result lower than 100%, but always higher than 98% of the maximum density.

Therefore, it was finally decided to use heavier compaction equipment. After the application of this equipment, the required density values were achieved, and the construction was completed. Figure 40 (left) shows the compaction machine used, and the final aspect of the sub-ballast layer with all testing points over 100% of the modified proctor (ADIF requirement).

Figure 40.- Sub-ballast layer; left: new compaction machine, right: final aspect of sub-ballast layer

Afterwards, dynamic load plate tests and Panda penetration tests were carried out to check the compaction status. Location of Panda and dynamic load plate tests (in the same location test) is shown in Figure 41, and also the results obtained.

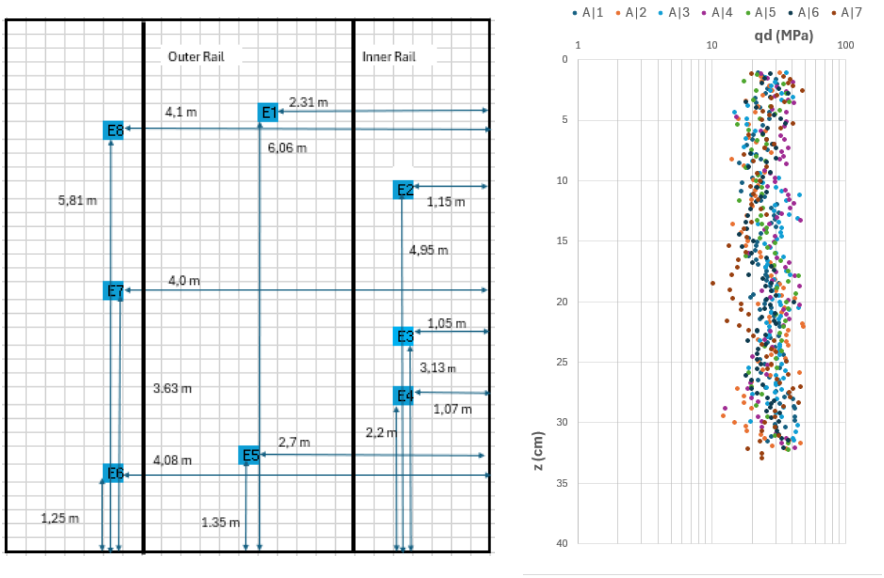

Figure 41.- Left: Location of Panda test on the Sub-ballast layer. Right: results obtained

As shown in the graphs above, most of the values ranged from 10 to 47 MPa, with an average value of approximately 28 MPa.

Figure 42 shows the values of settlement and vertical deformation modulus (E_{vd}) obtained at different test points, once the sub-ballast layer construction is finished.

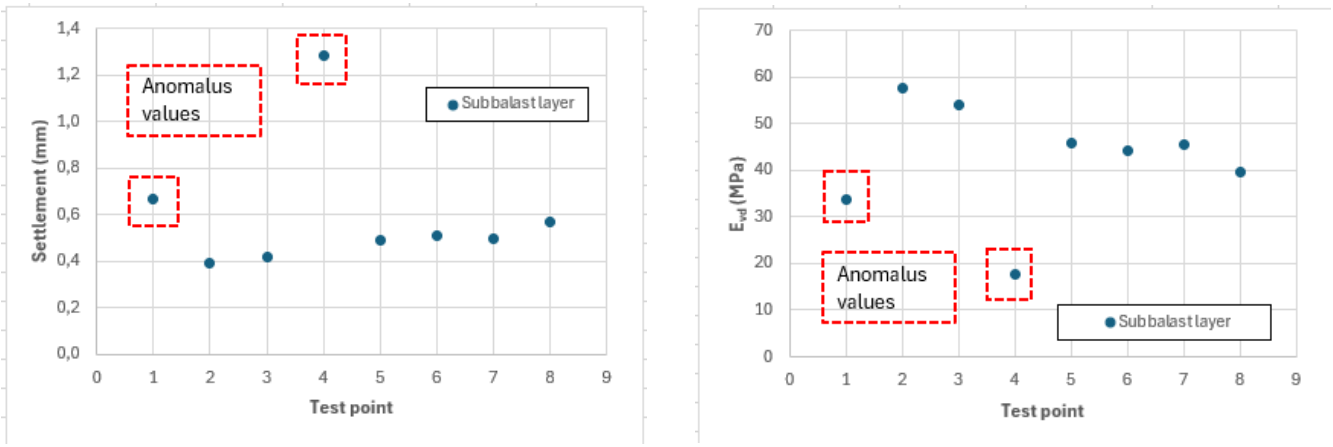

Figure 42.- Settlement (left) and modulus of vertical deformation (E_{vd}) (right) obtained in the different test points, once sub-ballast layer was finished

As can be seen in the above graphs, two values were identified as outliers and were not included in the calculation of average values. Settlement values are between 0.4 and 0.6 mm, while the average value for E_{vd} is 47 MPa.

5.5 BALLAST LAYER

The railway track section was covered with a layer of ballast that is 35 cm thick beneath the inner rail. This ballast was laid in two layers and comes from a quarry approved by ADIF for use on high-speed tracks.

Once the two layers of ballast were in place, the sleepers and the entire rail fastening system were installed. The ballast was then lightly compacted using a hand-held vibrator (Figure 43).

Figure 43.- Left: Ballast layer with sleepers, rails and fastening system. Right: Hand-held vibrator for ballast compaction

Finally, the track was levelled, as seen in Figure 44, to ensure that both rails were at the same height without any cant.

Figure 44.- Levelling of railway track sections.

Eleven tests were conducted on the ballast layer using the Panda equipment. The results and test locations are displayed in Figure 45.

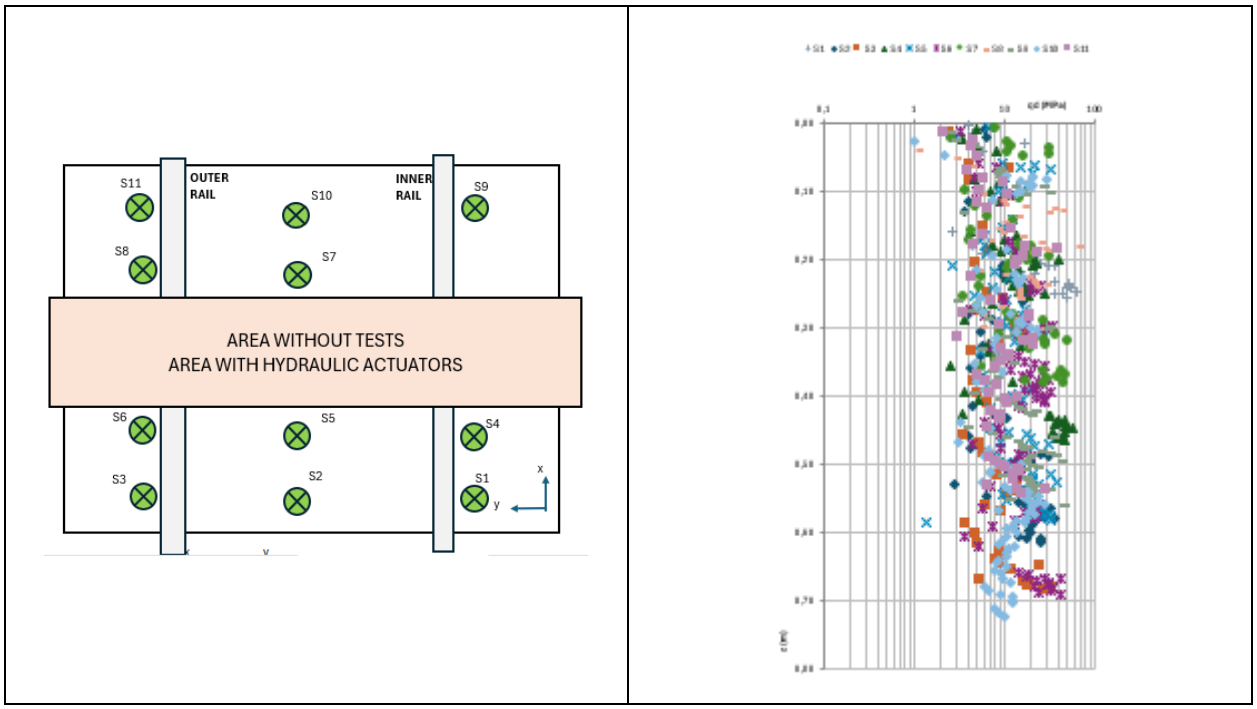

Figure 45.- Location of Panda tests and results at ballast layer

As shown in the graph above, the results obtained for the ballast layer exhibit a much wider variability than those corresponding to the underlying layers. In this case, the measured resistance values ranged from 4 to 60 MPa. The average value is 17.7 MPa, with 36% of the tests yielding values below 15 MPa.

Taking as a reference the work by Montero and Estaire (2025)[1], which includes an analysis of PANDA tests carried out by CEDEX both on in-service railway lines and at the CTB, it is indicated that, for the CTB, q_d values greater than 15 MPa are representative of an adequate compaction state of the ballast layer.

5.6 INSTRUMENTATION INSTALLED

5.6.1 GENERAL ASPECTS

The railway track section being studied was equipped with a range of sensors specifically designed to continuously and accurately record various physical parameters related to track behaviour. The arrangement of these devices was based on experimental criteria, aiming to gather information from both the different layers that compose the section (including ballast, sub-ballast and form layers, and embankment) and the surface, where the loads caused by rail traffic are most prominent. This instrumentation facilitates the analysis of phenomena linked to load transmission, deformability, contact pressure, and other geotechnical and structural parameters of interest. Table 1 details the sensors used and the physical variables recorded, which form the foundation for a comprehensive interpretation of railway infrastructure behaviour.

Table 1.- Types of instrumentation used in the present study

Type of sensor	Physical parameter	Identification	Measuring range
Laser system	Vertical displacement	LSV	±15 mm
LVDT		LVV	10-40 mm
Potentiometer		PTV	25 mm
Geophone	Vertical velocity	GEV	Up to 20 cm/s
Accelerometer	Vertical acceleration	ACV	±2/10/50 g
Pressure cell	Pressure	CP	1/2/5/10 bar
Temperature control	Temperature	TEMP	-50 to 100 ºC
Humidity control	Humidity	HUM	0 - 100%

The sensor nomenclature consists of three components: the first identifies the type of sensor, the second specifies its location relative to the sleeper, and the third denotes its position within the railway track section. The first component is detailed in Table 1, while the second is referenced to the sleeper numbering scheme illustrated in Figure 10. In addition to specifying the reference sleeper number, the nomenclature also indicates the position within the sleeper. For this purpose, three reference points are defined: the inner rail (I), the outer rail (E), and the centre (C). In some cases, however, it is not possible to place the instrumentation exactly at these

[1] Montero N. and Estaire J. (2022). El ensayo de penetración dinámica de energía variable para estimar la calidad de la banqueta de balasto. Revista Geotecnia, Nº 165. doi.org/10.14195/2184-8394_165_6

positions, requiring a slight displacement. When this occurs, the nomenclature reflects the direction of the displacement. For example, if a sensor is installed at the inner rail but shifted towards the centre of the sleeper, it is denoted as IC; conversely, if it is shifted towards the edge of the sleeper, the designation is II. The final parameter for naming is the location of the sensor in relation to the layer of the section or element where it has been placed. A distinction is made between: Rail (C): can be located on the head or the skid, outer frame of the CTB (MA), sleeper (TR), ballast (BA), sub-ballast (SB), form layer (CF), LECA embankment (LE), earth embankment (TE). Figure 46 illustrates the designation.

Below are some examples:

- LSV_0-E_PC-MA: laser system (LSV) positioned on Sleeper 0, on the outer rail (E) and measuring between the rail foot (PC) and the outer frame (MA).
- LVV_+2-C_BA: LVDT (LVV) positioned on Sleeper +2, at the centre of the sleeper (C) and measuring ballast layer (BA).
- ACV_0C_TR: accelerometer (ACV) positioned on sleeper slightly displaced towards the centre of sleeper (0C), measuring the sleeper (TR).

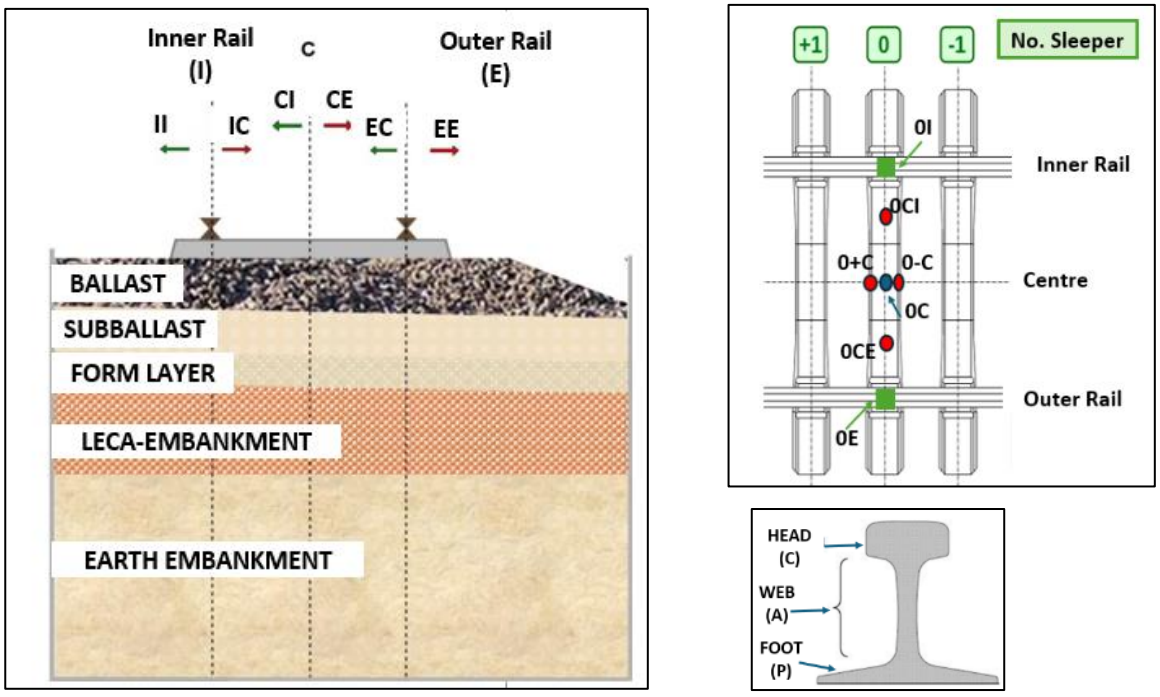

Figure 46.- Designation for sensors location with respect to the sleeper, rails and sections layers

The following sections describe the characteristics of the sensors installed. A distinction has been made between the instrumentation embedded inside the railway track section (internal instrumentation) and that installed on the surface (external instrumentation).

5.6.2 INSTRUMENTATION EMBEDDED IN THE RAILWAY TRACK SECTION

During the construction of the track section, most of the instrumentation was positioned beneath or near the central sleeper ("Sleeper 0"), which was designated as the reference point for load application. However, as discussed in the following sections, some sensors had to be relocated due to spatial constraints. Figure 47 illustrates the final layout of the instrumentation, showing its relative position with respect to the different track layers and the types of devices installed. As stated earlier, the precise location of each sensor can be inferred from its corresponding identifier.

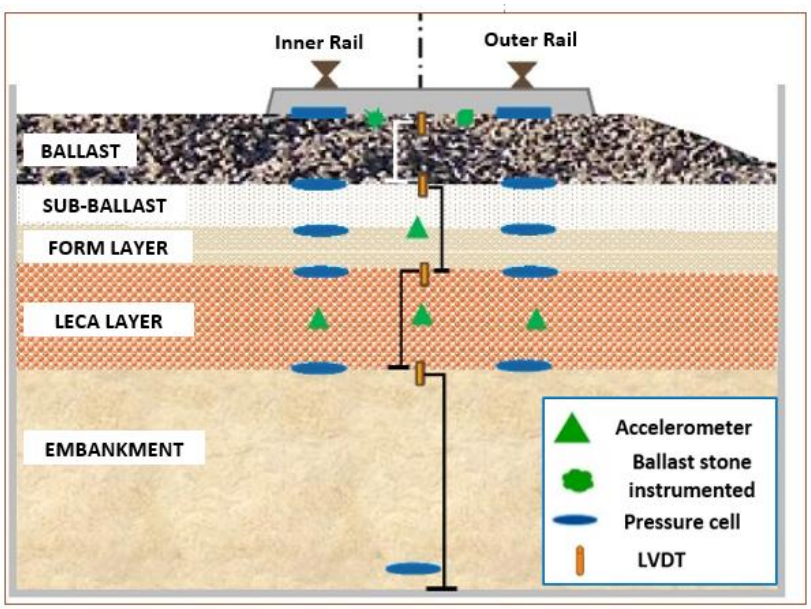

Figure 47.- Schematic diagram of the section with the instrumentation embedded within the railway track section

33 embedded sensors were installed, classified as follows:

a.- Linear Variable Differential Transformer (LVDT)

11 LVDTs were installed to measure the vertical displacements occurring within the different layers of the railway track section.

- 1 LVDT was located in the earth embankment, 30 cm below the base of the LECA level, where it had already been placed during previous tests.
- 4 LVDTs had their bases resting on the LECA bottom layer and their heads positioned on the surface of the LECA embankment, thus measuring the settlement of the LECA embankment.
- 2 LVDTs were anchored on the top surface of the LECA embankment, with their heads attached to the surface of the sub-ballast at the track axis, providing settlement measurements of both the sub-ballast and form layers.
- 4 LVDTs were fixed to the centre of a sleeper, with their bases connected to the sub-ballast surface and the heads to the sleeper, thereby recording the settlement of the ballast layer.

Table 2 describes the location details of the LVDT sensors embedded within the section, while Figure 48 shows a photograph of this type of sensor.

Table 2.- LVDTs position description and identification

Sleeper	Position	Level (m)(1)	Vertical displacement of	Identification
0	Centre	2.35 – 0.00	Earth embankment	LVV_0C_TE
0	Centre	2.05 – 0.99	LECA embankment	LVV_0EC_LE
-2	Centre	2.05 – 0.99	LECA embankment	LVV_-2C_LE
0	Centre to inner rail	2.05 – 0.99	LECA embankment	LVV_0CI_LE
+1	Centre	2.05 – 0.99	LECA embankment	LVV_+1C_LE
-1	Centre to outer rail	0.69 – 0.39	SB+FL layers	LVV_-1CE_CF+SB
+1	Centre to inner rail	0.69 – 0.39	SB+FL Layers	LVV_+1CI_CF+SB
-2	Centre to positive sleeper	0.39 – 0.00	Ballast layer	LVV_-2+C_BA
0	Centre to negative sleeper	0.39 – 0.00	Ballast layer	LVV_0-C_BA
0	Centre to positive sleeper	0.39 – 0.00	Ballast layer	LVV_0+C_BA
+2	Centre to positive sleeper	0.39 – 0.00	Ballast layer	LVV_+2-C_BA

(1) Level reference: sleeper bottom surface. The first number is the level of the LVDT base, and the second number is the level of the LVDT head

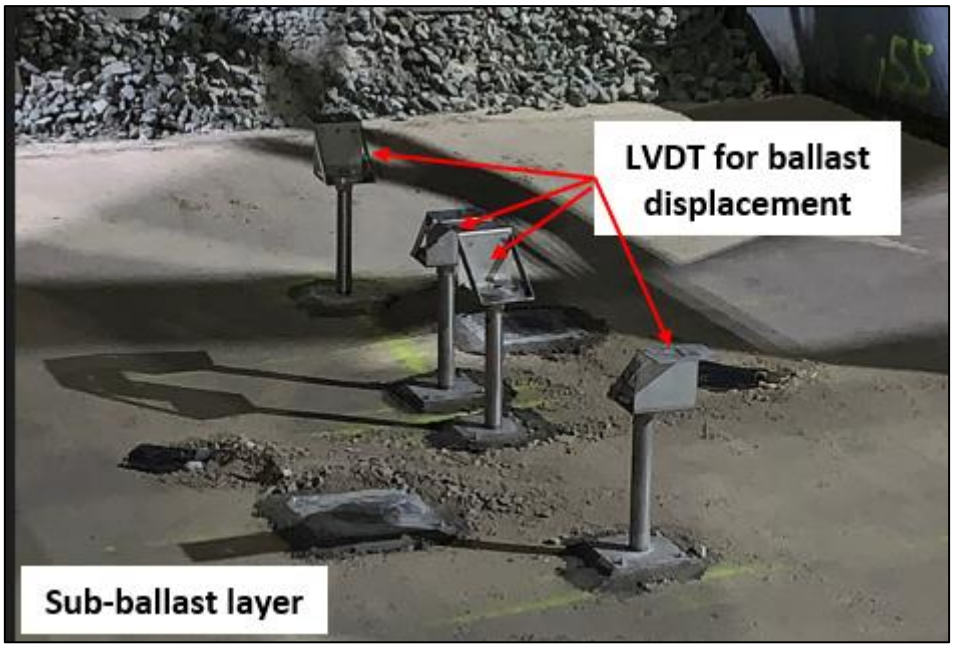

Figure 48.- Example of LVDT installed at CTB to measure vertical displacements

b- Geophones

2 geophones were installed to measure the velocity of the point at which they are installed. In this case, the sensors were embedded within the earth embankment, in an area that had not been excavated for the construction of the new section. Table 3 describes the location details of the geophones embedded within the section.

- 2 geophones were located at different depths within the earth embankment, beneath sleeper +2.

Table 3.- Geophones position and designation

Sleeper	Position	Level (m)[(1)]	Velocity at	Designation
+2	Centre to inner rail	2.50	Earth embankment	GEV2_+2CI_TE044
		2.35		GEV2_+2CI_TE137
[(1)] Level reference: sleeper bottom surface.				

c.- Accelerometers

8 accelerometers were installed at various locations within the test section to record the acceleration response of the material in the corresponding installation points:

- 3 accelerometers were located inside the LECA embankment.
- 3 capacitive accelerometers were placed at the interface between the formation layer and the sub-ballast.
- 1 triaxial IEPE accelerometer was placed at the ballast layer.
- 1 ballasted particle equipped with an accelerometer was located at the ballast layer.

Table 4 describes the location details of the accelerometers embedded within the section, while the figure shows the photograph of these sensors located at the mid-thickness of the LECA embankment.

Table 4.- Accelerometer position description and designation

Sleeper	Position	Level (m)[(1)]	Velocity at layer	Designation
0	Outer rail	1.60	LECA	ACV_0E_LE055
0	Centre	1.60	LECA	ACV_0C_LE055
0	Inner rail	1.60	LECA	ACV_0I_LE055
-1	Outer rail	0.73	Form layer-sub-ballast layer	ACV_-1E_CF-SB
0	Centre	0.69	Form layer-	ACV_0C_CF-SB
+1	Inner rail	0.65	sub-ballast layer	ACV_+1I_CF-SB
0	Outer rail to centre	0.00	Ballast layer	ACV_0-EC_BA
0	Inner rail to centre	0.00	Ballast layer	ACV_0-IC_BA
[(1)] Level reference: sleeper bottom surface.				

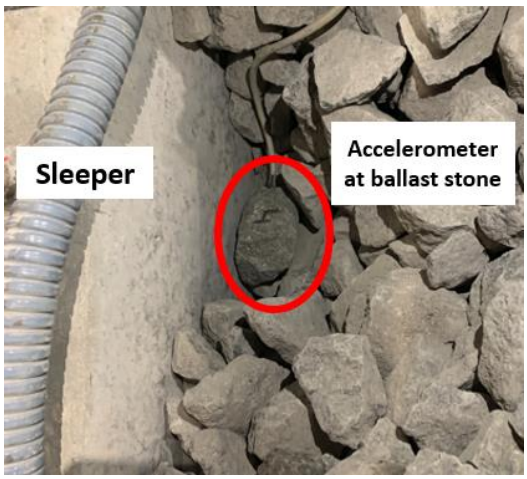

Figure 49.- Example of an accelerometer installed inside the railway track section (left) and instrumented ballast particle (right)

d.- Pressure cells

11 pressure cells were installed at the interfaces between the layers of the railway track section to quantify the stresses transmitted to each level.

- 1 pressure cell was embedded in the embankment, 30 cm below the LECA embankment bottom, where it had already been placed during previous tests.
- 2 pressure cells were located at the interface between the earth embankment and the LECA embankment. They measure the vertical pressure at the base of the LECA embankment.
- 2 pressure cells were located between the LECA embankment and the form layer. They measure the vertical pressure at the bottom of the form layer.
- 2 pressure cells were located at the interface between the form layer and the sub-ballast layer top. They measure the vertical pressure at the bottom of the sub-ballast layer.
- 2 pressure cells were located at the interface between the sub-ballast layer and the ballast layer. They measure the vertical pressure at the bottom of the ballast layer.
- 2 pressure cells were located at the interface between the top of the ballast layer and the bottom of the sleeper. They measure the vertical pressure at the bottom of the sleeper.

Table 5 describes the location details of the pressure cells embedded within the section, while the figure shows a photograph of this type of sensor.

Table 5.- Pressure cells position description and designation

Sleeper	Position	Level (m)[(1)]	Pressure at layer interface	Designation
0	Centre	2.30	Embankment	CP_0C_TE030
	Outer rail	2.05	Embankment - LECA	CP_0E_TE-LE
	Inner rail	2.05	Embankment - LECA	CP_0I_TE-LE
	Outer rail	1.03	LECA – Form layer	CP_0E_LE-CF
	Inner rail	0.95	LECA – Form layer	CP_0I_LE-CF

Sleeper	Position	Level (m)[1]	Pressure at layer interface	Designation
	Outer rail	0.73	Form layer - Sub-ballast	CP_0E_CF-SB
	Inner rail	0.65	Form layer - Sub-ballast	CP_0I_CF-SB
	Outer rail	0.43	Sub-ballast - Ballast	CP_0E_SB-BA
	Inner rail	0.35	Sub-ballast - Ballast	CP_0I_SB-BA
	Outer rail	0.00	Ballast - sleeper	CP_0E_TR-BA
	Inner rail	0.00	Ballast - sleeper	CP_0I_TR-BA
[1] Level reference: sleeper bottom surface.				

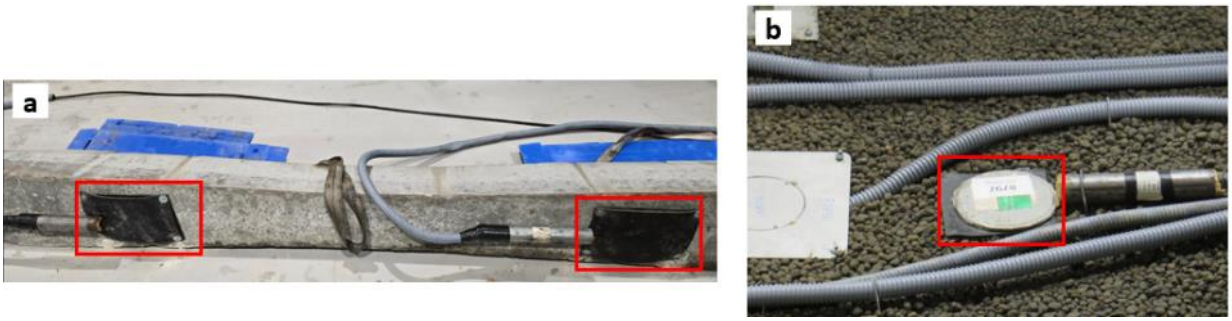

Figure 50.- Example of pressure cells installed in the test section. (a) at under sleeper, (b) at top of LECA embankment

e.- Temperature and humidity sensor

One sensor was installed to simultaneously measure humidity and temperature at the point of installation. In this case, the monitoring location corresponds to the mid-thickness of the LECA embankment, beneath sleeper +1, as shown in Table 6 and Figure 51.

Table 6.- Humidity and temperature sensor position description and designation

Sleeper	Position	Level (m)[1]	Layer	Designation
+1	Centre to outer rail	1.60	LECA	HUM_+1CE_LE055
				TEMP_+1CE_LE055
[1] Level reference: sleeper bottom surface.				

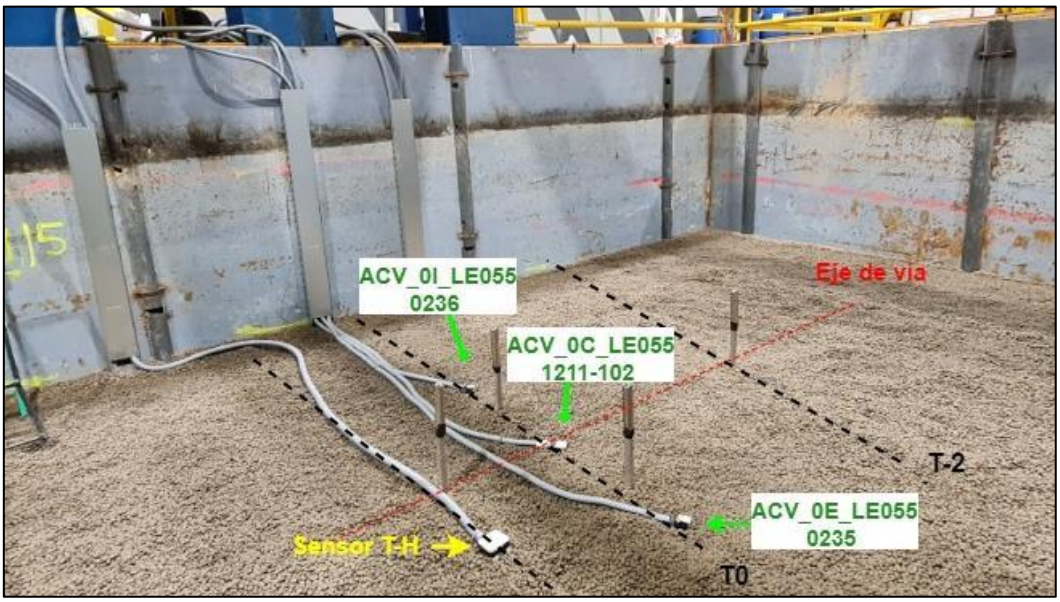

Figure 51.- Accelerometers and humidity-temperature sensor located at mid-thickness of LECA embankment

5.6.3 INSTRUMENTATION INSTALLED ON THE TEST SECTION SURFACE

As with the instruments embedded within the section, the external sensors were predominantly concentrated in the area around the central sleeper. Figure 52 presents a schematic layout showing the location of the surface sensors, together with the type of instruments installed and their precise position.

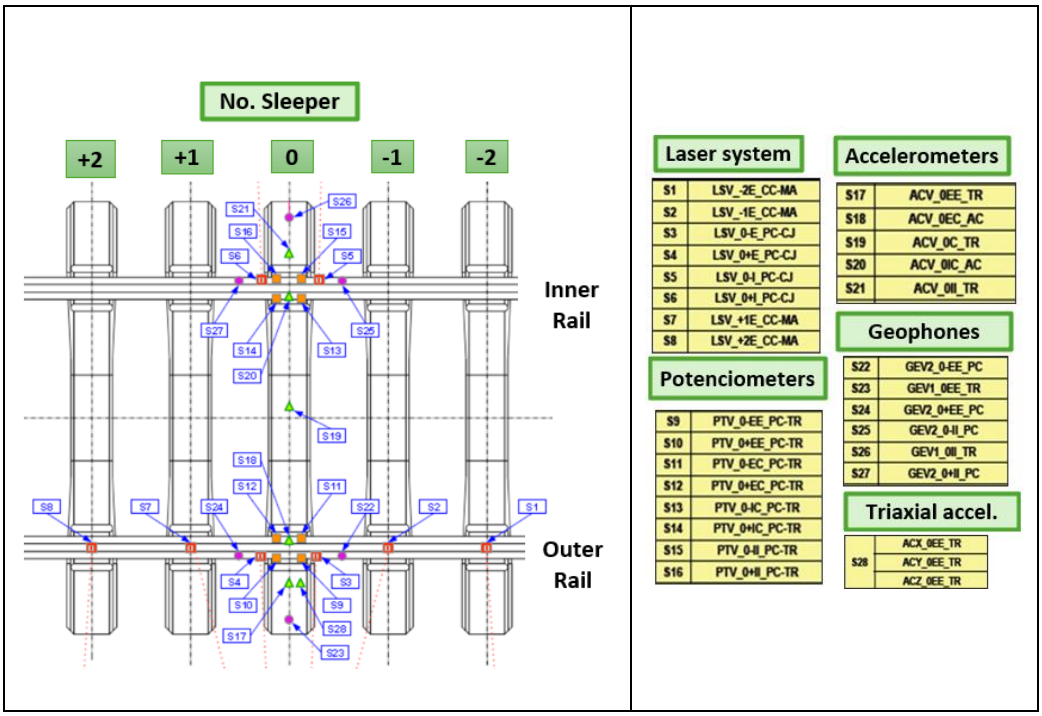

Figure 52.- Schematic diagram with external sensor locations

A total of 28 sensors were installed on the sleepers and rails.

a.- Laser system devices (LSV)

The 8 laser measurement systems are composed of an emitter, positioned outside the railway track section—specifically on the outer frame (MA)—and a series of receivers mounted directly on the rail. The receivers are attached at two critical points of the rail cross-section: the head (C) and the foot (P), thus enabling precise monitoring of the rail's response under loading. The spatial arrangement of these sensors, summarised in Table 7, is specifically designed to capture the vertical displacement of the entire track section.

Table 7.- Laser system position and designation

Sleeper	Position (1)	Designation
-2	Outer rail	LSV_-2E_CC-MA
-1	Outer rail	LSV_-1E_CC-MA
0	Outer rail towards sleeper with negative number	LSV_0-E_PC-MA
0	Outer rail towards sleeper with positive number	LSV_0+E_PC-MA
0	Inner rail towards sleeper with negative number	LSV_0-I_PC-MA
0	Inner rail towards sleeper with positive number	LSV_0+I_PC-MA
+1	Outer rail	LSV_+1E_CC-MA
+2	Outer rail	LSV_+2E_CC-MA

(1) See details of Figure 10 to identify positive and negative numbers of sleepers

(2) Measurement unit: mm

Figure 53 presents a photograph showing several of the laser systems installed on the outer rail. The central sleeper (0) and the positively numbered sleeper are also indicated. In addition, two of the lasers are labelled with their respective numbering to facilitate interpretation.

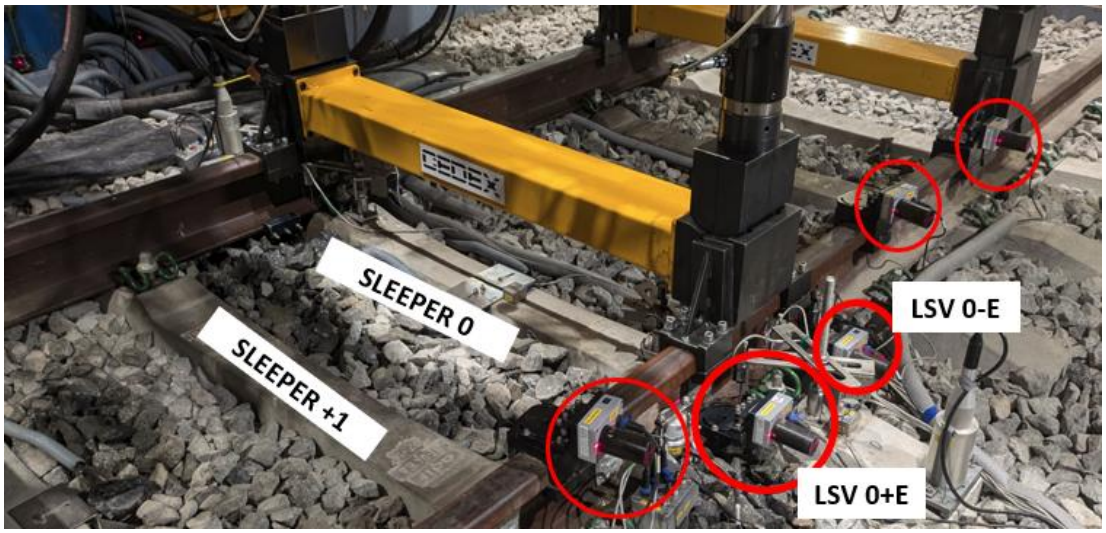

Figure 53.- Laser systems located at outer rail and some designations.

b.- Potentiometers (PTV)

The 8 installed potentiometers were used to record the vertical displacements of the rail pad. Their locations and designations are detailed in Table 8.

Table 8.- Potentiometer description and designation

Sleeper	Position [(1)]	Designation
0	Outer rail towards end of sleeper and towards sleeper with negative no.	PTV_0-EE_PC-TR
	Outer rail towards end of sleeper and towards sleeper with positive no.	PTV_0+EE_PC-TR
	Outer rail towards centre of sleeper and towards sleeper with negative no.	PTV_0-EC_PC-TR
	Outer rail towards centre of sleeper and towards sleeper with positive no.	PTV_0+EC_PC-TR
	Inner rail towards centre of sleeper and towards sleeper with negative no.	PTV_0-IC_PC-TR
	Inner rail towards centre of sleeper and towards sleeper with positive no.	PTV_0+IC_PC-TR
	Inner rail towards end of sleeper and towards sleeper with negative no.	PTV_0-II_PC-TR
	Inner rail towards end of sleeper and towards sleeper with positive no.	PTV_0+II_PC-TR

[(1)] See detail of Figure 10 to identify positive and negative numbers of sleepers
[(2)] Measurement unit: mm

Figure 54 presents a photograph of several potentiometers installed on the outer rail. Generic labels were added to enhance clarity.

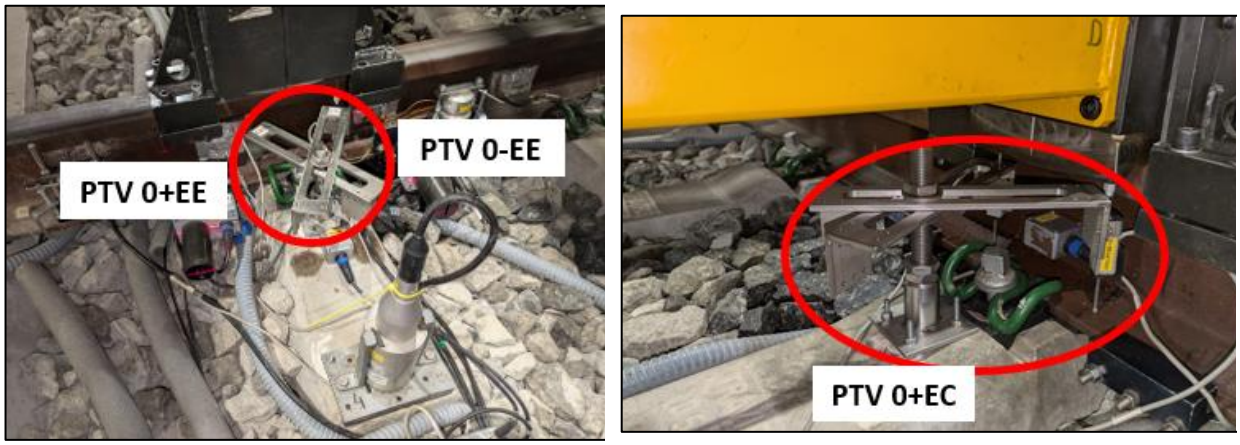

Figure 54.- Examples of potentiometers positioned at outer rail

c.- Geophones (GEV): Total number: 6.

6 geophones were installed at the rail foot (PC) and on the sleeper (TR) to record the velocity induced by train load. Their natural frequencies are 1 Hz and 2 Hz, respectively. Table 9 provides the detailed locations of these geophones, and Figure 55 shows an example of a geophone located at a sleeper.

Table 9.- Geophone description and designation

Sleeper	Frequency (Hz)	Position [1]	Designation
0	2	Outer rail towards end of sleeper and towards sleeper with negative no.	GEV2_0-EE_PC
	1	Outer rail towards end of sleeper	GEV1_0EE_TR
	2	Outer rail towards end of sleeper and towards sleeper with positive no.	GEV2_0+EE_PC
	2	Inner rail towards end of sleeper and towards sleeper with negative no.	GEV2_0-II_PC
	1	Inner rail towards end of sleeper	GEV1_0II_TR
	2	Inner rail towards end of sleeper and towards sleeper with positive no.	GEV2_0+II_PC

[1] See details of Figure 10 to identify positive and negative numbers of sleepers

[2] Measurement unit: cm/s

Figure 55.- Geophone located at sleeper

d.- Accelerometer (ACV)

6 accelerometers were installed at the rail web (AC) and on the sleepers (TR) to record the acceleration induced by the train passages. Table 10 provides the detailed locations of these accelerometers, and Figure 56 shows an example of an accelerometer located at one sleeper.

Table 10.- Accelerometer description and designation

Sleeper	Position (1)	Designation
0	Outer rail towards end of sleeper	ACV_0EE_TR
	Outer rail towards centre of sleeper	ACV_0EC_AC
	Centre of sleeper	ACV_0C_TR
	Inner rail towards centre of sleeper	ACV_0IC_AC
	Inner rail towards end of sleeper	ACV_0II_TR
	Outer rail towards end of sleeper (2)	ACV_0EE_TR

(1) See details of Figure 10 to identify positive and negative numbers of sleepers
(2) Accelerometer that measures in all three directions (X, Y, Z)
(3) Measurement unit: g

Figure 56.-Example of accelerometer located at sleeper

6. TESTING PROGRAM AND RESULTS

6.1 INTRODUCTION

The behaviour of the test section is evaluated using three types of tests:

1) Static Tests: These tests primarily determine the static stiffness of the railway track section.
2) Dynamic Tests: in this testing phase, the section is subjected to the passage of a specific type of train travelling at various speeds, from 15 to 400 km/h.
3) Fatigue Tests: during these tests, the section first endures the passage of one million axles of a designated passenger train at 300 km/h; and secondly, the passage of half a million axles of a designated freight train at 80, 100 and 120 km/h.

As mentioned above, two types of trains were considered: a passenger train, specifically the Siemens S-103, and a freight train corresponding to the Type 7 train in Eurocode 1 (EN 1991-2:2025) (see more details at section 2.2).

Extensive instrumentation installed both within the different layers of the section and on the track surface, as detailed in section 5.6, allows for the recording of various physical parameters, including vertical pressures, displacement, speed, and acceleration. This data, gathered during each of the aforementioned tests, will illustrate the behaviour of the track section.

Additionally, based on the experience from tests conducted at the CTB on typical sections of high-speed lines, comparisons in behaviour will be possible. The following sections provide a detailed description of each of the test groups mentioned above. Table 11 indicates the summary of the tests carried out for the railway track section under study.

Table 11.- Summary of the tests carried out

Date	Test	Test stage
26/04/2024	Static test	After railway track construction
04/07/2025	Static test	After railway stabilisation
07/07/2025 to 07/10/2025	Dynamic test for passenger train	Passing-by of a passenger train at 15/25/50/100/150/200/250/275/300/315/340/350/400 km/h
30/07/2025	Static test	After dynamic test for passenger train
27/10/2025 to 27/11/2025	Fatigue test for passenger train	Passing-by of a passenger train at 300 km/h
28/11/2025	Static test	After fatigue test for passenger train

Date	Test	Test stage
2/12/2025 to 3/12/2025	Dynamic test for freight train	Passing-by of a freight train at 40/80/100/120 km/h
5/12/2025 to 18/12/2025	Fatigue test for freight train	Passing-by of a freight train at 80, 100 and 120 km/h
19/12/2025	Static test	After fatigue test for freight train

6.2 STATIC TESTS

6.2.1 GENERAL ASPECTS

This study analyses five static tests performed at different moments of the testing period to determine the static track stiffness. The track stiffness is used to assess the quality of the track and its potential degradation due to the load transmitted by the train passages. Table 12 shows some features of the static tests performed.

Table 12.- Static tests performed in the present study

Date	Test stage
26/04/2024	After railway track construction
04/07/2025	After railway track stabilisation by the passage of 64,000 axles.
30/07/2025	After dynamic tests for passenger train
28/11/2025	After fatigue tests for passenger train
19/12/2025	After fatigue test for freight train

In the CTB facility, three pairs of servo-hydraulic actuators are installed along the track, with each pair separated by 1.5 meters. For the static tests, only the central pair of actuators, referred to as Actuators B, is utilised, while the other two pairs (Actuators A and C) remain unused. The load from actuators B is applied simultaneously on both rails at the central sleeper, named “Sleeper 0”. This point also serves as a reference for measuring the distances of the laser sensors, used to determine the track stiffness. The arrangement of the actuators is illustrated in Figure 57.

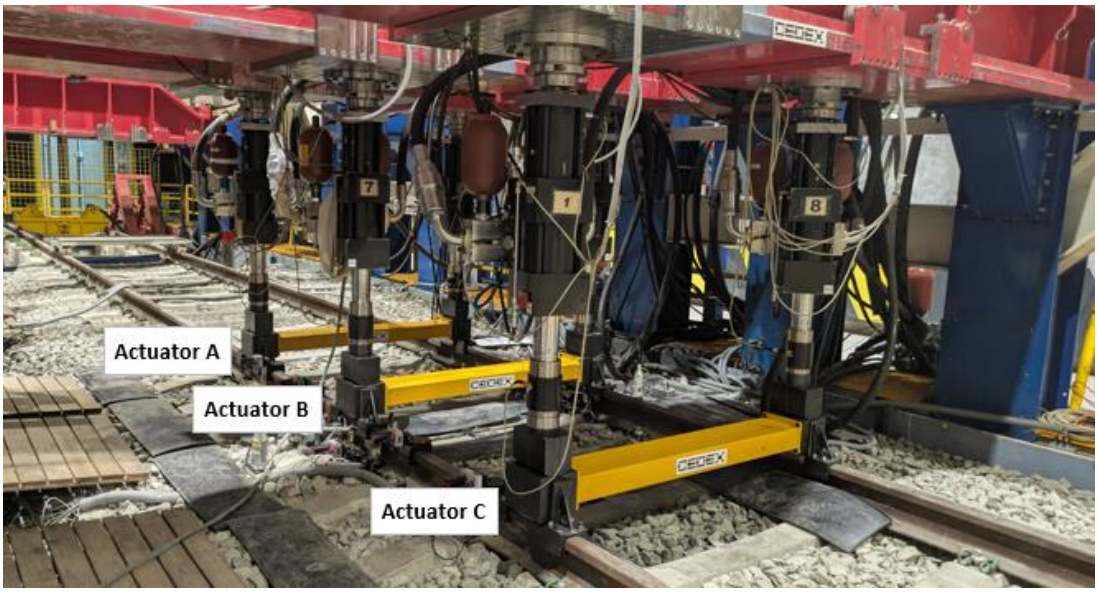

Figure 57.- Hydraulic actuators disposition in CTB

The static tests usually consist of one loading–unloading cycle in which a maximum load of 94 kN is reached, applying the load at a rate of 0.084 kN/s, as can be seen in Figure 58. A minimum load of 2.5 kN was applied to avoid loss of contact between the actuators and the rails. The duration of each static test was 22 minutes.

This test configuration is inspired by the standard used by ADIF to test the rail pads (Especificación Técnica ET 03.360.570.0 "Placas elásticas de asiento para sujeción VM". "Ensayo de rigidez vertical secante 20 / 95 KN". ADIF. 1ª edición, diciembre de 2005).

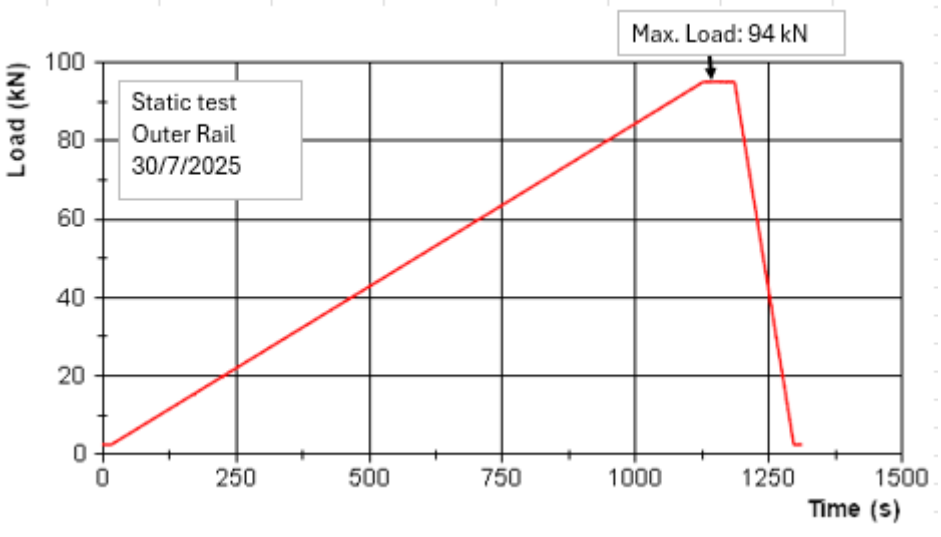

Figure 58.- Time – load history example applied at outer rail in static test

The rail vertical displacements were recorded with six laser systems distributed along the inner rail (as seen in Figure 59) and two situated at both sides of the central sleeper in the outer rail.

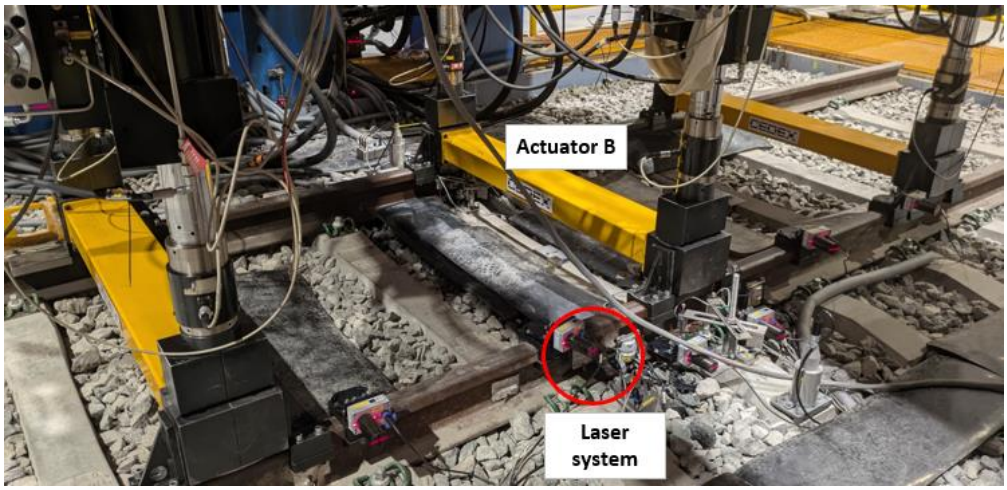

Figure 59.- Detail of laser system located at Actuator B

Figure 60 (left) shows the evolution with time of the rail displacement, measured with all the laser systems installed in both rails, in one of the static tests. These data will be used to analyse the rail displacement as a function of the load applied, as shown in Figure 60 (right). It can be seen that the deflection curves are clearly non-linear so railway stiffness deduced from them should always be referred to the load at which it is being calculated.

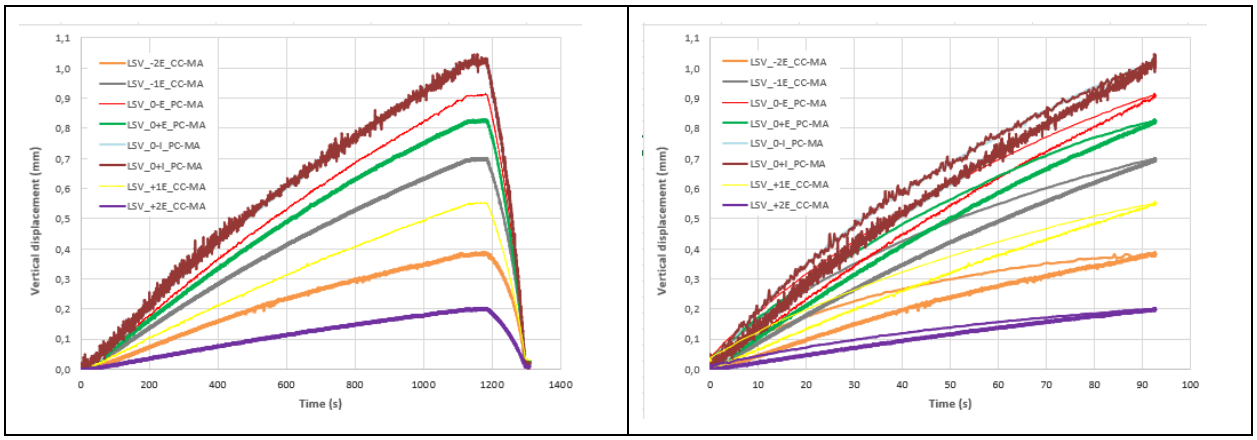

Figure 60.- Vertical displacement logged by laser systems during a static test

From those time-vertical displacement graphs, the rail deflections measured in the eight laser systems for any time can be obtained and plotted as a function of their distance from the load application point. By plotting rail displacement as a function of position, the points can be fitted assuming that the track follows a Winkler-type behaviour, quantified by Equation 1, from which the value of the track stiffness (K) can be determined.

$$\delta(x,t) = \frac{Q}{K}\, e^{-\frac{|x-vt|}{L}} \left[cos\left(\frac{|x-vt|}{L}\right) + sin\left(\frac{|x-vt|}{L}\right)\right] \qquad (1)$$

As can be seen later, the very good agreement between measurements and theory shows

that the rail deflections due to a vertical single load can be predicted with high accuracy, assuming the rail track follows a Winkler-type behaviour.

6.2.2 STATIC TEST AFTER RAILWAY TRACK CONSTRUCTION

Figure 61 shows the displacements recorded by all laser systems during the static test performed after railway track construction (left) and those displacements versus the load applied (right). This test was performed on 26/04/2024.

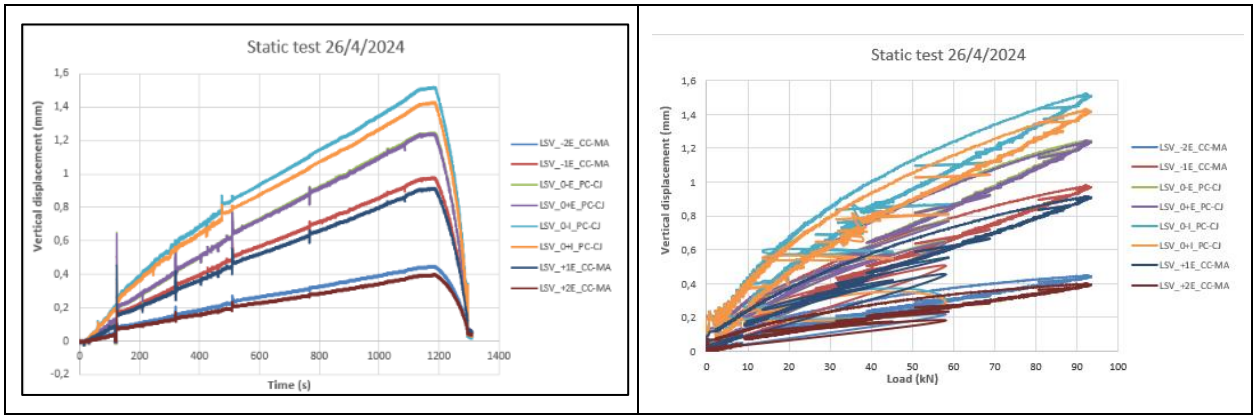

Figure 61.- Vertical displacement versus time (left) and versus load (right) logged during static test performed 26/4/24

The graph above illustrates how the displacements correspond to the load history experienced during the static test.

The highest displacements were observed in the lasers positioned on the central sleeper (Sleeper 0). Specifically, the laser on Sleeper 0 of the outer track recorded a vertical displacement of 1.5 mm, while the one on the inner rail registered a displacement of 1.4 mm. In contrast, the lowest displacements were noted on the instrumented sleepers that are farthest from the point of load application, known as Sleeper +2 and -2, which exhibited maximum displacements of 0.4 mm.

By applying Winkler's theory, we can determine the stiffness of the system. It's important to highlight that stiffness is a parameter that depends on the load applied. In this instance, the stiffness of the system is calculated based on the maximum load applied, which is 94 kN.

Figure 62 presents the experimental data collected during the static test on April 26, 2024, alongside Winkler's theoretical curve. The measurements from the lasers positioned on the outer rail are represented in blue, while those from the lasers on the inner rail are shown in red. The distance from the actuator point refers to the load point applied at Sleeper 0.

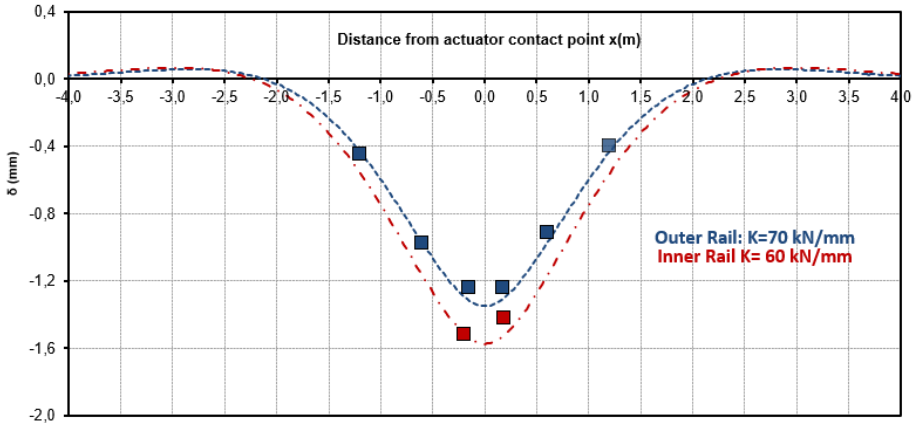

Figure 62: Stiffness values obtained for static test on 26/04/2024

The stiffness values measured for the railway track section constructed with LECA material on the embankment are approximately 65 kN/mm. When we compare these values to those obtained in our facility from testing high-speed line sections that consist entirely of earth embankments, it is evident that the stiffness values for the LECA material are somewhat lower. However, it is important to note that the section needs to be stabilised before testing. We anticipate that after stabilisation, and with the passage of trains, the stiffness will increase.

6.2.3 STATIC TEST AFTER SECTION STABILIZATION

The railway track section was stabilised by running the Siemens S-103 train (see section 2.2 for more details) at 80 km/h. Stabilisation consisted of running 64,000 axles, corresponding to a cumulative load of one million tonnes. The static test was conducted on July 4, 2025.

Figure 63 illustrates the movements recorded by all laser systems during this static test, both over time and in relation to the applied load.

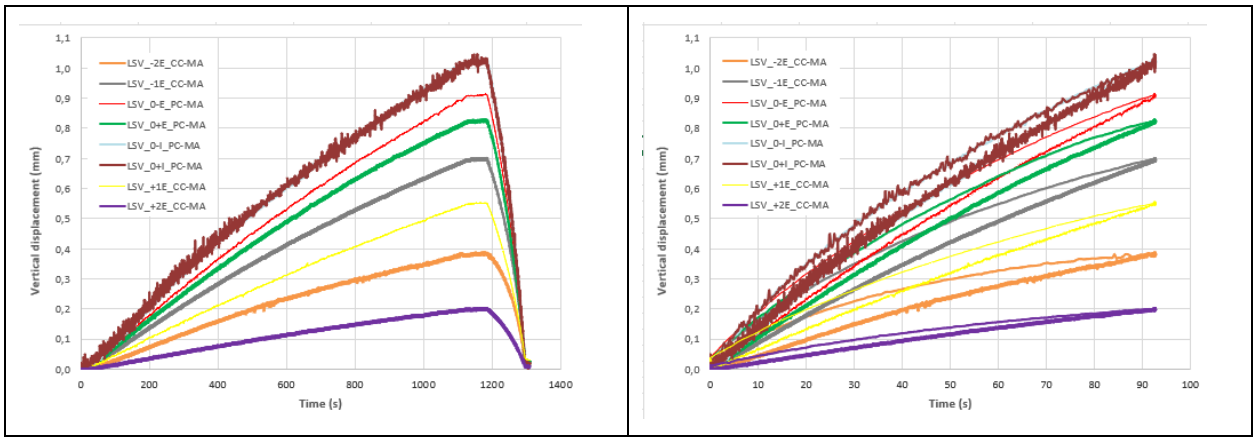

Figure 63.- Laser system displacement logged at static test versus time (left) and versus load (right)

As shown in the figures above, the maximum displacements recorded for Sleeper 0 are approximately 0.8 to 1 mm. In contrast, the minimum displacements are observed in sleepers +2 and -2, with values around 0.4 mm.

Figure 64 presents the stiffness values measured at both the outer and inner rails according to Winkler's theory.

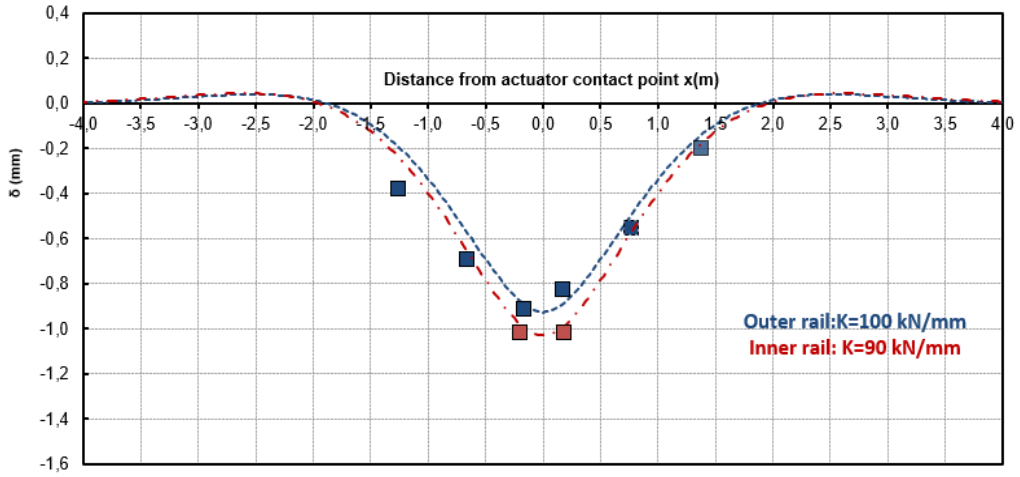

Figure 64.- Stiffness values obtained for static test on 04/07/2025

After stabilising the track, the overall stiffness of the section is measured at 100 kN/mm. This value is significantly higher than the one recorded after the completion of the embankment construction. The measured stiffness of 100 kN/mm is consistent with the magnitudes typically used at the CTB when testing other types of railway track sections.

6.2.4 STATIC TEST AFTER DYNAMIC TESTS FOR PASSENGER TRAIN

To assess the condition of the section under test after the dynamic tests (train S-103 passing at speeds of 5 to 400 km/h), a static test was conducted on July 30, 2025.

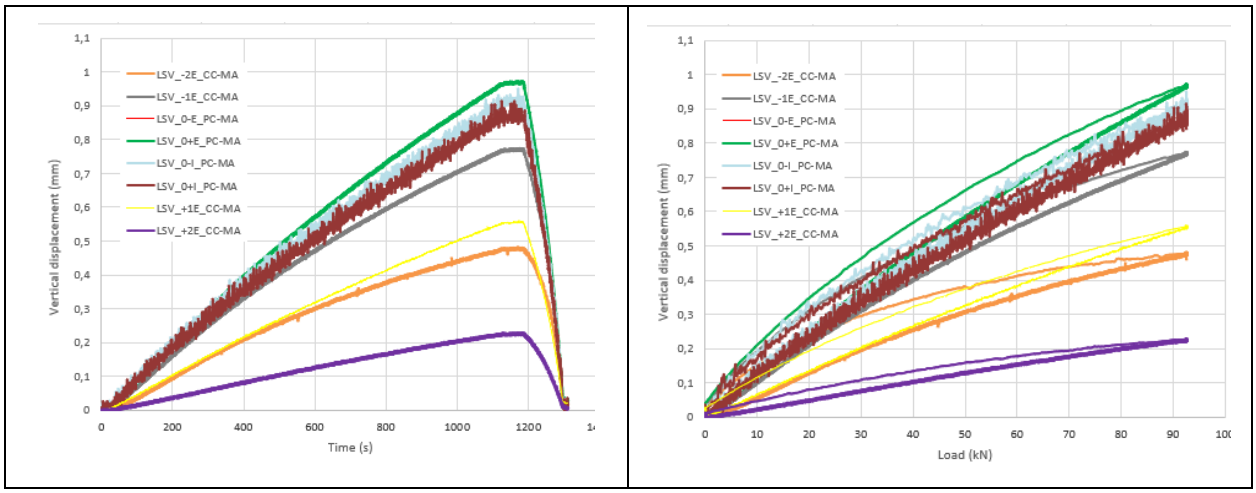

Figure 65.- Laser system displacements versus time (left) and load (right) at static test performed on 30/07/2025

As shown in the figures above, the maximum displacements recorded for Sleeper 0 are approximately 0.8 to 1 mm. In contrast, the minimum displacements are observed in sleepers +2 and -2, with values around 0.4 mm.

Figure 66 presents the stiffness values measured at both the outer and inner rails according to Winkler's theory.

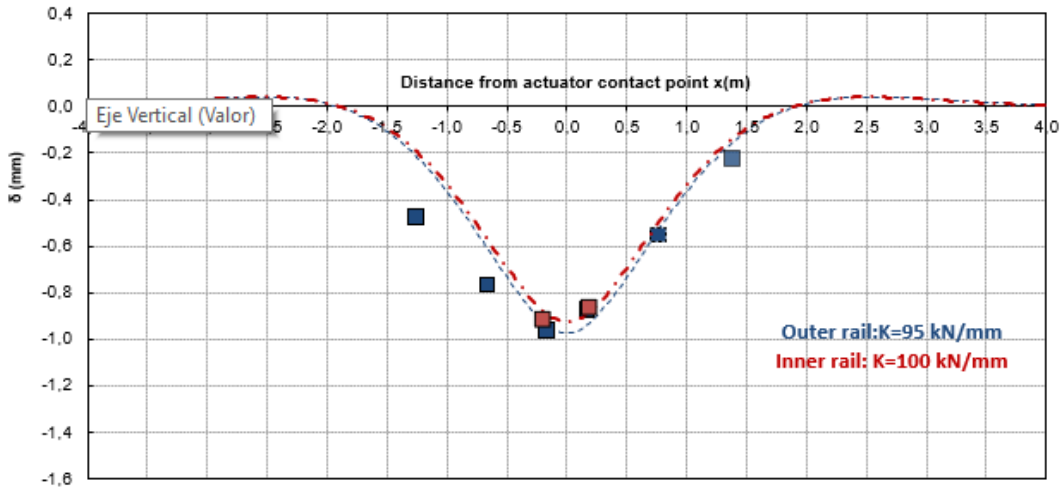

Figure 66.- Stiffness values obtained for static test on 30/07/2025

After conducting the dynamic tests, the overall stiffness of the section was measured at 100 kN/mm, which is the same value as before the tests.

6.2.5 STATIC TEST AFTER FATIGUE TEST FOR PASSENGER TRAIN

To assess the condition of the section under test after the fatigue tests with the passenger train (train S-103 passing at a speed of 300km/h for one million axles), a static test was conducted on November 28, 2025.

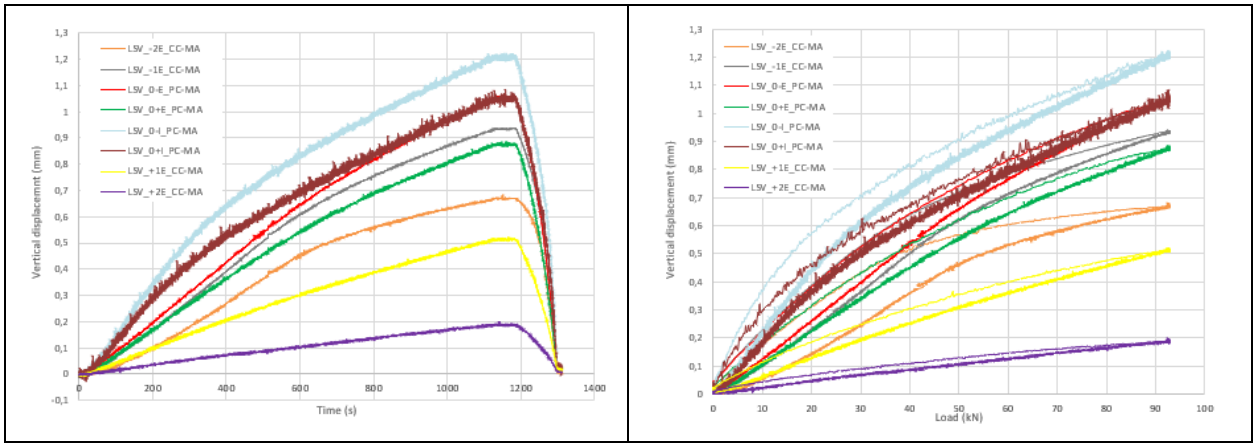

Figure 67.- Laser system displacements versus time (left) and load (right) at static test performed on 28/11/2025

As shown in the figures above, the maximum displacements recorded for Sleeper 0 are approximately 1.1 to 1.2 mm. In contrast, the minimum displacements are observed in sleepers +2 and -2, with values ranging from 0.2 to 0.7 mm.

Figure 68 presents the stiffness values measured at both the outer and inner rails according to Winkler's theory.

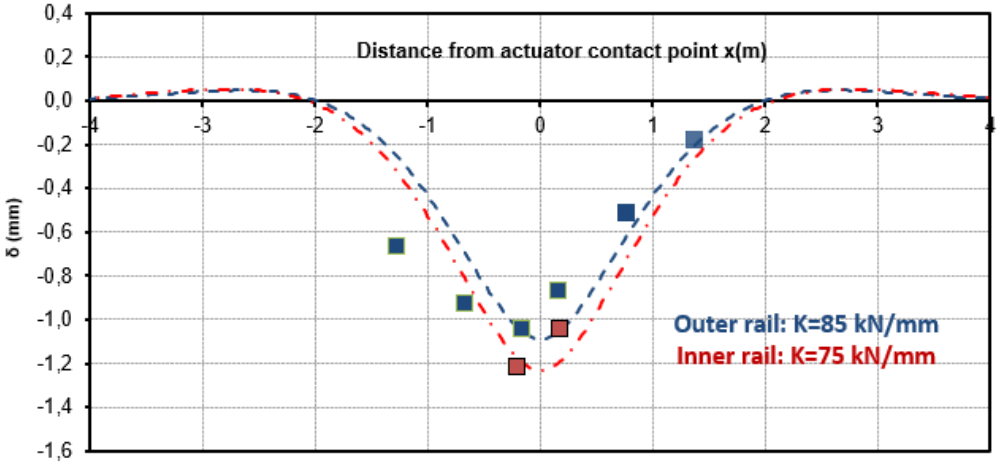

Figure 68.- Stiffness values obtained for static test on 28/11/2025

After conducting the fatigue tests with the passenger train, the overall stiffness of the section was measured at 80 kN/mm, which is lower than previous results.

6.2.6 STATIC TEST AFTER TESTING FREIGHT TRAINS

To assess the condition of the section under test after the dynamic and fatigue tests with the freight train (passing at speeds of 80/100/120 km/h for one million axles), a static test was conducted on December 19, 2025.

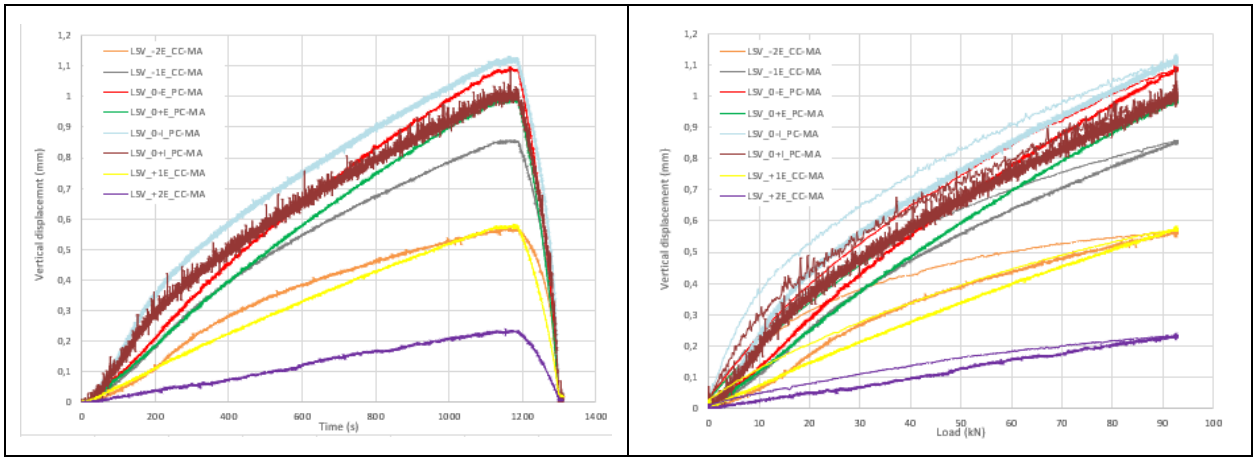

Figure 69.- Laser system displacements versus time (left) and load (right) at static test performed on 19/12/2025

As shown in the figures above, the maximum displacements recorded for Sleeper 0 are approximately 1.1 to 1.0 mm. In contrast, the minimum displacements are observed in sleepers +2 and -2, with values ranging from 0.2 to 0.6 mm.

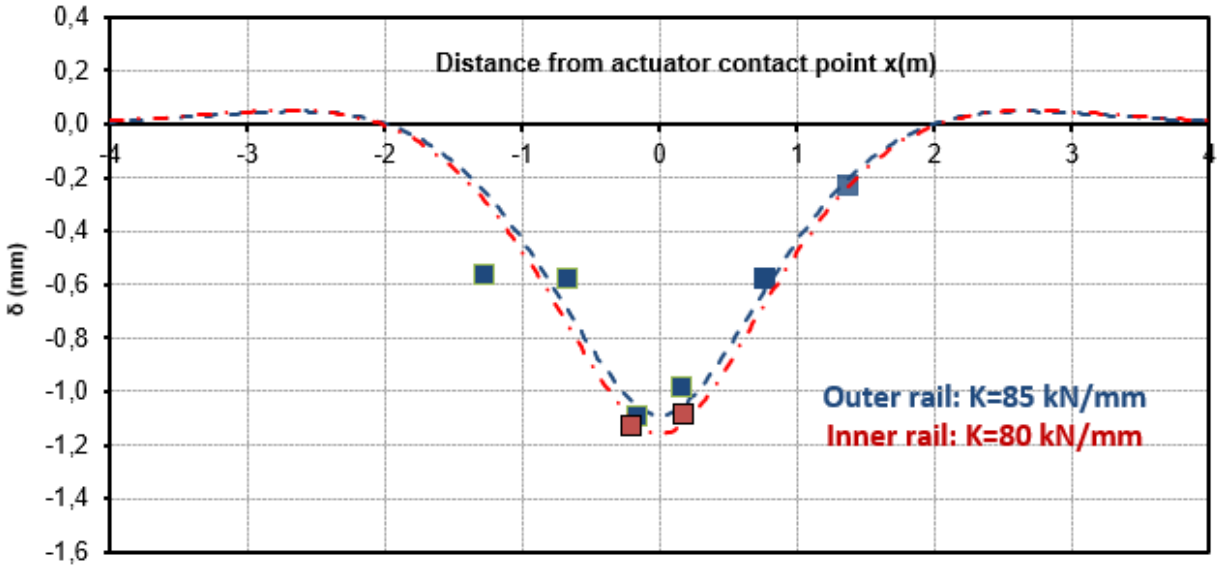

Figure 70.- Stiffness values obtained for static test on 19/12/2025

After conducting the tests with the freight train, the overall stiffness of the section was measured at 80 kN/mm, which is similar to that obtained before these tests.

6.2.7 SUMMARY OF TRACK STIFFNESS VALUES OBTAINED IN THE STATIC TEST

As described in the previous sections, a series of static tests were conducted at the most representative stages of the study in order to characterise the condition of the railway section. These tests were performed at key moments throughout the experimental programme to capture the response of the track structure. Table 13 presents a summary of the results obtained from the static tests, enabling the evolution of the railway section to be analysed as a consequence of train passages during the dynamic characterisation phase and the subsequent fatigue tests.

Table 13.- Summary of static test results

Date	Track stiffness [K (kN/mm)]		Test stage
	Inner rail	Outer rail	
26/04/2024	60	70	After railway track construction
04/07/2025	90	100	After railway track stabilisation by the passage of 64,000 axles.
30/07/2025	100	95	After dynamic tests for passenger train
28/11/2025	75	85	After fatigue tests for passenger train
19/12/2025	80	85	After fatigue test for freight train
Note: K value is obtained for a Q = 94 kN/axle.			

Taking into account CEDEX experience in the determination of track stiffness, based on measurements performed both on in-service railway lines and on the experimental models tested at the CTB, it can be concluded that track stiffness values (K) within the range of 85 to 100 kN/mm may be considered representative of an adequate stiffness of the railway section.

6.2.8 STATIC PRESSURE MEASUREMENTS

The railway track section is equipped with instrumentation that includes pressure cells designed to measure the pressure exerted at the interfaces of various layers. These pressure cells are strategically placed in the layer interfaces of the track section: at the sleeper bottom, in direct contact with the ballast layer; between the ballast and the sub-ballast layers; between the sub-ballast and the subgrade layers; between the subgrade layer and the top of the LECA embankment; and finally, between the base of the LECA embankment and the earth embankment. A diagram, incorporated in Figure 71, shows the arrangement of the pressure cells, all of which are located in the vertical plane corresponding to the central section (Section 0), with one cell positioned beneath the outer rail and another beneath the inner rail.

Measuring pressure at the sleeper–ballast interface is particularly challenging due to the granular nature of the ballast, which results in discrete point contacts rather than a uniform load distribution. This condition may significantly affect the accuracy and reliability of pressure measurements. To enhance measurement reliability, the procedure described by Merino and

Bendahman[2] was adopted. This methodology consists of installing the pressure cell between elastomeric elements and incorporating a steel plate between the ballast and the lower elastomeric element to promote a more uniform stress transfer to the sensor.

Figure 71 displays the pressure values recorded in the pressure cells during the static tests, as function of their location depth. Additionally, the boundaries of each layer that comprises the railway track section are indicated. Ultimately, the theoretical pressure curves, which are expected to be recorded as a function of depth, were also included in the figure.

These theoretical pressure curves come from Fadum theory, considering a vertical stress for z=0 m of 110 kPa ±20%, that corresponds to the pressure on the ballast layer surface transmitted by the sleeper under a static load of a passenger train axle load (about 188 kN) acting on the horizontal sleeper area (0.65 m^2), and taking into account a distribution load factor between sleepers of 0.4, due to Winkler theory.

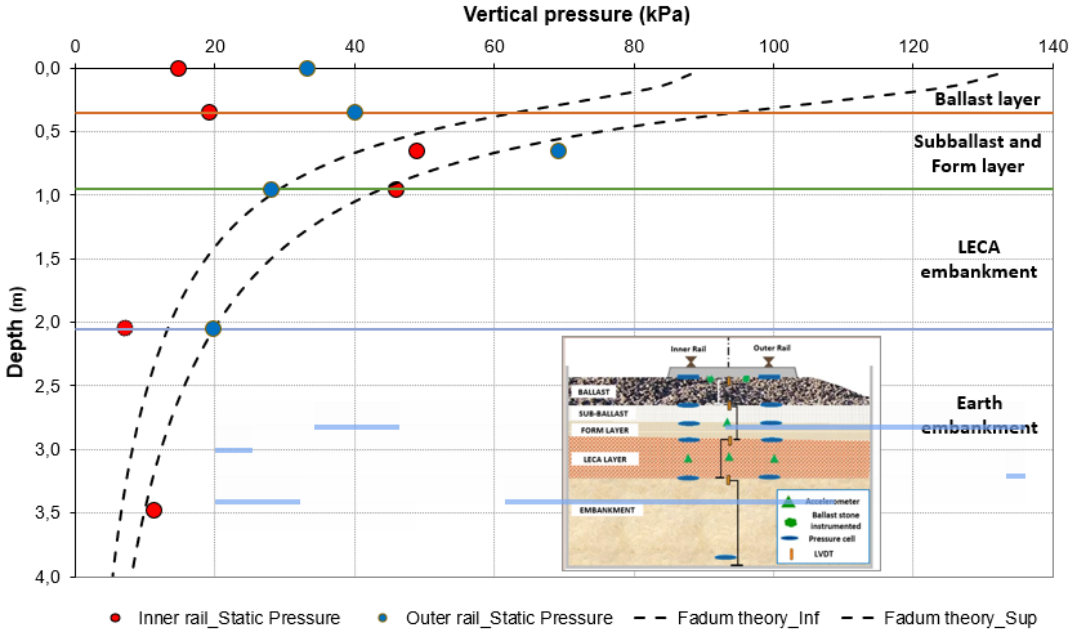

Figure 71.- Pressure measurements recorded by pressure cells during static tests

The results presented in the figure above indicate that the values obtained from the pressure cells are in substantial agreement with the theoretical predictions. The most significant differences are observed in the pressure cells installed between the sleeper and the ballast, in spite of all the efforts made during the arrangement of those pressure cells to avoid this problem, as previously described.

[2] Medidas de presión bajo una sección de traviesa sometida a cargas verticales. S. Merino y K. Bendahman. 2025. Ingeniería Civil 205.

6.3 DYNAMIC CHARACTERISATION TESTS

6.3.1 GENERAL ASPECTS

6.3.1.1 *MODELLED SPEEDS*

25 dynamic tests were conducted to simulate the pass-by of passenger trains at various speeds ranging from 15 to 400 km/h. The specific speeds tested were 15, 25, 50, 100, 150, 200, 250, 275, 300, 315, 325, 340, 350, 375, and 400 km/h. In the case of freight trains, only four passing speeds were considered in the modelling: 40, 80, 100, and 120 km/h.

To increase the amount of available data and facilitate a more comprehensive comparison of the results, certain passenger train speed scenarios were analysed in duplicate. The nomenclature used in the figures is defined below:

- The designation “Pass-1” refers to passenger train cases modelled during the first test campaign that includes 15 velocities (15/ 25/ 50/ 100/ 150/ 200/ 250/ 275/ 300/ 315/ 325/ 340/ 350/ 375/ 400).
- The designation “Pass-2” refers to passenger train cases modelled to replicate selected passing speed scenarios that include 10 velocities (50/ 100/ 150/ 200/ 250/ 275/ 300/ 315/ 340/ 350).
- The designation “Freight” refers to the tests in which freight trains were modelled.
- The last part of the names (_0-E//_0+E//_0-I//_0+I) defines the position of the measuring instrument relative to the sleeper. Further details are provided in section 5.6.1.

  [Example: *Pass-1_0-E*: Passenger train analysed in the initial testing phase. The sensor is positioned at Sleeper 0, with a slight offset towards the sleepers assigned negative numbering, on the outer rail].

Figure 72 displays, as examples, the records of the load applied during the test period for a passenger train passing at 15 km/h (left) and 400 km/h (right), highlighting the difference in the load signal passing time. The train takes approximately 50 seconds to pass-by through the central section at a speed of 15 km/h, and about 2 seconds at a speed of 400 km/h. The passenger train used in all these tests was a Siemens S-103, whose characteristics were detailed in section 2.2.

The behaviour of the railway track section during the passage of freight trains at speeds of 40, 80, 100, and 120 km/h was also studied. Similarly, Figure 73 shows the difference in the recorded load applied when the freight train is travelling at 40 km/h and 120 km/h.

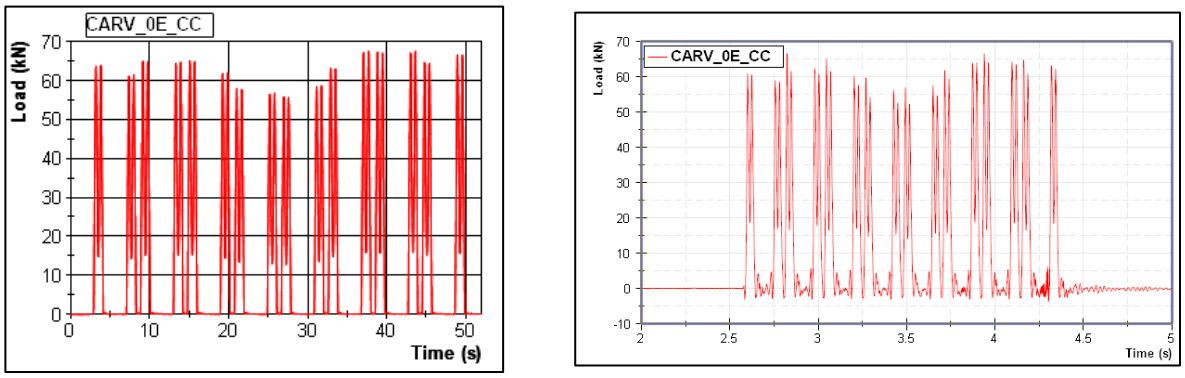

Figure 72.- Time-load history (load/wheel) for passenger train at 15 km/h (left) and 400 km/h (right)

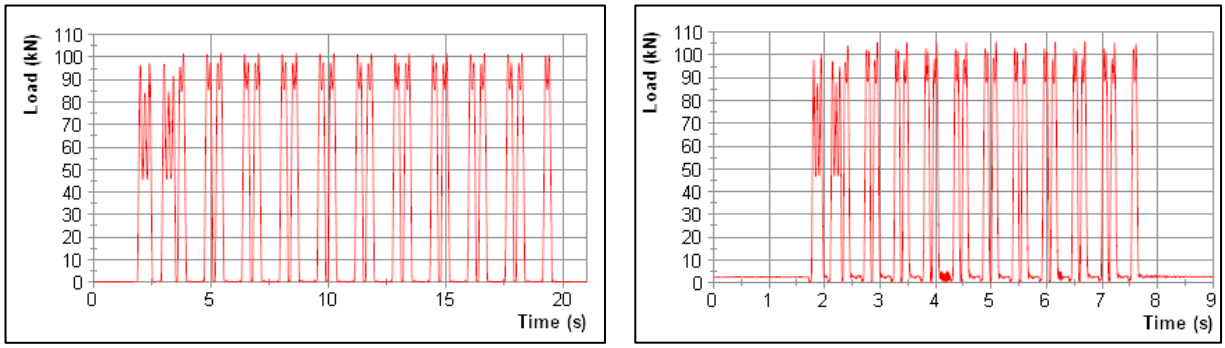

Figure 73.- Time-load history (load/wheel) for freight train at 40 km/h (left) and 120 km/h (right)

6.3.1.2 *INSTRUMENTATION ANALYSED*

In all dynamic tests, the behaviour of the railway track section is analysed by studying the instrumentation installed not only on the track surface but also within the section itself.

As previously mentioned, dynamic testing involves the recording of various physical magnitudes using a diverse array of instruments. Table 14 collects a list of these physical magnitudes along with the corresponding equipment used for their measurement. Additionally, it includes the unit of measurement, the number of devices and the DIAdem[3] channel name example.

Table 14.- Instrumentation used in dynamic tests

Physical magnitude	Unit	Instrumentation	No.	DIAdem channel example
Time	s	Chronometer	1	Time MGCplus_1
Load applied by hydraulic actuators	kN	Pressure cell	6	CARV_0E_CC

[3] DIAdem is a data analysis and reporting software developed by National Instruments, designed for the efficient processing, visualization, and automated reporting of large experimental datasets.

Physical magnitude	Unit	Instrumentation	No.	DIAdem channel example
Total railway track section vertical displacement	mm	Laser system	8	LSV_0+E_PC-MA
Pad vertical displacement	mm	Potentiometer	8	PTV_0+EE_PC-TR
Ballast layer vertical displacement	mm	LVDT	4	LVV_0+C_BA
Sub-ballast and form layers vertical displacement	mm	LVDT	2	LVV_+1CI_CF+SB
LECA embankment vertical displacement	mm	LVDT	4	LVV_0CE_LE
Pressure under sleeper	kPa	Pressure cell	2	CP_0E_TR-BA
Pressure in the interface ballast - sub-ballast layer	kPa	Pressure cell	2	CP_0E_SB-BA
Pressure in the interface sub-ballast - form layer	kPa	Pressure cell	2	CP_0E_CF-SB
Pressure in the interface form layer - LECA embankment	kPa	Pressure cell	2	CP_0E_LE-CF
Pressure in the interface LECA embankment - earth embankment	kPa	Pressure cell	2	CP_0E_TE-LE
Sleeper acceleration	g	Accelerometer	3	ACV_0C_TR
Sleeper velocity	cm/s	Geophone	2	GEV1_0EE_TR

Note that the analysis will primarily focus on the values obtained from the instrumentation located nearest to the central sleeper (0), where the test boundary conditions fairly represent the real track conditions. However, the other sensors were also monitored and helped to validate the results presented.

The upcoming sections present the results for each of the recorded physical magnitudes for dynamic tests with both passenger and freight trains.

6.3.1.3 *RESULT ANALYSIS BY DYNAMIC AMPLIFICATION FACTOR CURVES*

Dynamic amplification factor (*DAF*) curves are dimensionless relationships that describe how the vertical response of a track-ground system increases with train speed, as seen in the example shown in Figure 74.

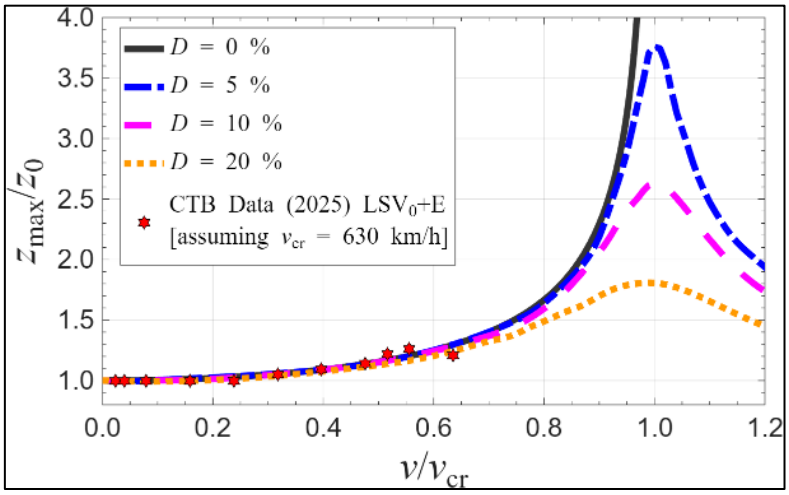

Figure 74.- DAF curves - Maximum track vertical displacement (normalised to the static vertical displacement of the track) vs. dimensionless train speed for different damping ratios

A *DAF* curve provides the ratio between the maximum vertical rail deflection (z_{max}) – for a particular train speed – and the corresponding static rail deflection (z_0), plotted versus the train speed (v) normalised to the critical speed of the railway track section (v_{cr}). Each *DAF* curve corresponds to a different damping ratio (D).

According to the literature (Heelis et al., 1999[4]; Estaire et al., 2018[5]), the damping ratio is below 20% and commonly close to 10%. Recent studies by the Laboratorio de Geotecnia-CEDEX indicate that the critical speed of Spanish high-speed lines (HSL) built on good-quality ground is around 600 km/h. Since the current maximum commercial speed for HSL is 300 km/h, operation remains in the $v/v_{cr} < 0.5$ range, where the *DAF* curves for $D \leq 20\%$ are practically equal. Therefore, for analytical purposes, it is appropriate to use the zero-damping curve, which admits an explicit expression (Equation 1):

$$DAF_{D=0\%} = \frac{z_{max}}{z_0} = \frac{1}{\sqrt{1-(v/v_{cr})^2}} \qquad \textit{Equation 1}$$

DAF curves can be used in two complementary ways: (i) to predict speed-dependent dynamic rail deflections, and (ii) to infer the critical speed and damping ratio of railway track sections. Practical guidance on how to apply the DAF curves for both purposes is provided in Estaire et al.

[4] Heelis, M. E., Collop, A. C., Dawson, A. R., Chapman, D. N. & Krylov, V. V. 1999. Transient effects of high speed trains crossing soft soil. In *Proceedings of the 12th European Conference on Soil Mechanics and Geotechnical Engineering*. Barends et al. (eds): Vol. 3, 1809-1814

[5] Estaire, J., Crespo-Chacón, I., Santana, M. 2018. A procedure to determine the critical speed of railway tracks based on the Winkler´s hypothesis and static FEM simulations. *Minisymposium on Computational modelling of beams on foundations with application to rail tracks. 6th European Conference on Computational Mechanics (ECCM 6)* Glasgow (UK), 11-15 June 2018: 1045-1056

(2025)[6], who also demonstrate the validity of the *DAF* curves using in-situ measurements over a wide range of train speeds.

6.3.2 VERTICAL DISPLACEMENTS OF THE ENTIRE RAILWAY TRACK SECTION

The laser system installed on the rail, as shown in Figure 75, records the rail deflection that must be interpreted as the total movement of the entire railway track section as trains pass by. For example, Figure 76 illustrates the vertical displacement recorded by the laser system located at the outer rail on Sleeper 0 during the simulation of a passing passenger train at 300 km/h (left) and of a freight train at 100 km/h (right). In this case, negative values indicate downward movements.

Figure 75.- Detail of the laser system used to measure the vertical displacements of the railway track section

[6] Estaire, J., Crespo-Chacón, I., Tijera, A. 2025. Validating theoretical dynamic amplification factors using in-situ measurements for a wide range of train speeds. *Proceedings of the Institution of Mechanical Engineers, Part F: Journal of Rail and Rapid Transit*. Vol. 240, Issue 1. https://doi.org/10.1177/09544097251368973

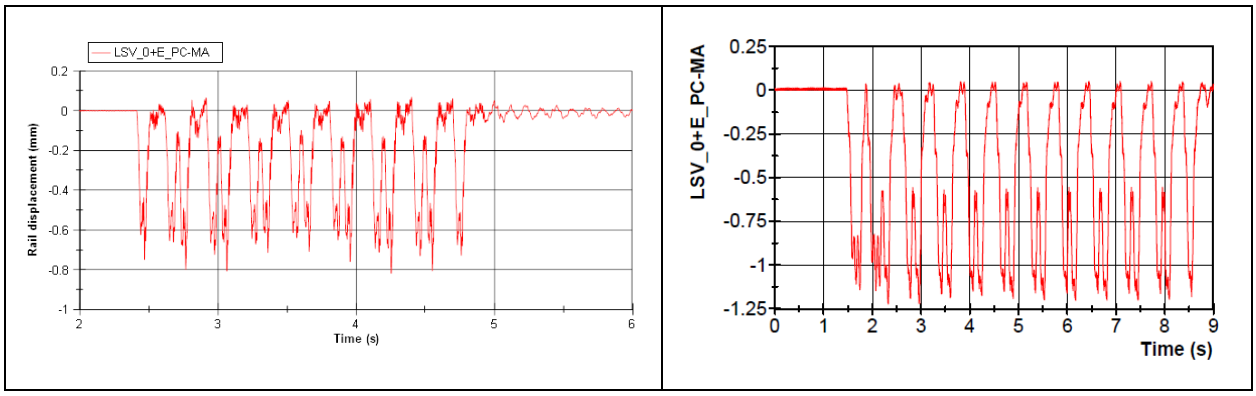

Figure 76.- Vertical displacement recorded by laser system for a passenger train at a speed of 300 km/h (left) and for a freight train at a speed of 100 km/h

As shown in Figure 76, the laser system clearly reflects the load signal applied during the dynamic tests corresponding to the axles of the modelled train.

For each train speed and each train type (passenger and freight), the values of rail deflection were plotted against train speed, resulting in the graph shown in Figure 77 for the movements recorded at both sides (+ and -) of Sleeper 0 on the outer (E) and inner (I) rails.

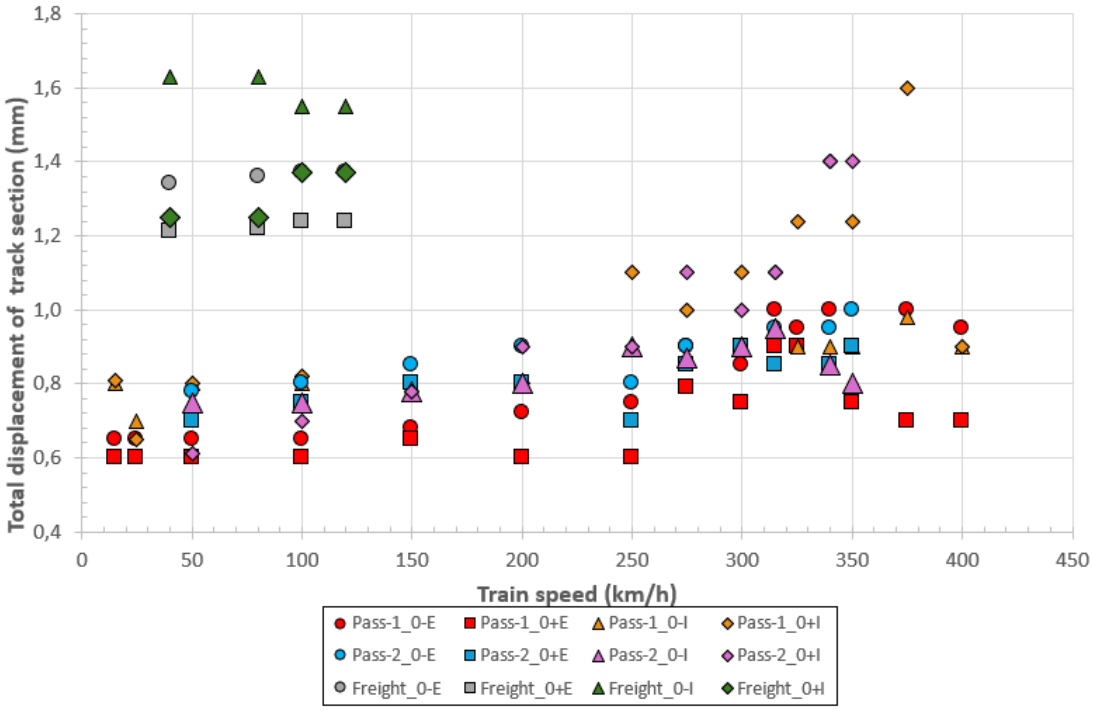

Figure 77.- Total displacement of the track section at different passing-by train speeds

Table 15 summarises the range of results obtained for each testing campaign involving passenger and freight trains.

Table 15.- Ranges of total displacements of the railway track section

Type of train	Vertical displacement (mm)	
	Outer rail	Inner rail
Passenger (Pass 1)	0.65-1.00	0.65-0.98[1]
Passenger (Pass 2)	0.70-1.00	0.60-0.95[2]
Freight	1.21-1.37	1.25-1.36[3]

[1] 1.60 including anomalous values; [2] 1.25 including anomalous values;
[3] 1.63 including anomalous values

Several observations can be drawn from the above figure and table:

- The vertical deflection of the total section increases with increasing train speed.
- Higher vertical displacements are observed in the freight train simulations, as expected due to the higher load (225 *vs*. 155 kN/axle).
- The second round of passenger train tests (Pass-2) shows slightly higher settlement values than the first round, probably due to the degradation of the mechanical behaviour of the ballast layer.
- Settlement values are comparable for both rails.
- For speeds exceeding 250 km/h, the deflection values measured by the 0+I laser were deemed unreliable and therefore classified as anomalous. These records were considered non-representative for interpretation purposes because they deviated from the general trend of the remaining measurements and were associated with isolated sensor-specific behaviour. Their exclusion does not alter the global trends discussed in the report, which remain consistent when considering the complete dataset.

6.3.3 CRITICAL SPEED OF THE RAILWAY TRACK SECTION

This section presents the calculation of the critical speed of the railway track section, based on the vertical displacement values obtained for the entire section (6.3.2) and in accordance with the criteria established in Chapter 6.3.1.3.

It is shown in this report that the vertical rail displacements measured in the CEDEX track box clearly exhibit the expected dynamic amplification associated with increasing train speed in

railway lines. To obtain the critical speed (v_{cr}) of the section, the procedure reported by Estaire et al. (2025)[7], which takes advantage of the DAF curves, is used.

Data used to obtain the critical speed of the railway section

Vertical rail displacements were measured for a wide range of simulated train speeds, from 15 to 400 km/h. Measurements were obtained on both the inner and outer rails using laser sensors placed on both sides of each rail. These sensors were designated as LSV0-E, LSV0+E, LSV0-I and LSV0+I.

Pre-processing of the experimental data prior to fitting the DAF curves

Two preliminary processing steps were applied to the raw measurements to ensure consistency prior to fitting the *DAF* curves:

1. Averaging between rails.

   For the present purpose, the track structure and subgrade conditions are assumed to be identical beneath both rails of the section. For this reason, the vertical displacements obtained under the inner and outer rails were averaged for each test run. This provides a single representative vertical displacement for the section at each train speed (v).

2. Averaging repeated tests at identical speeds.

   Several speeds were tested more than once. To prevent these speeds from having disproportionate weight in the fitting procedure, the results from repeated tests were averaged to obtain a single displacement value for each unique speed.

After applying these two steps, one vertical rail displacement value (z_{max}) was available for each of the distinct simulated train speeds in the campaign.

Normalisation of the vertical displacements to the static value

The comparison between the measurements and the theoretical *DAF* curves requires normalising the measured vertical rail displacements to the static value. The vertical rail displacement recorded at the lowest test speed (15 km/h) was taken as a proxy for the static value (z_0). Examination of the experimental trend confirms that the displacement vs. speed curve approaches this value asymptotically as the speed decreases, thus validating the approximation.

Estimation of the critical speed

To determine the critical speed, two independent least-squares fittings (Fit A and Fit B) were performed between the normalised measurements and the theoretical zero-damping *DAF* curve:

- Fit A (full average dataset).

[7] Estaire, J., Crespo-Chacón, I., Tijera, A. 2025. Validating theoretical dynamic amplification factors using in-situ measurements for a wide range of train speeds. *Proceedings of the Institution of Mechanical Engineers, Part F: Journal of Rail and Rapid Transit*. Vol. 240, Issue 1. https://doi.org/10.1177/09544097251368973

To perform Fit A, all available speed–displacement pairs were included. This fit yielded a critical speed of 550 km/h (see Figure 78).

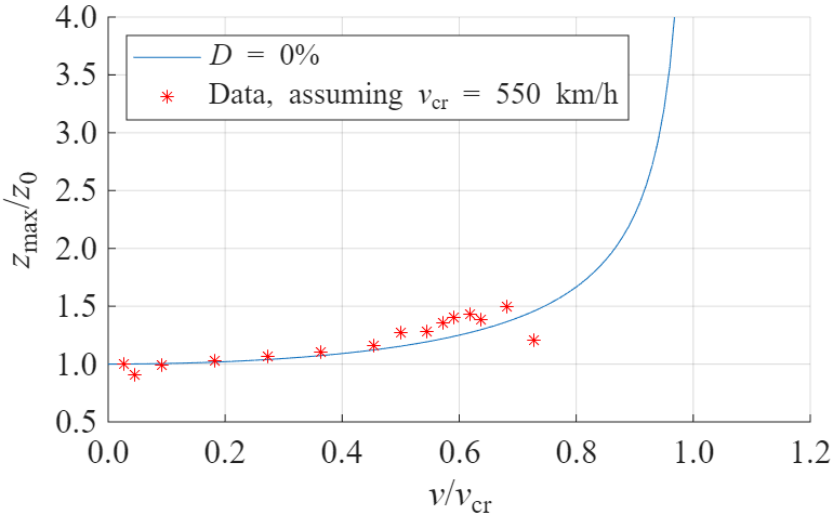

Figure 78.- Fit A.

- Fit B (excluding the 400 km/h point).

  To perform Fit B, the measurement corresponding to 400 km/h was removed on the basis that it deviates from the overall trend described by the remaining data. This may be associated with local variability in the measurement process or the inherent scatter typical of very high-speed tests. The resulting fit provided a critical speed of 490 km/h (see Figure 79). In this case, the fitting can be considered extremely good.

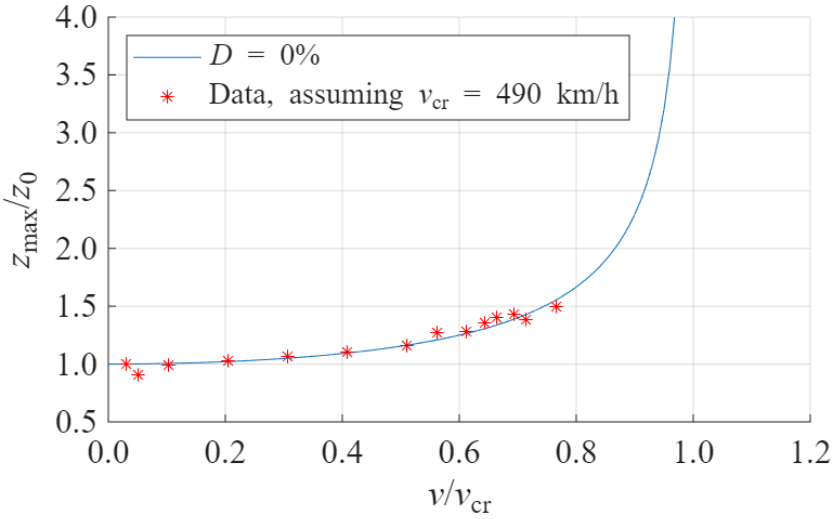

Figure 79.- Fit B.

The values of the critical speed obtained from Fit A and Fit B are taken, respectively, as the maximum and minimum limits for this parameter.

Therefore, the final estimate of the critical speed of this railway section was taken as the midpoint of the range defined by these two fits, that is:

$$v_{cr} = 520 \pm 30 \text{ km/h.}$$

Assessment of the representativeness of the estimated critical speed

To assess how representative the critical speed of 520 km/h is of all the original measurements, an additional fitting (Fit C) was performed using the complete set of displacement records from the four laser sensors (LSV0-E, LSV0+E, LSV0-I and LSV0+I). For this purpose, each sensor's own displacement at 15 km/h was taken as its corresponding static value, and the same fitting procedure previously applied to the averaged data was followed. When the normalised displacements from all sensors were adjusted to the zero-damping DAF curve, the resulting critical speed was 519 km/h (see Figure 80). This value is practically identical to the previously estimated 520 km/h, confirming that the adopted critical speed is fully representative of the entire dataset.

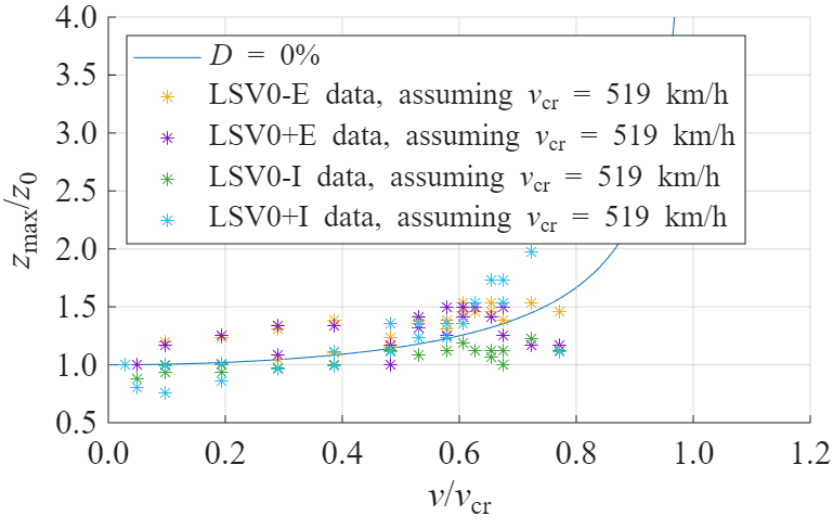

Figure 80.- Fit C.

In addition, a comparison plot using v_{cr} = 520 km/h is given in Figure 81, showing that the measurements fall closely on the theoretical zero-damping *DAF* curve assuming this critical speed, confirming the internal consistency of the estimation procedure. It is worth noting that this critical speed is slightly higher than the value reported by Fortin (1983)[8] for a real high-speed track in France (500 km/h).

[8] Fortin, J. P. 1983. Dynamic track deformation. French Railway Review, Vol. 1,1: 3-12

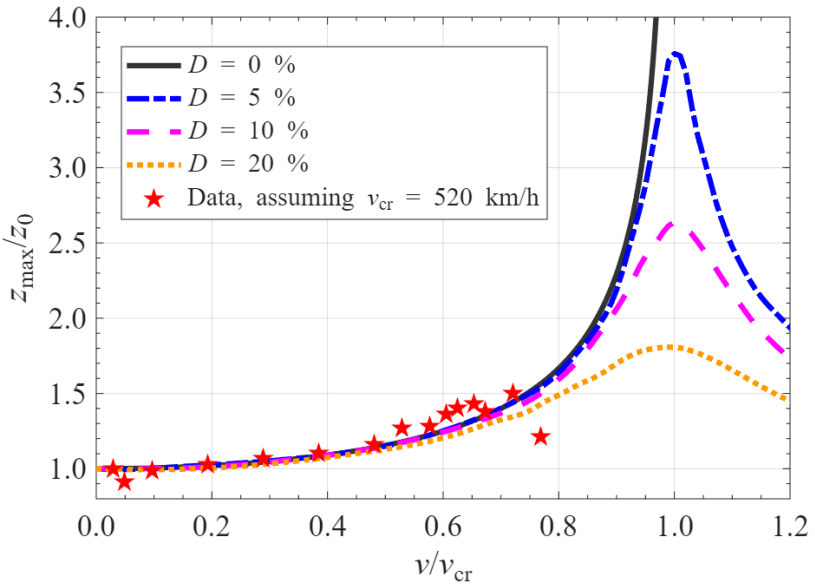

Figure 81.- Normalised deflection vs. dimensionless train speed for the processed CTB data, assuming a representative critical speed of 520 km/h, together with the DAF curves for different damping ratios.

Based on these premises, the trend of the recorded displacements can be represented as a function of the amplification related to the critical velocity. Thus, Figure 82 shows the total displacement of the track section and the bands that define the upper and lower limits of the displacements, calculated using Equation (1) -in 6.3.1.3-, considering the upper bound of the critical speed of the railway track section (V_{cr}=550km/h), as determined in 6.3.2, and a value of z_0 assumed for V_{train}=0.

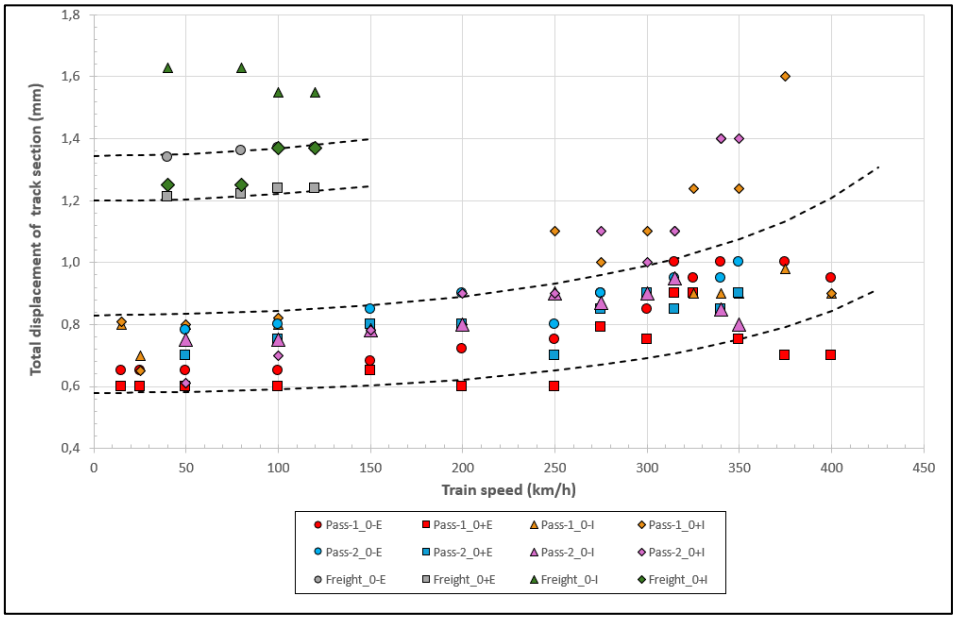

Figure 82.- Total displacement of the track section at different passing-by train speeds with bands related to critical speed

6.3.4 DYNAMIC TRACK STIFFNESS

Similar to the approach used for static tests, it is possible to calculate track stiffness for dynamic tests, which is referred to as dynamic stiffness. This calculation is based on the relationship between the actual load applied by the hydraulic actuators at each modelled speed and the corresponding rail deflection (measured as mean values of deflections recorded by the two laser systems at the outer rail).

Figure 83 illustrates the value of the ratio between the average actual load applied and the rail deflection (referred to as *railway vertical stiffness*) against the train speed values for which the calculation was performed. Also, the bands that define the upper and lower limits of the dynamic stiffness, calculated using Equation (1) -in 6.3.1.3-, considering the upper bound of the critical speed of the railway track section (V_{cr}=550km/h), as determined in 6.3.2, and a value of z_0 assumed for V_{train}=0. The initial values of these curves (90 and 105 kN/mm²) correspond to the static stiffness obtained from the tests.

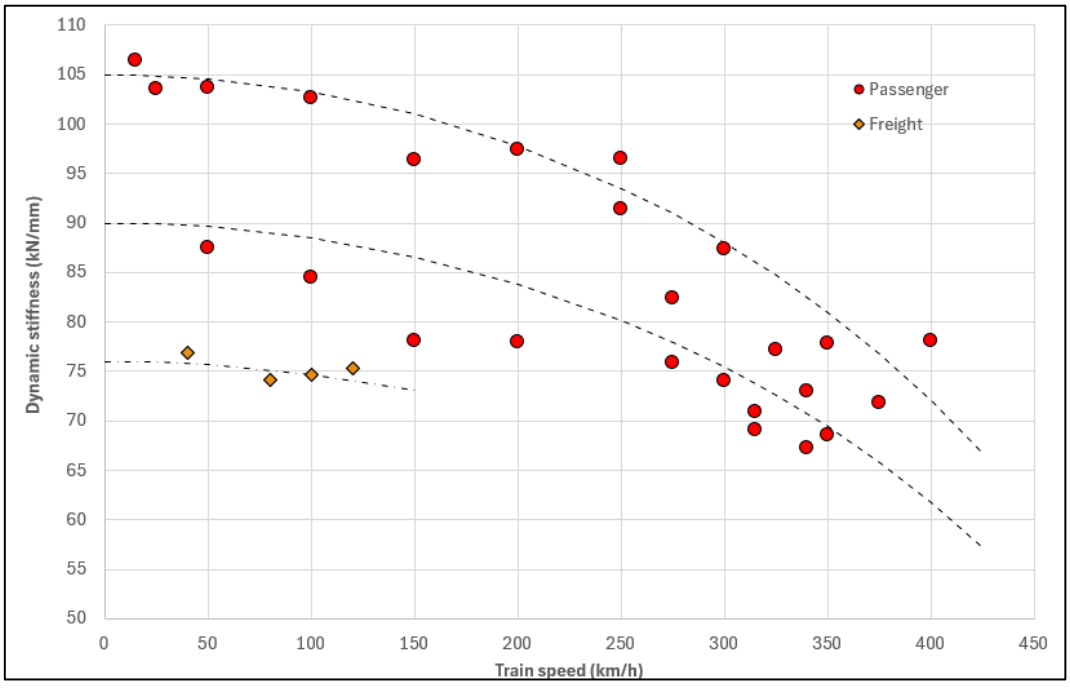

Figure 83.- Dynamic stiffness calculated in the dynamic test and bands related to critical speed

The figure above illustrates that the dynamic stiffness values ranged from 67 to 107 kN/mm for passenger trains and 74 to 77 kN/mm for freight trains. It shows that this stiffness decreases as the speed of the train increases. Additionally, the figure presents the range of values that encompass the results, taking into account the critical velocity.

6.3.5 VERTICAL DISPLACEMENTS OF THE UNDER-RAIL PAD

Potentiometers were installed to record the vertical displacements occurring on the under-rail pad, as shown in Figure 84. Figure 85 illustrates the displacements recorded by the potentiometer located on the central sleeper (Sleeper 0) of the outer rail in the test of a passenger train modelled at a speed of 300 km/h. For these sensors, positive values indicate downward vertical displacements.

Figure 84.- Detail of the potentiometers used to measure the vertical displacements of the under-rail pad

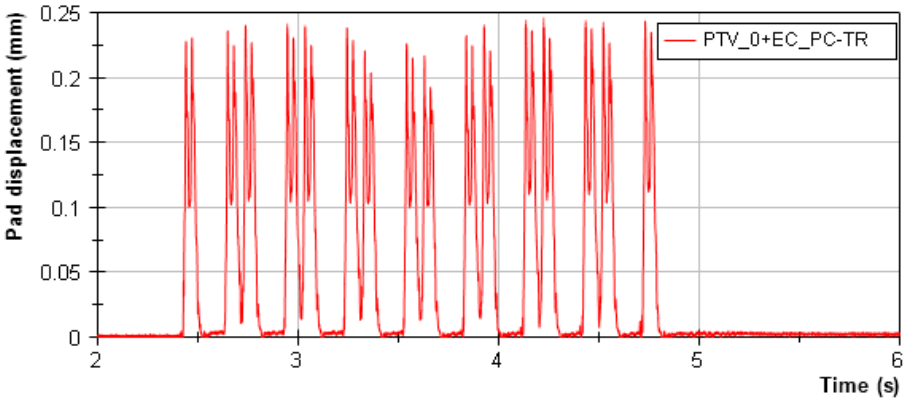

Figure 85.- Data recorded by the potentiometer measuring the vertical displacement of the under-rail pad

As shown in Figure 85, the potentiometer measurements clearly reflect the load signal applied during the dynamic tests depicted in Figure 72 (left).

The displacements recorded in the under-rail pad can be interpreted as the variation in the pad thickness during dynamic tests. Figure 86 illustrates this variation as a function of the train speed, for both passenger and freight trains. The graph presents two sets of data points: one for the inner rail and the other for the outer rail. Each point represents the average value recorded at a given train speed, calculated from the four potentiometers installed in each of the pads. The bands that define the upper and lower limits of the displacements, added to the figure, were calculated using Equation (1) -in 6.3.1.3-, considering the upper bound of the critical speed of the railway track section (V_{cr}=*550km/h*), as determined in 6.3.2, and a value of z_0 assumed for V_{train}=0.

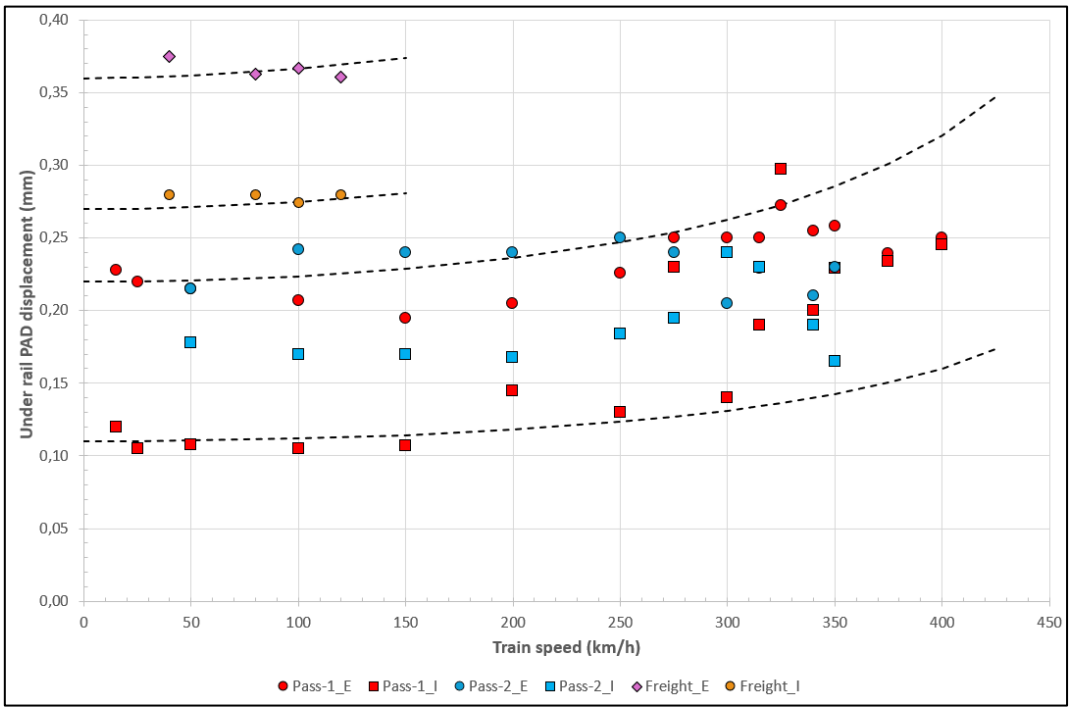

Figure 86.- Under-rail pad displacement at different passing-by train speeds

Table 16 summarises the range of results obtained for each testing campaign involving passenger and freight trains. In addition, it provides the vertical deformation of the under-rail pad.

Table 16.- Rail pad movement range and deformation

Type of train	Vertical movement (mm)		Deformation (%)[1]	
	Outer rail	Inner rail	Outer rail	Inner rail
Passenger (Pass 1)	0.20 - 0.27	0.10 - 0.30	2.8 - 3.9	1.5 - 4.3
Passenger (Pass 2)	0.20 - 0.25	0.16 - 0.24	2.9 - 3.1	2.4 - 3.4
Freight	0.36 - 0.37	0.27 - 0.28	5.2 - 5.4	3.9 - 4.0

[1] Pad thickness: 7 mm

Several observations can be drawn from the above figure and table:

- The vertical displacements of the under-rail pad increase with increasing train speed.
- Freight trains systematically reach higher displacement levels than passenger trains, with values ranging between 0.27 mm for the inner rail and 0.37 mm for the outer rail, due to the higher loads applied.

- In the case of freight trains, axle load is the dominant factor, leading to increased pad deformation even at moderate speeds. For the speed range considered, velocity plays a secondary role relative to the axle load.
- In passenger trains, movement levels are smaller, and the structural response shows a clearer dependence on speed, with movement magnitudes increasing with velocity. The movement range is approximately 0.10 – 0.28 mm, with significantly higher values observed at speeds exceeding 300 km/h.
- In the case of passenger trains, inner rail deflections ranged from 0.17 – 0.27 mm, while outer rail values lie between 0.12 and 0.22 mm.
- When comparing the two passenger train testing campaigns, it is observed that the second series (Pass-2) generally yields slightly higher settlement values than the first series (Pass-1) at comparable speeds.
- Concerning sensor positioning, in both freight and passenger trains, higher displacement values are consistently measured by the potentiometers located on the inner rail compared to those on the outer rail.

6.3.6 VERTICAL DISPLACEMENTS OF THE BALLAST LAYER

The vertical displacement of the ballast layer was monitored using two LVDTs linked to the central sleeper (section 0) and an additional two LVDTs linked to adjacent sleepers. In the present work, only the measurements obtained from the LVDTs linked to the central sleeper (section 0) are presented, while the data from the neighbouring sleepers were used to verify the overall behaviour of the ballast layer under train passages.

The LVDTs were installed at the mid-span section of the sleepers, positioned near the lateral edges in that zone (sides 0- and 0+). Each transducer was arranged between the top surface of the sub-ballast layer and the underside of the sleeper, as shown in Figure 87. With this configuration, the recorded displacements correspond to the relative movement between these two points. These records are interpreted as the displacements of the ballast layer, assuming that there is full and permanent contact, during the duration of all the tests, between the sleeper bottom and the top surface of the ballast layer.

Figure 87.- Instrumentation for ballast displacement measurement. Base of LVDT fixed at the top of the sub-ballast layer (left). Head of LVDT fixed at the sleeper (right).

Figure 88 displays the values recorded by the LVDTs linked to the central sleeper, when a passing-by of a passenger train at 300 km/h (left) and of a freight train at 100 km/h (right) are modelled. Similar to previous recordings, instrumentation accurately reflects the loads applied. In these sensors, negative values indicate downward vertical movements.

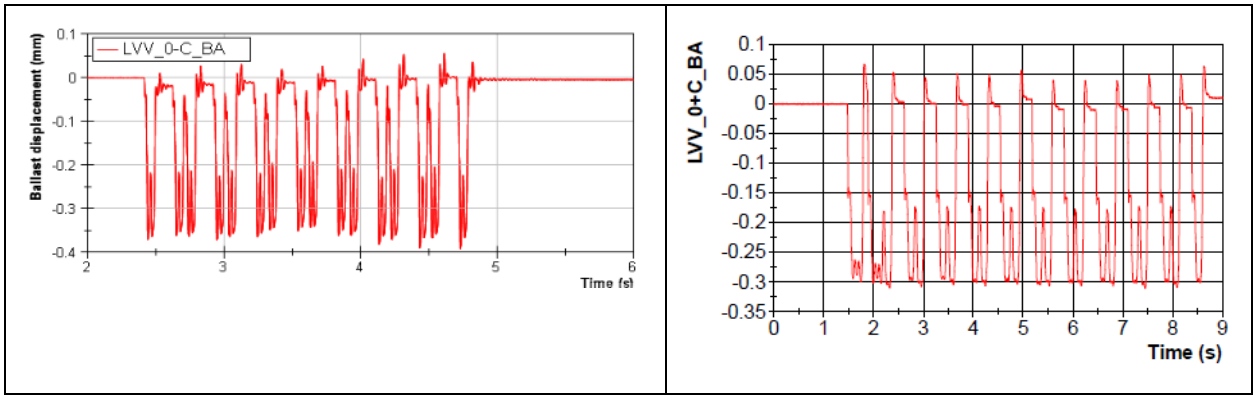

Figure 88.- Data recorded by the LVDTs measuring the vertical displacement of the ballast layer for a passenger train at 300 km/h (left) and a freight train at 100 km/h (right)

Figure 89 presents the measurements obtained from the LVDTs positioned on either side of the central sleeper (0+ and 0−) during the two testing phases (Pass-1 and Pass-2). The bands that define the upper and lower limits of the displacements, added to the figure, were calculated using Equation (1) -in 6.3.1.3-, considering the upper bound of the critical speed of the railway track section (V_{cr}=*550km/h*), as determined in 6.3.2, and a value of z_0 assumed for V_{train}=0.

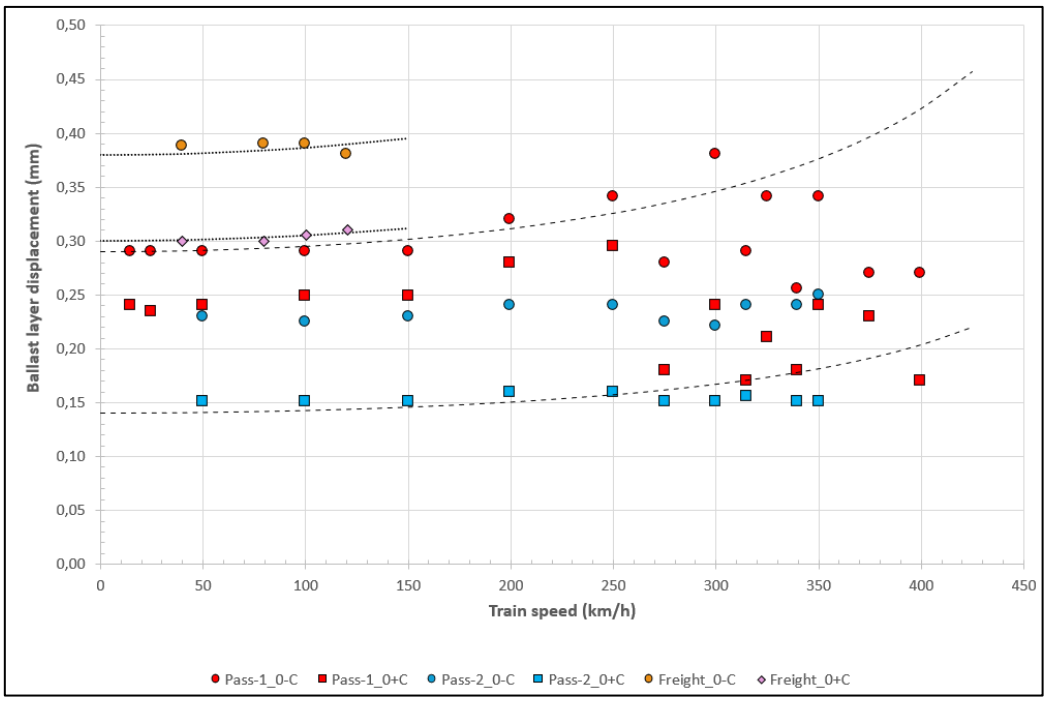

Figure 89.- Ballast vertical displacements recorded at the central sleeper at different passing-by train speeds

Table 17 summarises the range of results obtained for each testing campaign involving both passenger and freight trains. In addition, it provides the settlement expressed as a percentage of ballast layer thickness.

Table 17.- Ballast layer displacement range and deformation

Type of train	Vertical displacement (mm)		Layer deformation (%)[1]	
	Sleeper side 0-	Sleeper side 0+	Sleeper side 0-	Sleeper side 0+
Passenger (Pass 1)	0.25-0.38	0.18-0.29	< 0.10	< 0.08
Passenger (Pass 2)	0.22-0.25	0.15-0.16	< 0.07	< 0.05
Freight	0.38-0.39	0.30-0.31	< 0.10	< 0.08

[1] Ballast layer thickness below the centre of Sleeper 0 = 386 mm

Some conclusions, based on the above figure and table, are:

- The displacements recorded under freight trains are greater than those measured under passenger trains, due to the higher loads applied by the freight trains.
- The values obtained at the sleeper side (0−) are higher than those recorded at the (0+) side.
- The first test series (Pass-1) exhibits higher values than those measured during the second series (Pass-2), probably due to a certain degradation of the mechanical behaviour of the ballast layer as a whole.
- The measured displacements show a clear dependence on train speed, increasing progressively up to 250 km/h. At higher speeds, the ballast layer measurements exhibit greater variability.
- At present, no clear explanation can be provided for the lack of continuity observed in the trend recorded by the sensors located on the central sleeper.
- Nevertheless, the records obtained from the sensors located on sleepers 2+ and 2− confirm that the general trend of displacement growth with increasing speed persists throughout the full range of tested speeds. Figure 90 presents the vertical displacement values obtained in sleeper 2+, where the dotted lines show the clear trend of the increase in displacements with increasing train speed.

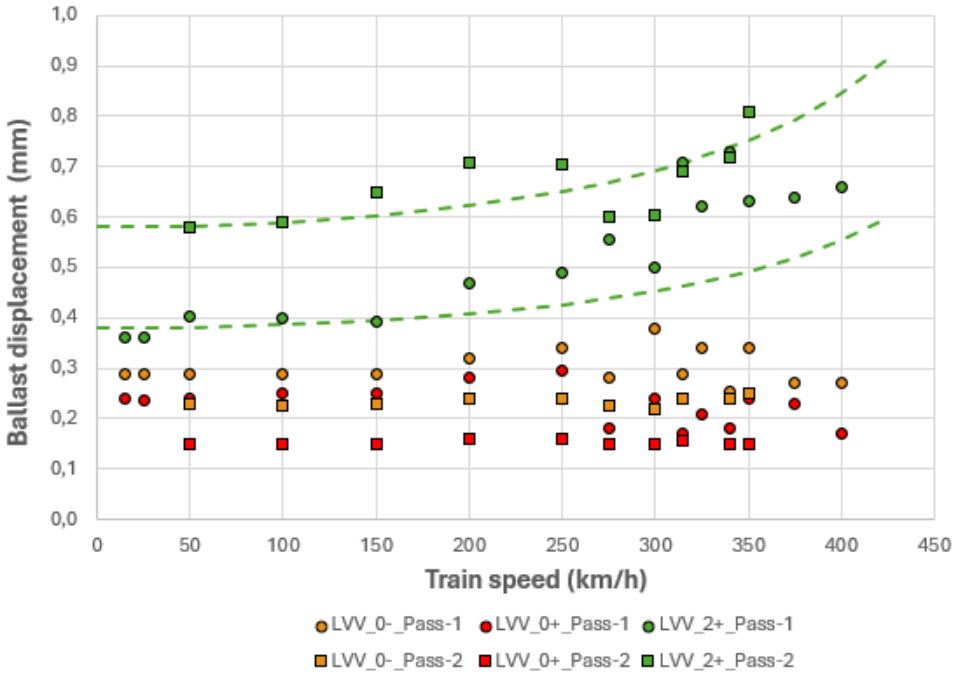

Figure 90.- Ballast vertical displacements recorded at the central sleeper and at Sleeper +2 at different passing-by train speeds

6.3.7 VERTICAL DISPLACEMENTS OF THE SUB-BALLAST AND FORM LAYERS

The form and sub-ballast layers were constructed using granular material, each with a thickness of 30 cm. Installed instrumentation, which consists of LVDTs, measures the vertical displacements of both layers together. Figure 91 illustrates a moment during the construction of the sub-ballast layer, depicting the lower form layer and the placement of tubes where instrumentation was installed to measure the vertical movement of both layers.

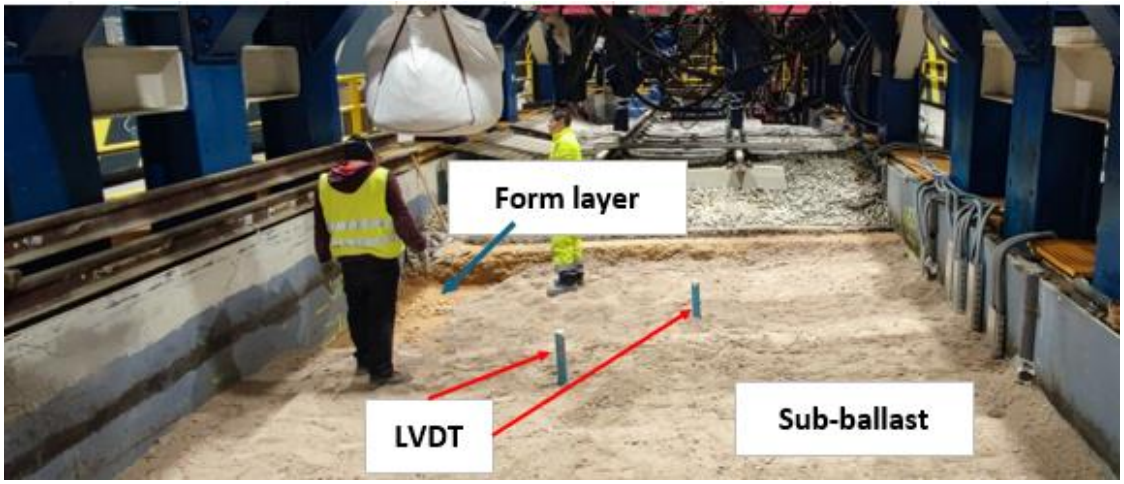

Figure 91.-Installation of LVDTs to measure the vertical displacement of both the sub-ballast and form layers together

Figure 92 displays the values recorded by the LVDT positioned at the central section, with a passing-by passenger train at 300 km/h (left) and a freight train at 100 km/h (right). Similar to previous recordings, the instrumentation accurately reflects the loads applied. In these sensors, negative values indicate downward vertical movements (towards the inside of the railway track).

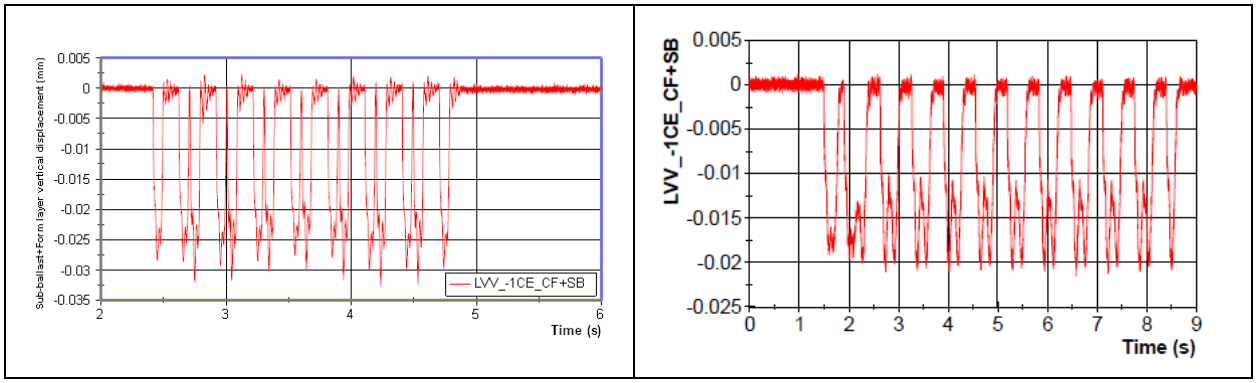

Figure 92.-Data recorded by the LVDT measuring the vertical displacement of the sub-ballast and form layers for passenger train at 300 km/h (left) and freight train at 100 km/h (right)

Like other sensors, the movements in the sub-ballast and form layers are mainly downward, while their vertical upward displacements are negligible.

Figure 93 shows the values recorded at the sub-ballast and form layers during the dynamic tests. The bands that define the upper and lower limits of the displacements, added to the figure, were calculated using Equation (1) -in 6.3.1.3-, considering the upper bound of the critical speed of the railway track section (V_{cr}=*550km/h*), as determined in 6.3.2, and a value of z_0 assumed for V_{train}=0.

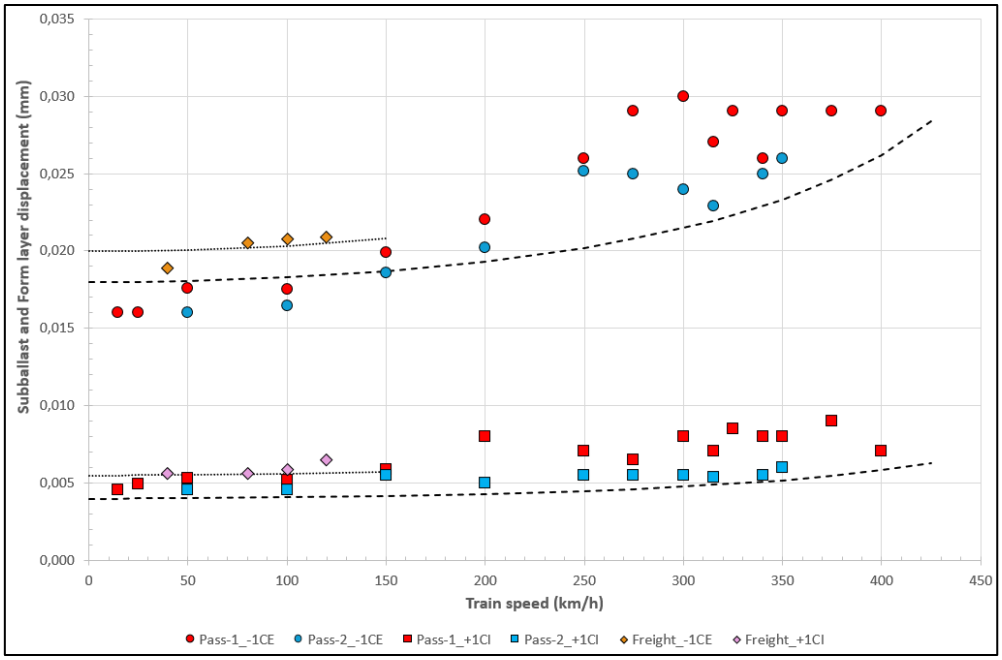

Figure 93.- Sub-ballast and form layers vertical displacements recorded at different passing-by train speeds

Table 18 summarises the range of results obtained for each testing campaign involving passenger and freight trains. In addition, it provides the deformation of the sub-ballast and form layers, considered as a unique layer.

Table 18.- Sub-ballast and form layers displacement range and deformation

Type of train	Vertical displacement (mm)		Layer deformation [1]	
	Outer rail	Inner rail	Outer rail	Inner rail
Passenger (Pass 1)	0.016-0.030	0.004-0.009	<0.005	<0.002
Passenger (Pass 2)	0.016-0.026	0.004-0.006	<0.005	<0.001
Freight	0.019-0.021	0.005-0.006	<0.004	<0.001

[1] Sub-ballast and form layer thickness = 600 mm

Some conclusions, based on the above figure and table, are:

- The vertical displacements of the sub-ballast and form layers increase with increasing train speed.
- Vertical displacements are minimal, ranging from 0.004 to 0.030 mm, corresponding to a thickness variation around 0.005%.
- These minimal vertical displacements are probably due to the high compaction of these layers obtained during the execution phase, as previously indicated in section 5.4.
- The inner rail exhibits lower displacements compared to the measurements recorded on the outer rail.
- Displacement values recorded for freight trains are marginally higher than those obtained for passenger trains. Specifically, the outer rail exhibits an increase of 5%, while the inner rail shows no measurable difference.
- The first series of passenger train tests exhibits marginally greater vertical displacements compared to the second series.

6.3.8 VERTICAL DISPLACEMENTS OF LECA EMBANKMENT

The LECA embankment was constructed on top of the existing earth embankment. It consists of 1.1 meters of LECA material, measured beneath the inner rail. To monitor the vertical movements of this layer, four LVDTs were installed: two in the central section (Section 0) and two below the adjacent sleepers (Sections +2 and -2). This report focuses only on the measurements from the central section; however, data from the Sections +2 and -2 were also analysed to validate the results obtained. Figure 94 shows the location of the LVDTs used to measure LECA embankment vertical displacements: the base was located at the earth embankment top surface, and the head was positioned at the LECA layer top.

Figure 94.-Installation of LVDTs to measure LECA embankment vertical displacements

Figure 95 displays the values recorded by the LVDT positioned in the central section during a passing passenger train at 300 km/h and a freight train at 100 km/h. Similar to previous recordings, the instrumentation accurately reflects the loads applied. In these sensors, negative values indicate downward vertical movements.

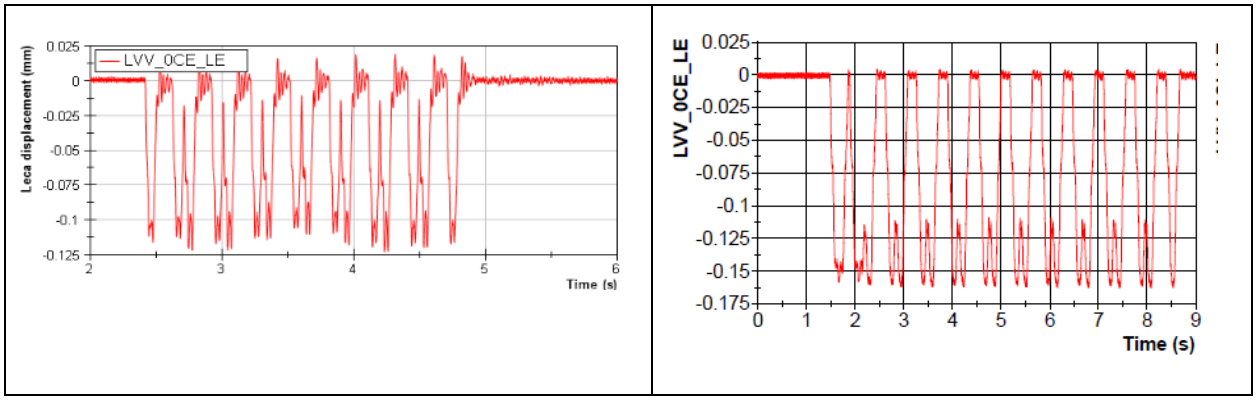

Figure 95.- Data recorded by the LVDT measuring the vertical displacement of the LECA embankment for a passenger train at 300 km/h (left) and a freight train at 100 km/h (right)

Figure 96 shows the values recorded at the LECA embankment during the dynamic tests by the two LVDTs located at the central section (Section 0) at inner (I) and outer (E) rail. The bands that define the upper and lower limits of the displacements, added to the figure, were calculated using Equation (1) -in 6.3.1.3-, considering the upper bound of the critical speed of the railway track section (V_{cr}=*550km/h*), as determined in 6.3.2, and a value of z_0 assumed for V_{train}=0.

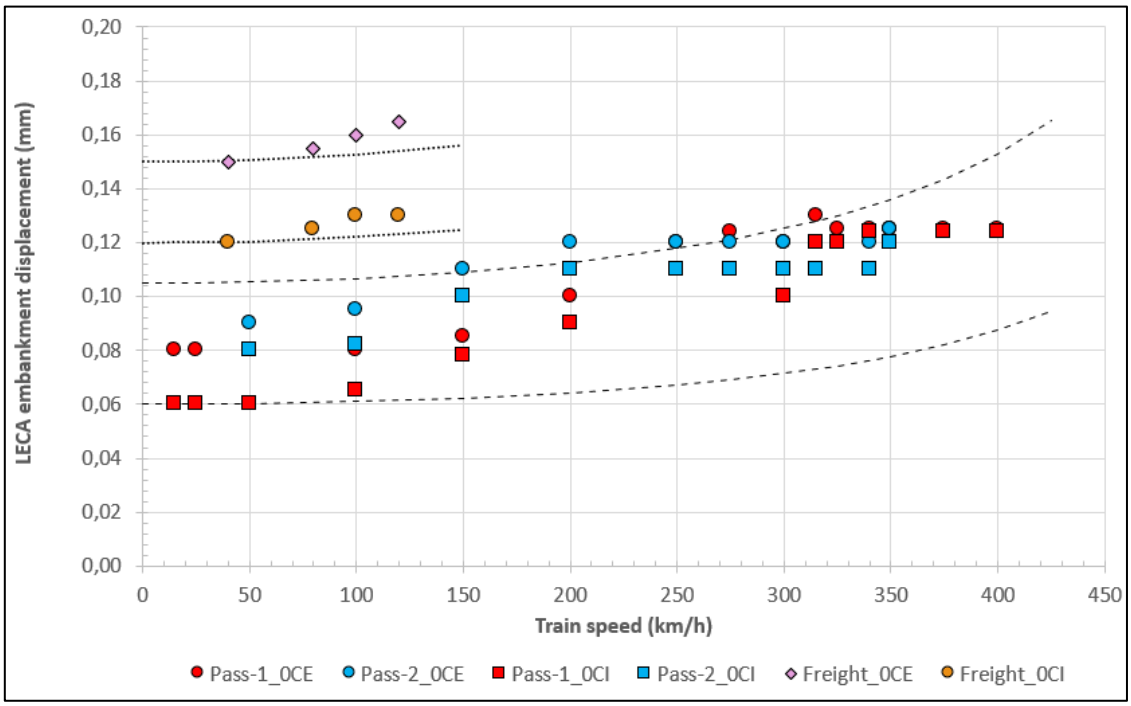

Figure 96.- LECA embankment vertical displacements recorded at different passing-by train speeds

Table 19 summarises the range of results obtained for each testing campaign involving passenger and freight trains and the deformation of the LECA embankment.

Table 19.- LECA embankment displacement range and deformation

Type of train	Vertical displacement (mm)		Layer deformation [1]	
	Under Outer rail	Under Inner rail	Under Outer rail	Under Inner rail
Passenger (Pass 1)	0.08-0.13	0.06-0.12	<0.015	<0.013
Passenger (Pass 2)	0.09-0.12	0.08-0.12	<0.012	<0.010
Freight	0.15-0.17	0.12-0.13	<0.015	<0.013
[1] LECA embankment thickness ≈ 1100 mm				

Some conclusions, based on the above figure and table, are:

- The vertical displacements of the LECA embankment increase with increasing train speed.
- The greatest displacements are induced by freight trains due to their higher loads applied.

- The second testing campaign for passenger trains (Pass-2) exhibited marginally higher displacement values.
- Higher vertical displacements are observed on the outer rail.
- The deformation of the LECA embankment can be considered negligible.

6.3.9 GLOBAL ANALYSIS OF VERTICAL DISPLACEMENTS

The previous sections detailed the vertical displacements recorded in each layer of the railway track section. Additionally, the total displacement of the section, as recorded by the laser systems, is also available.

This section analyses all the vertical displacements mentioned earlier. It is important to note that only the most significant displacements, specifically downward displacements obtained in the central sleeper (0), where the test boundary conditions fairly represent the real track conditions, or alternatively, in the nearest section (sleeper), will be examined.

Figure 97 illustrates the vertical displacements recorded in various layers during the tests with passenger trains at different speeds: the rail pad (orange), the ballast layer (green), the sub-ballast and form layers (blue), the LECA embankment (purple), the entire railway track section - recorded by laser at rail- (red), and the sum of the total displacements recorded in all layers (grey).

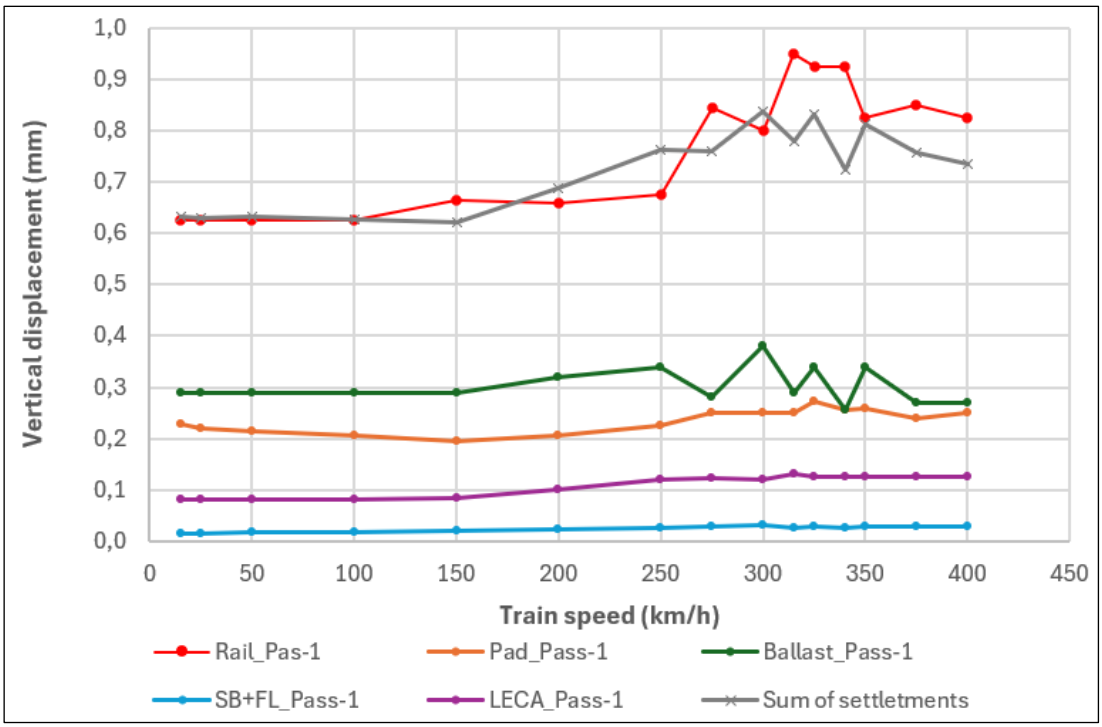

Figure 97.- Vertical displacements recorded for each railway track section layer at different passing-by train speeds

The analysis of the figure makes it possible to highlight the following facts:

- The total displacement of the section, measured by the laser system in the rail, closely aligns with the sum of the vertical displacements of the layers that form the railway track section.
- The most significant vertical displacements occur within the ballast layer, followed by the under-rail pad.
- The displacements in the LECA embankment are around a third of the displacement in the ballast layer.
- The displacements measured in the sub-ballast and form layers can be considered negligible

Table 20 summarises the contribution of each layer of the railway track section to the overall vertical displacement for different passenger train speeds.

Table 20.- Contribution of each layer to total vertical displacement of railway section

Train speed (km/h)	Rail Pad (%)	Ballast layer (%)	Sub-ballast+Form layers (%)	LECA embankment (%)	Earth embankment (%)
15	37.1	47.1	2.6	13.0	0.2
25	36.2	47.7	2.6	13.2	0.4
50	35.5	47.9	2.9	13.2	0.4
100	34.7	48.7	2.9	13.4	0.2
150	33.0	49.1	3.4	14.4	0.1
200	31.5	49.2	3.4	15.4	0.4
250	31.6	47.5	3.6	16.8	0.5
275	36.5	40.9	4.2	18.1	0.3
300	32.0	48.6	3.8	15.4	0.2
315	35.8	41.5	3.9	18.6	0.2
325	35.3	44.1	3.8	16.2	0.5
340	38.4	38.4	3.9	18.8	0.4
350	34.2	45.0	3.8	16.6	0.4
375	35.9	40.5	4.4	18.8	0.5
400	37.0	39.9	4.3	18.5	0.3
Maximum	38.4	49.2	4.4	18.8	0.5
Minimum	31.54	38.43	2.60	13.01	0.10
Mean	34.98	45.09	3.57	16.02	0.33
Std Dev	2.11	3.84	0.58	2.22	0.14
Coef. Var. (%)	0.06	0.09	0.16	0.14	0.42

It can therefore be concluded that the ballast layer accounts for approximately 45% of the total displacement, followed by the rail pad with 35%, the LECA embankment with 16%, the combined contribution of the sub-ballast layer and subgrade with 4%, and the earth embankment is lower than 0.4%.

6.3.10 VERTICAL VELOCITIES IN SLEEPERS

Velocities of the sleeper vibration during the train pass-by were recorded by geophones installed on the sleepers. Figure 98 provides a detailed view of one of these geophones (up), and the records taken at the central sleeper (Sleeper 0) when the passenger train passes at 300 km/h (left) and the freight train at 80 km/h (right).

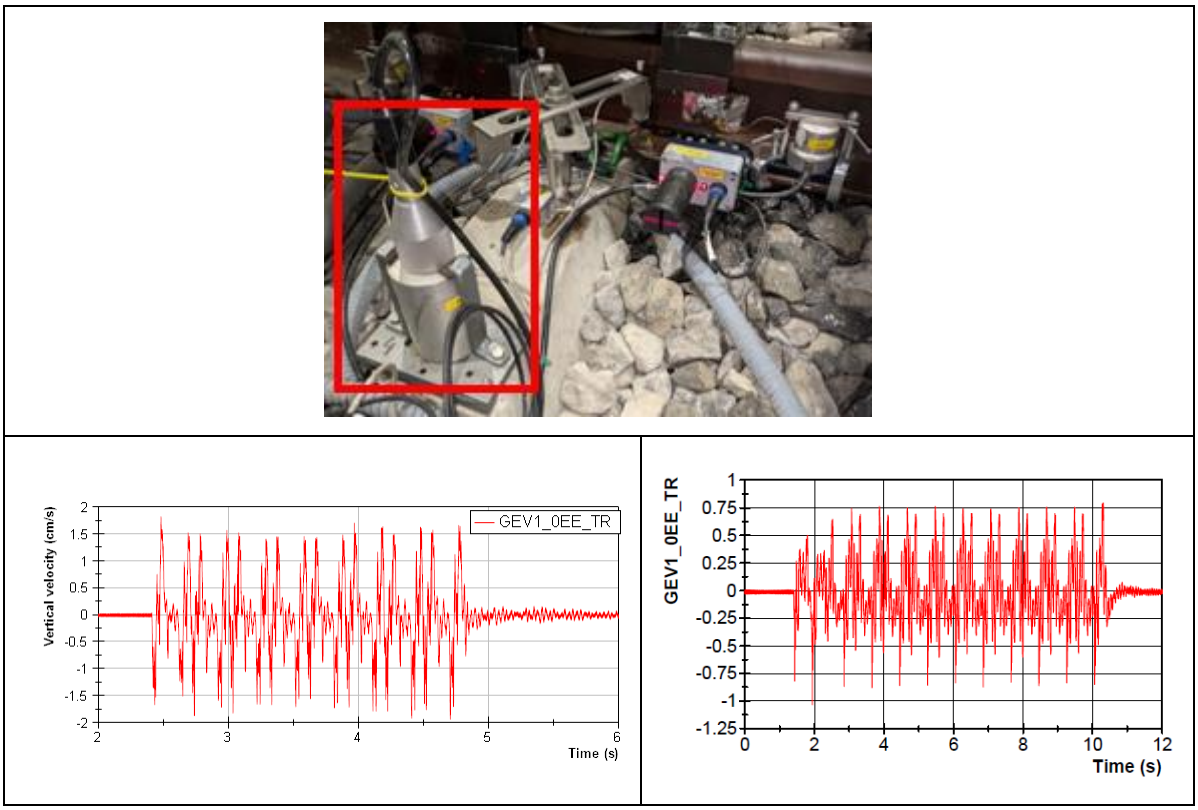

Figure 98.- Geophone installed on the sleeper (up) and its record for passenger train at 300 km/h (left) and freight train at 80 km/h (right)

As illustrated in the figure above, the sleeper experiences both positive and negative velocities, each averaging approximately 1.5 cm/s for a train moving at 300 km/h.

Positive velocities are associated with the downward vertical movement of the sleeper caused by the train passage. The velocity momentarily reaches zero when the sleeper reaches its maximum displacement. This phenomenon is graphically illustrated in the figure using Winkler's theory.

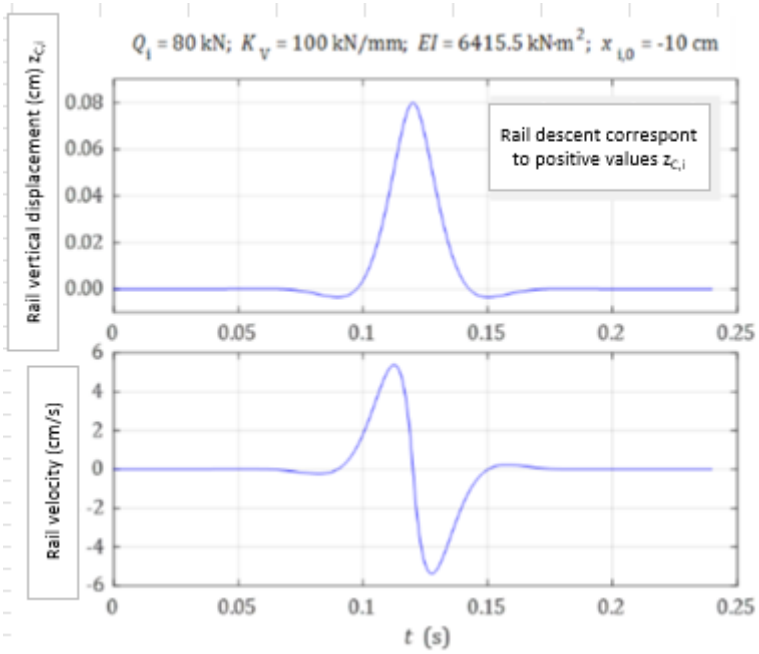

Figure 99.- Relationship between vertical displacement and velocity according to Winkler's theory

Figure 100 presents the peak velocity values measured at the central sleeper (Sleeper 0) for both passenger train test campaigns (Pass-1 and Pass-2) and for the freight train. It also identifies whether the data correspond to the instrumentation installed on the inner rail (I) or the outer rail (E). The figure illustrates the representative bands of sleeper velocity values as a function of train speed. The results are differentiated between freight (orange dotted lines) and passenger trains and, for passenger trains, between measurements recorded on the inner (green dotted lines) and outer rails (black dotted line).

Table 21 summarises the range of results obtained for each testing campaign involving passenger and freight trains.

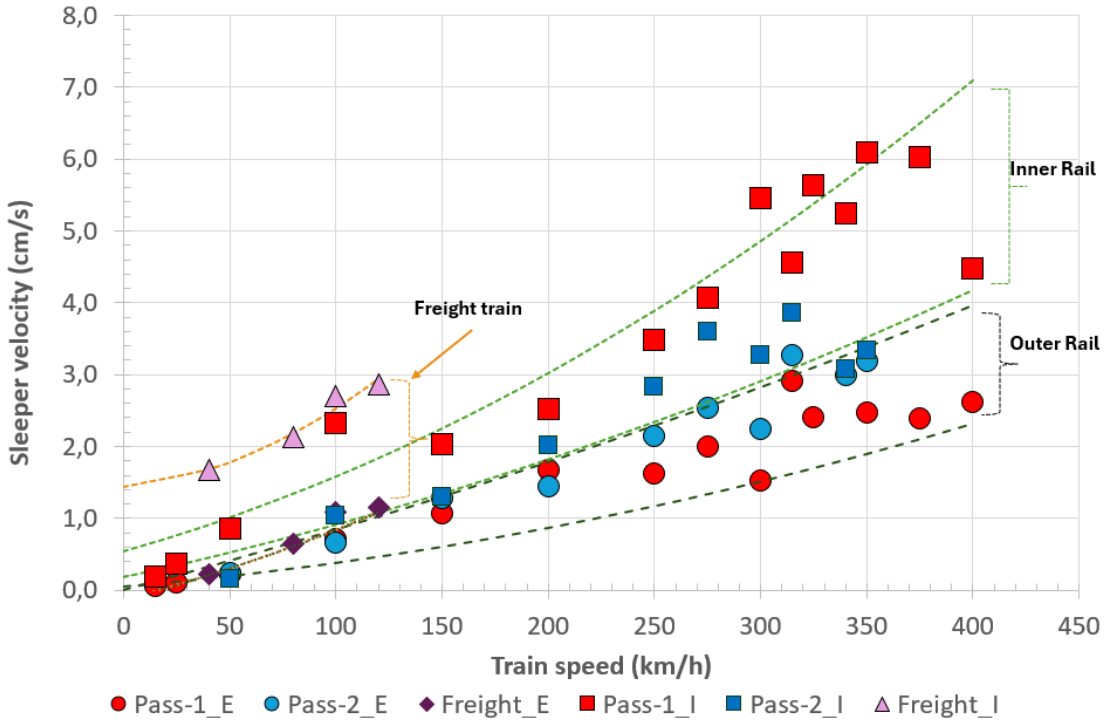

Figure 100.- Peak vertical sleeper velocity recorded at different train speeds

Table 21.- Peak vertical sleeper velocity range

Type of train	Peak vertical velocity (cm/s)	
	Outer rail	Inner rail
Passenger (Pass 1)	0.06 - 2.93	0.19 - 6.05
Passenger (Pass 2)	0.24 - 3.28	0.15 - 3.86
Freight	0.22 - 1.16	1.67 - 2.87

Some conclusions, based on the above figure and table, are:

- The velocities measured at the sleepers increase with increasing train speed.
- The values obtained from the instrumentation on the inner rail are consistently higher than those recorded on the outer rail.
- The sleeper velocities measured in the second testing phase of the passenger train (Pass-2) are marginally higher than those recorded during the first phase (Pass-1).
- For a train speed, in the case of freight trains, the sleeper velocities exceed those recorded for passenger trains, with this effect being more evident in the measurements taken on the inner rail.

6.3.11 VERTICAL ACCELERATIONS IN SLEEPERS

Accelerations experienced by the sleepers as trains pass by were measured using accelerometers, similar to the one depicted in Figure 101 (up). An example of the recorded data is illustrated on the bottom part of the figure.

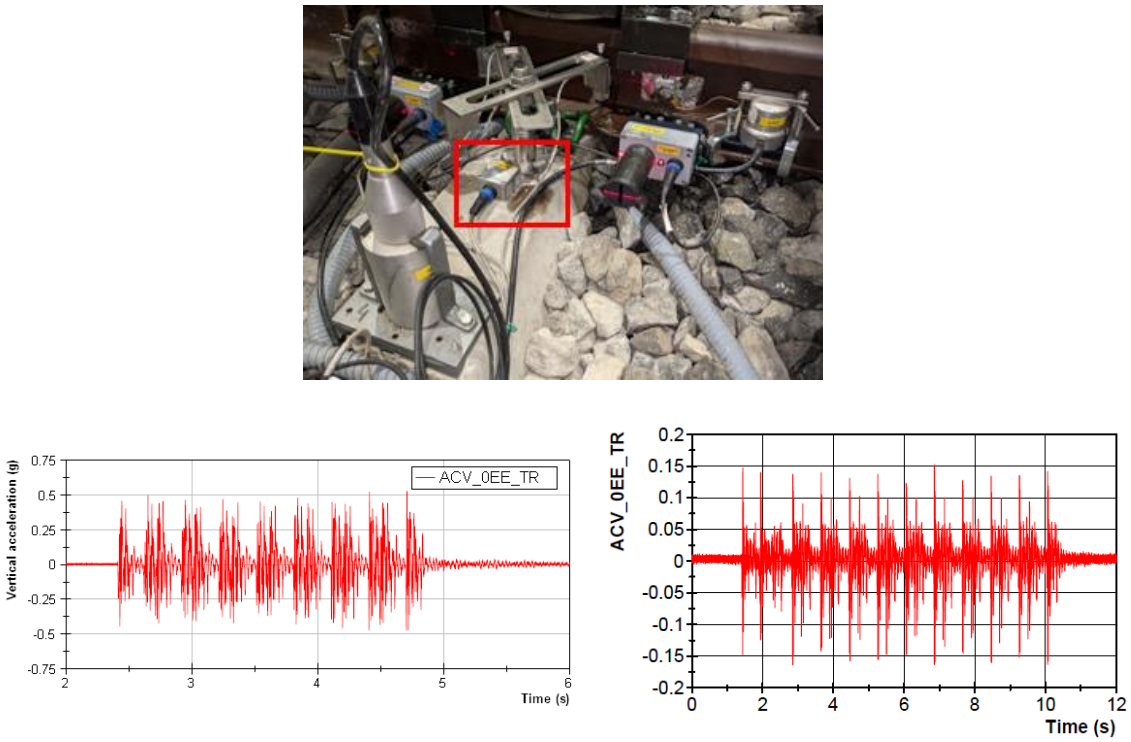

Figure 101.- Accelerometer installed at sleeper (up) and its record at 300 km/h passing-by passenger train (left) and for freight train at 80 km/h (right)

Similar to the speed values, the acceleration records at the central sleeper show both positive and negative values, which can be understood in the same manner as discussed in the previous section. In this instance, the maximum acceleration values are approximately 0.5g during the passing-by train at 300 km/h.

Figure 102 shows the representative values of the sleeper acceleration recorded for each of the train passages analysed. The acceleration values obtained during the first and second series of passenger train tests (Pass-1 and Pass-2), as well as those recorded for freight trains, were included. Measurements from both accelerometers—installed near the inner rail (I) and the outer rail (E)—were presented. The value ranges were also included, with a distinction made between measurements obtained on the inner (green dotted line) and outer rails (black dotted line).

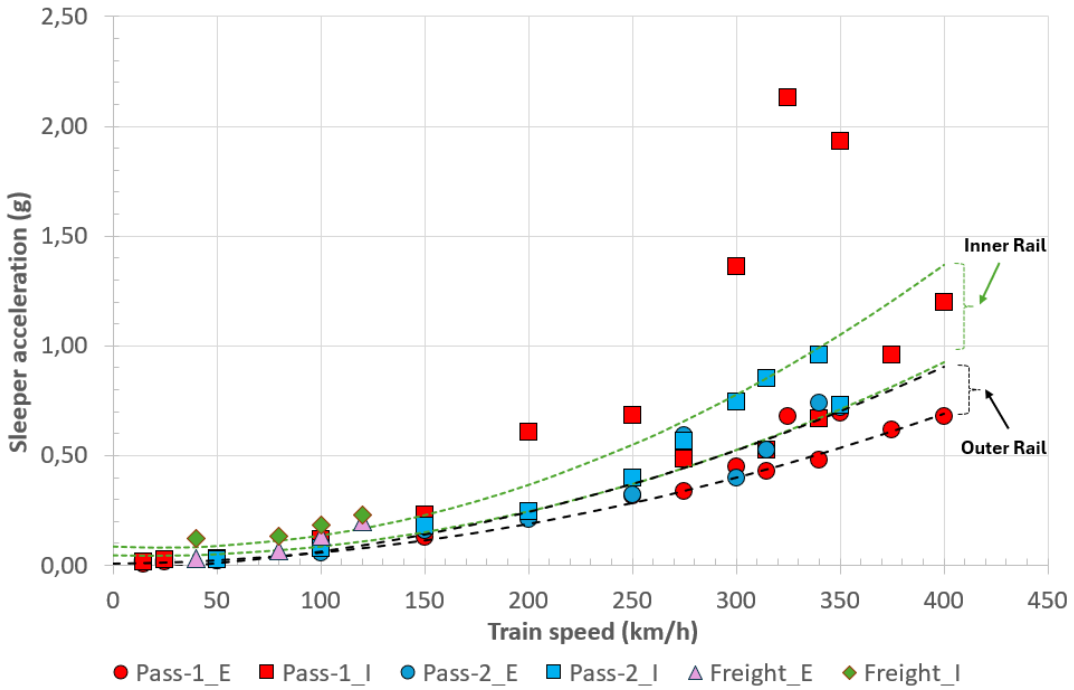

Figure 102.- Representative vertical sleeper acceleration recorded for different train speeds

Table 22 summarises the range of results obtained for each testing campaign involving passenger and freight trains.

Table 22.- Representative vertical sleeper acceleration range

Type of train	Peak vertical sleeper acceleration (g)	
	Outer rail	Inner rail
Passenger (Pass 1)	0.006 - 0.693	0.014 - 2.130
Passenger (Pass 2)	0.018 - 0.395	0.024 - 0.960
Freight	0.030 - 0.199	0.122 - 0.230

Some conclusions, based on the above figure and table, are:

- The acceleration at the sleeper increases with increasing train speed.
- For a particular train speed, the values obtained for freight trains are similar to those of passenger trains.
- No significant differences were observed between the first and second test campaigns for passenger trains.
- The measurements obtained on the inner rail are consistently slightly higher than those recorded on the outer rail.

- Unusually high sleeper acceleration values were recorded for speeds between 300 and 350 km/h on the accelerometer installed near the inner rail. These measurements are considered unrepresentative of the overall structural response.

6.3.12 BALLAST PARTICLE ACCELERATIONS

The ballast layer includes a ballast particle instrumented with a triaxial accelerometer capable of measuring acceleration along the three spatial axes, as shown in Figure 49.

Figure 103 presents an example of the records obtained during the dynamic characterisation tests for the passage of a passenger train at 300 km/h and a freight train at 100 km/h, corresponding to the most relevant direction: the vertical direction (z-axis).

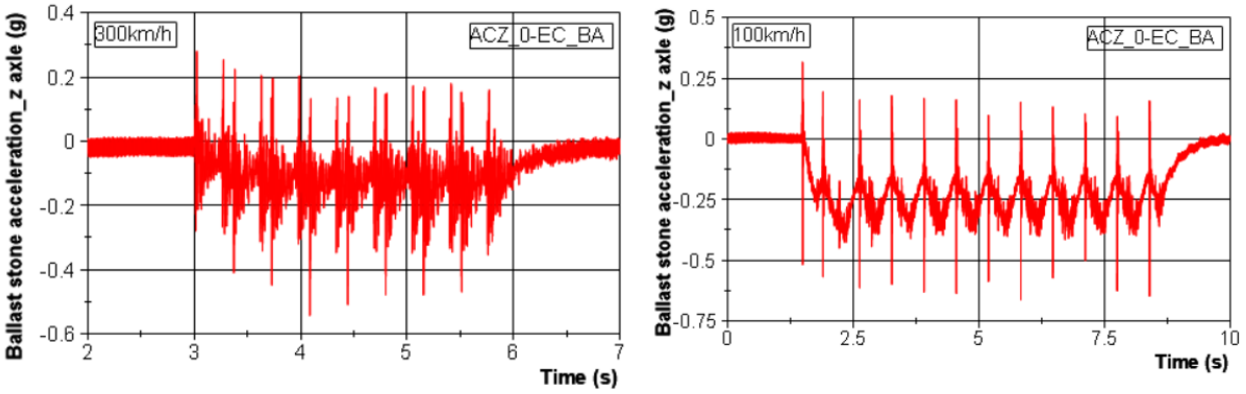

Figure 103.- Ballast particle register at ballast layer for a passenger train passing at 300 km/h (left) and a freight train at 100 km/h (right)

In both records, the passage of the train bogies can be clearly distinguished. In addition, the signals exhibit a range that includes both positive and negative acceleration values.

Figure 104 presents the representative acceleration values recorded by the instrumented ballast particle on the z-axis for the modelled train speeds. The results are differentiated according to the first (Pass-1) and second passages (Pass-2) of the passenger train, the freight train, and the location of the instrumentation on the inner or outer rail. The corresponding value ranges are also included to facilitate the identification of trends.

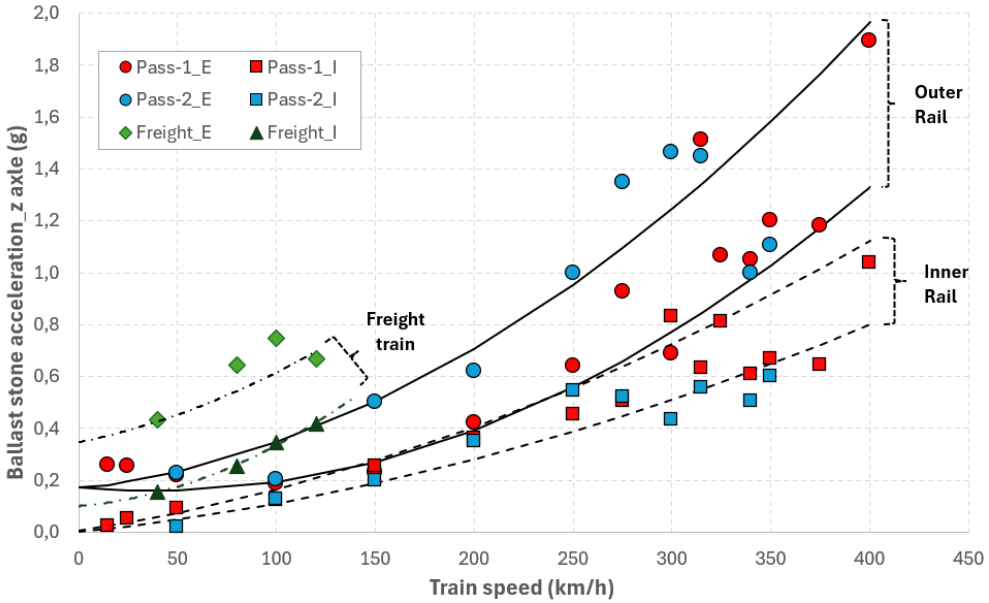

Figure 104.- Ballast particle acceleration recorded for different train speeds

Table 23 summarises the range of results obtained for each testing campaign involving passenger and freight trains.

Table 23.- Ballast particle acceleration range

Type of train	Ballast acceleration _Vertical direction (g)	
	Outer rail	Inner rail
Passenger (Pass 1)	0.21 - 1.85	0.02 - 1.04
Passenger (Pass 2)	0.20 - 1.50	0.02 - 0.55
Freight	0.43 - 0.75	0.16 - 0.42

Some conclusions, based on the above figure and table, are:

- The acceleration at ballast particle increases with increasing train speed.
- For a given train speed, the values obtained for freight trains are higher than those of passenger trains.
- No significant differences were observed between the first and second test campaigns for passenger trains.
- The measurements obtained on the outer rail are consistently slightly higher than those recorded on the inner rail.

6.3.13 ACCELERATION INSIDE THE RAILWAY SECTION

As described in Chapter 5.6.2, in addition to the accelerometers installed on the rails, sleepers, and ballast particles, similar instrumentation has also been deployed within the railway section. Specifically, accelerometers are installed at the interface between the sub-ballast and form layers, as well as at mid-depth within the LECA embankment layer.

Figure 105 presents the maximum acceleration values recorded at the different modelled passenger train speeds, together with the depth of the sensors at which these values are measured. Two distinct zones have been identified, within which similar trends in acceleration response are observed.

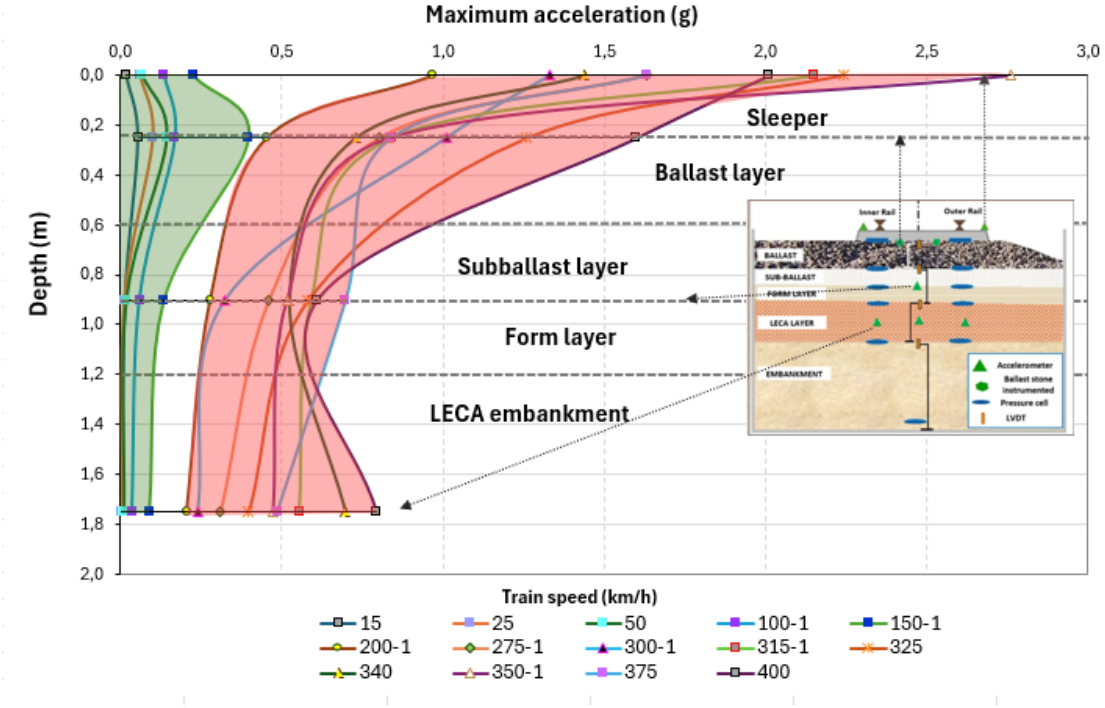

Figure 105.- Maximum accelerations recorded at passenger train models at different depths of the railway section

As shown in the figure above, at low speeds (up to 150 km/h), highlighted in the green zone, the highest acceleration values are recorded in the ballast particles located at the sleeper–ballast interface. At greater depths, the acceleration progressively decreases.

In the red zone, corresponding to speeds of 200 km/h and above, the curves exhibit a change in trend, with peak accelerations occurring at the sleeper level and decreasing with increasing depth of the sensor location. However, for passing speeds of 340, 375, and 400 km/h, the acceleration measured at mid-depth within the LECA embankment is slightly higher than that recorded at the interface between the form and sub-ballast layer.

6.3.14 DYNAMIC PRESSURE MEASUREMENTS

The dynamic pressures in the track section were measured using the pressure cells previously described, installed at the different layer interfaces along Section 0, with one sensor under each rail. Since the challenges associated with obtaining reliable data at the sleeper–ballast interface have already been discussed, the same installation procedure (Merino & Bendahman, 2025) was applied here to ensure adequate stress transfer to the sensors. In the dynamic tests, only the pressure cells located under the outer rail provided valid measurements; the sensors under the inner rail experienced measurement errors and their data were therefore excluded in this analysis.

Figure 106 provides an example of the pressure time histories recorded by two cells during the passage of a train at 300 km/h. In particular, the measurements at the sleeper–ballast (SL-BA) interface and LECA embankment and form layer (LE-CL) are presented, clearly demonstrating the ability of the pressure cells to resolve the individual bogies.

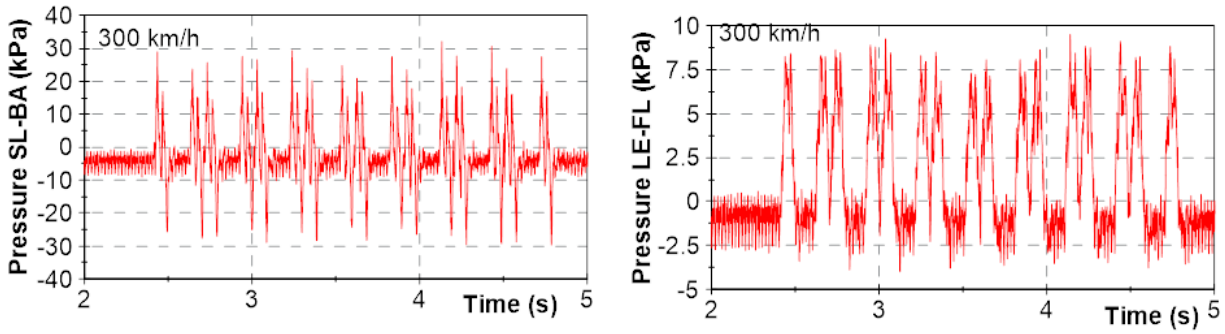

Figure 106.- Pressure cells register at the interface sleeper-ballast and LECA embankment-form layer for a train passing at 300 km/h

Figure 107 illustrates the pressure measurements recorded by the cells installed at the different interfaces, expressed as a function of train speed.

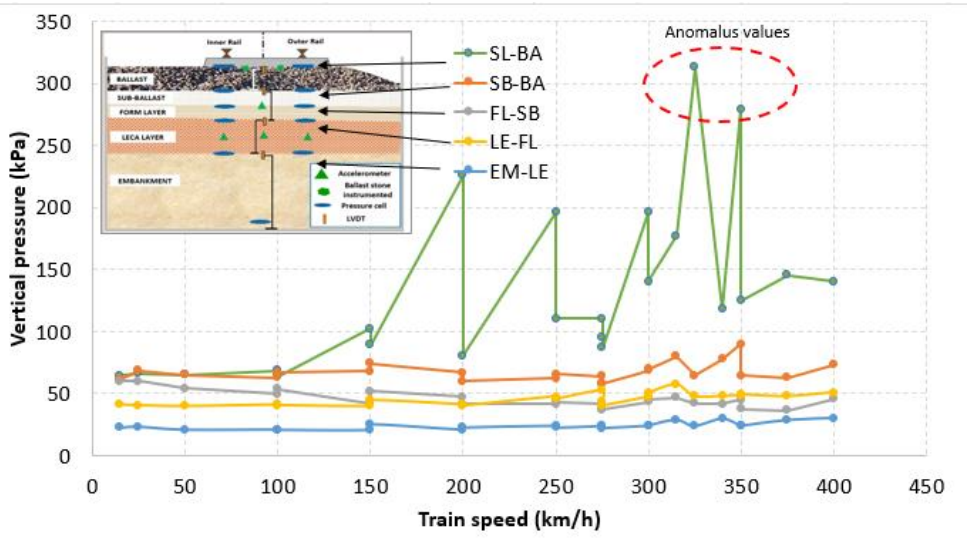

Figure 107.- Vertical pressure recorded at each interface at different train speeds

To provide a clearer representation of the trend in the pressures recorded at different speeds, Figure 108 presents the lowest values obtained from all sensors, excluding those located at the sleeper–ballast interface.

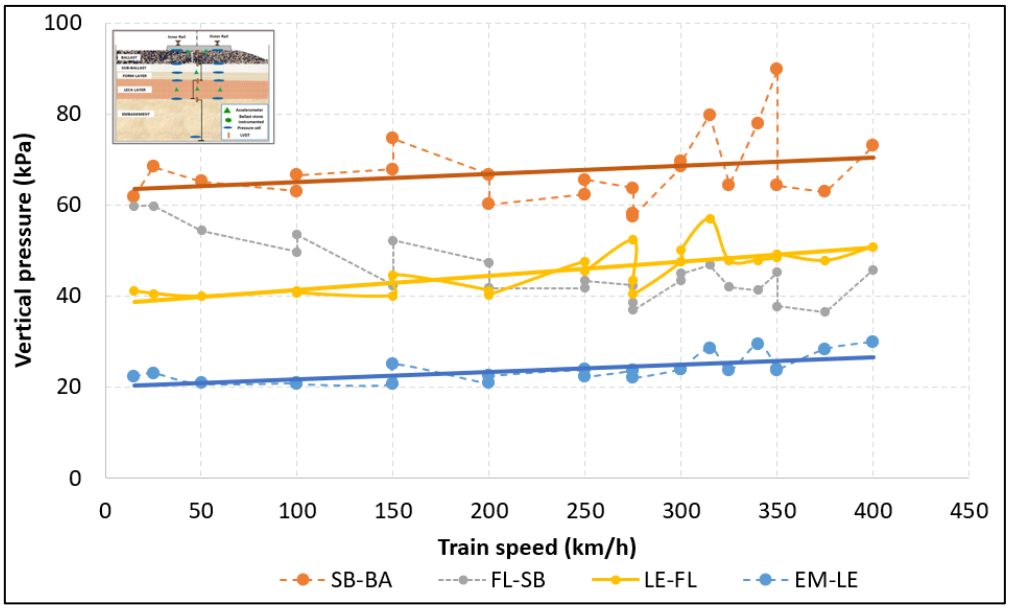

Figure 108.- Vertical pressure recorded at different interfaces at different train speeds

Figure 109 presents the pressure values recorded at the sleeper–ballast interface (SL-BA). In addition, the range of variation considered as representative is also indicated.

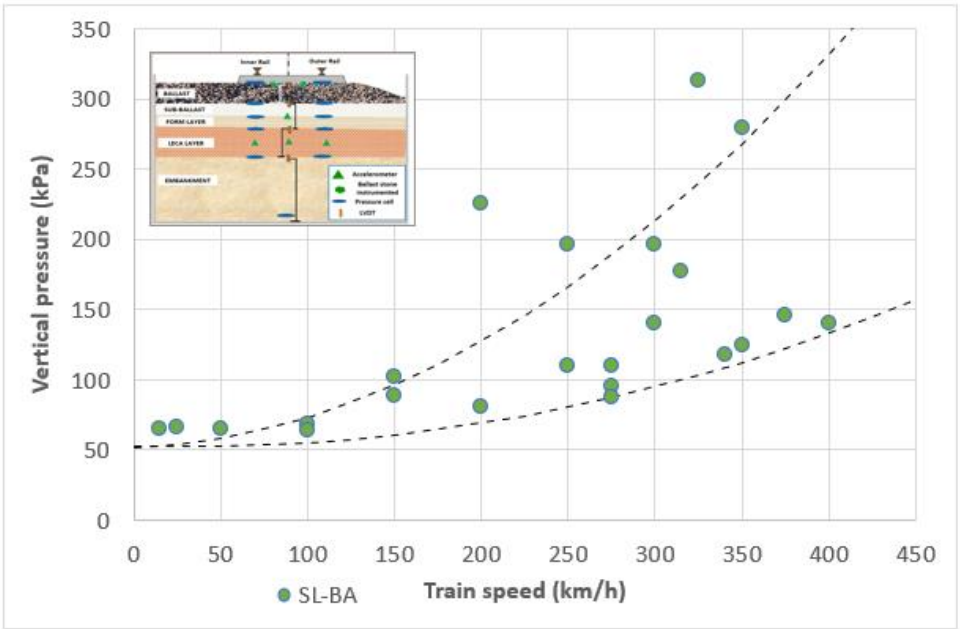

Figure 109.- Vertical pressure recorded at sleeper-ballast interface at different train speeds

Several conclusions can be drawn from the figures above:

- In general, the recorded pressure decreases with increasing depth of the instrumentation.
- At the deeper interfaces (EM-LE, LE-FL and SB-BA), the pressure increase factor with increasing train speed ranges from 1.10 to 1.25.
- For speeds above 250 km/h, the pressure measured at the embankment–LECA interface (EM-LE) is slightly higher than that recorded at the upper subgrade interface.
- The pressure variation recorded at the sleeper–ballast (SL–BA) interface increases with speed, exhibiting a variation ratio of approximately 2.5.
- The highest pressure values are observed at the sleeper – ballast (SL-BA) interface. At this location, a couple of unusually high readings are identified and are considered anomalous.

Figure 110 shows the pressure values recorded in the pressure cells during the dynamic tests as a function of their location depth, together with the boundaries of the track layers and the theoretical pressure profile expected for this section. The pressure values obtained from the static tests are also included (blue and red circles). For the dynamic tests, the mean values (for all train speeds), along with the corresponding minimum and maximum pressures, are reported.

These theoretical pressure curves come from Fadum theory, considering a vertical stress for z=0 m of 130 kPa ±30%, that corresponds to the pressure on the ballast layer surface transmitted by the sleeper under a static load of a passenger train axle load (about 150 kN) acting on the horizontal sleeper area (0.65 m2), and taking into account a distribution load factor between sleepers of 0.4, due to Winkler theory and a dynamic amplification of 1.45, according to 6.3.3.

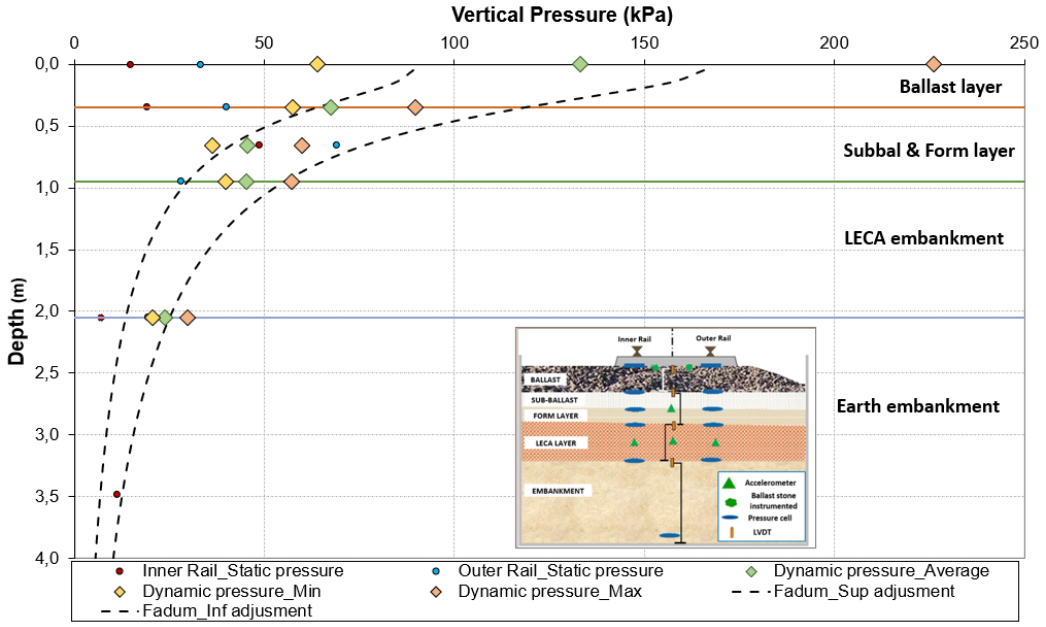

Figure 110.- Pressure values obtained during dynamic test (values obtained during static tests are also identified)

As illustrated in the figure above, the pressure values derived from the dynamic tests show good agreement with the predictions of Fadum's theory. Conversely, the dynamic-to-static pressure ratio is about 6 at the sleeper–ballast interface and varies between 1.2 and 1.8 across the other interfaces.

6.3.15 RELATIONSHIP BETWEEN BALLAST LAYER DISPLACEMENTS AND SLEEPER–BALLAST CONTACT PRESSURE AND ITS VARIATION WITH TRAIN SPEED

The representation of the vertical deformation of the ballast layer as a function of the simulated train speed, shown in Figure 111, does not display a strictly monotonic trend over the full range of tested velocities. In particular, the vertical deformation, as measured by the displacement sensor called LVV_0-C_BA does not increase as would be expected from 250 to 400 km/h. Figure 111 also shows the sleeper-ballast contact-pressure as a function of the train speed. Excluding the measurements for train speeds below 50 km/h, which are clearly outliers, a good correlation is visually observed between these two curves.

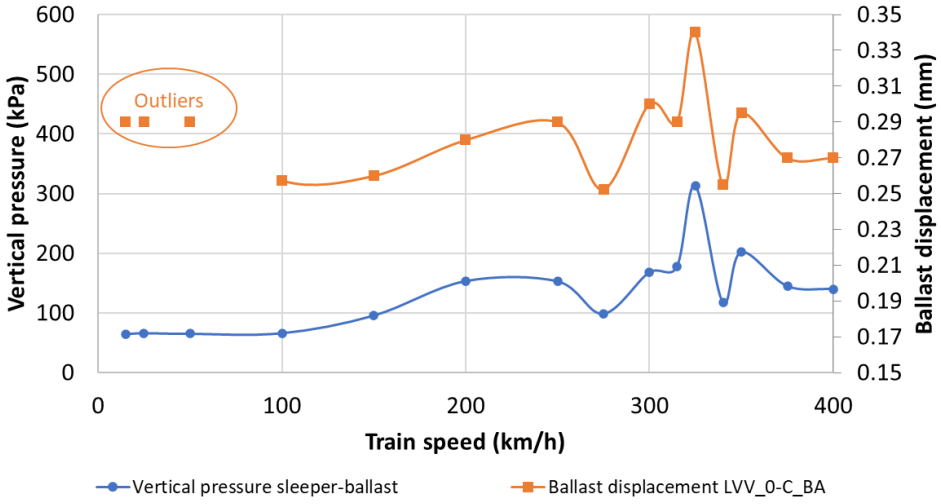

Figure 111.- Sleeper-ballast contact pressure (left vertical axis) and vertical deformation of the ballast layer (right vertical axis) as a function of train speed.

In fact, this good correlation is clearly evidenced in Figure 112, where the ballast contact pressure is plotted on the horizontal axis, and the vertical deformation of the ballast layer is plotted on the vertical axis. The data points follow a well-defined linear trend, indicating a coherent mechanical response in which higher sleeper-ballast contact pressures systematically correspond to larger vertical deformations of the ballast layer. The Pearson correlation coefficient associated with the corresponding linear fit is 0.95. This behaviour suggests that the ballast layer response is primarily governed by the stress state transmitted through the sleeper, as expected.

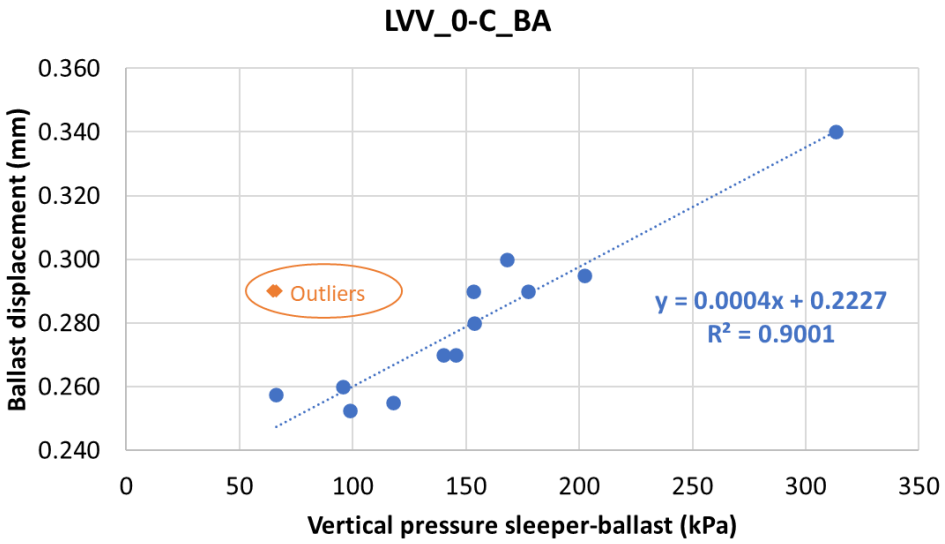

Figure 112.- Vertical deformation of the ballast layer as a function of the sleeper-ballast contact pressure.

When Figure 111 and Figure 112 are interpreted jointly, the strong and consistent correlation between contact pressure and vertical deformation indicates that the ballast material behaves in a mechanically coherent manner under the applied loading conditions. Therefore, the apparent non-monotonicity with train speed observed in Figure 1 is not attributed to an intrinsic change in the mechanical response of the ballast layer, but rather to deviations between the theoretical command signal and the actual loading signal effectively applied during the tests.

6.4 FATIGUE TESTS

6.4.1 GENERAL ASPECTS

The primary objective of the fatigue testing programme is to quantify the potential degradation of the individual layers constituting the railway track section. This degradation is associated with the cumulative mechanical actions induced by the repeated passage of train loads.

The procedure followed at CTB implies that fatigue tests are conducted by reproducing the dynamic loads generated by the passage of a standard high-speed train (specifically the Siemens S-103) operating at a nominal speed of 300 km/h. The testing protocol is designed to apply a sequence of cyclic loads equivalent to the cumulative effect of one million axles, thereby enabling the assessment of long-term mechanical performance and potential degradation mechanisms within the track components under realistic service conditions.

It should be noted that, in this case, the section was also subjected to fatigue tests produced by the passage of 400,000 axles of a freight train operating at speeds of 80, 100, and 120 km/h.

To evaluate the performance of the different components of the track section, data from all sensors were collected approximately every 10,000 axles. These acquisitions were performed

once the simulated train load had finished and with all actuators fully lifted, i.e., under zero-load conditions (recorded as files 000). Additionally, a full train passage was captured roughly every 50,000 axles, following a procedure analogous to that used during the dynamic characterisation of the track (files of type ABC).

In this study, the vertical displacements of the layers composing the railway track section were the priority, as these are most directly related to long-term settlement phenomena. However, the vertical velocity and acceleration of the sleeper vibration were also analysed. These measurements enable the quantification of potential degradation of the section as a function of the number of accumulated axles in the section and the corresponding accumulated load.

In conventional fatigue analyses of ballasted track, the accumulated settlement is typically represented as a function of the total gross tonnage or of the number of load cycles. This approach is appropriate when all cycles are applied under identical loading conditions, particularly when the train speed is kept constant.

However, in the present test programme, the loading applied to the track comes not only from passenger trains but also from freight trains, and, moreover, the same freight train loading was applied at three different speeds. Since train speed affects the dynamic response of the track, the accumulated tonnage alone is no longer sufficient to compare the degradation produced under different testing conditions.

To account for the influence of speed, we introduce a parameter that represents the effective dynamic load applied in each wheel passage. This parameter is referred to as the "*dynamic load index*" in this report and is defined as the product between the static wheel load (Q) and the dynamic amplification factor (*DAF*), which quantifies the increase in rail and track deformation due to train speed. A detailed description of the *DAF* is provided in 6.3.1.3.

The accumulated value of this parameter [$\Sigma(DAF \cdot Q)$] is therefore used as the horizontal axis in the settlement plots. This choice reflects the fact that the severity of each loading cycle (i.e., its capacity to produce permanent deformation in the ballast) depends not only on the applied load but also on the dynamic enhancement induced by speed. As a result, $\Sigma(DAF \cdot Q)$ provides a physically meaningful measure that allows a consistent comparison of settlement rates across the different test velocities, while remaining fully compatible with the conventional interpretation of fatigue in railway tracks.

Table 24 presents the rounded values of the number of accumulated axles, loads and dynamic load index in the test section for each test phase performed.

Table 24.- Accumulated number of axles and load for each test

Accumulated	Stabilization	Dynamic-Passenger	Fatigue-Passenger	Dynamic-Freight	Fatigue-Freight	TOTAL
Axle	64,000	200,000	1,000,000	20,000	400,000	1,684,000

Accumulated	Stabilization	Dynamic-Passenger	Fatigue-Passenger	Dynamic-Freight	Fatigue-Freight	TOTAL
Load (t)	926,000	4,000,000	14,500,000	455,000	9,000,000	28,881,000
Dynamic load index (t)	1,000,000	3,500,000	17,300,000	300,000	6,400,000	28,500,000

6.4.2 PERMANENT SETTLEMENT AT BALLAST LAYER

Figure 113 illustrates the evolution of the permanent vertical displacement observed in the ballast layer compared to the number of accumulated axles recorded in the railway track section. The representative slopes that characterise the evolution of settlement were also determined and graphically represented by dotted lines. The data of the settlements correspond to the two LVDTs installed on the central sleeper, positioned symmetrically about its midpoint, one on each side of the edge, as shown in Figure 87 (right).

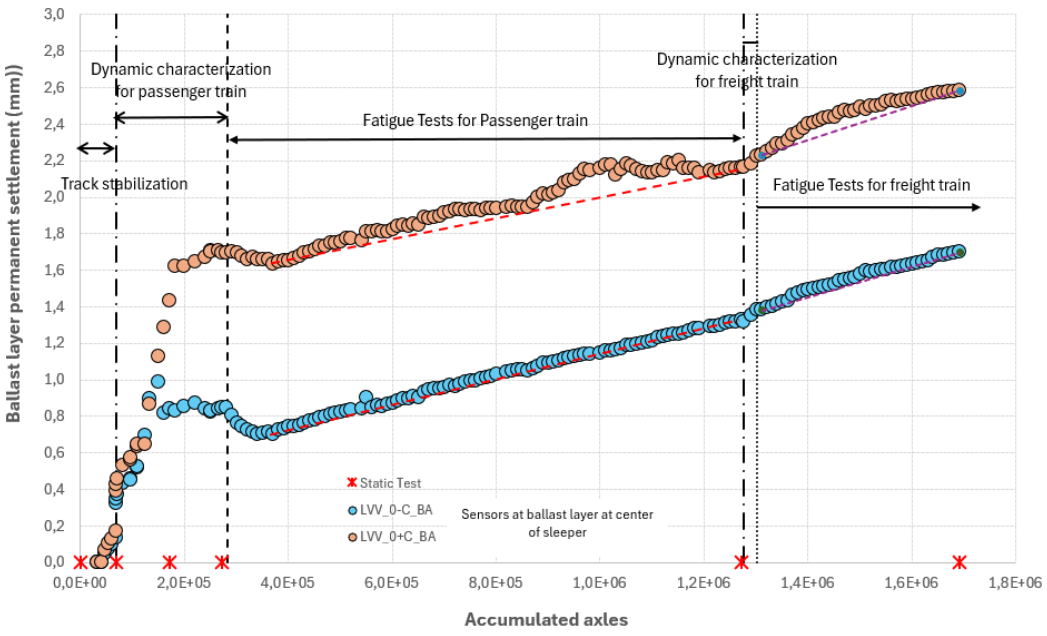

Figure 113.- Ballast layer permanent settlement recorded at accumulated axles

Figure 114 shows the permanent ballast layer settlement for the accumulated load supported by the railway track section.

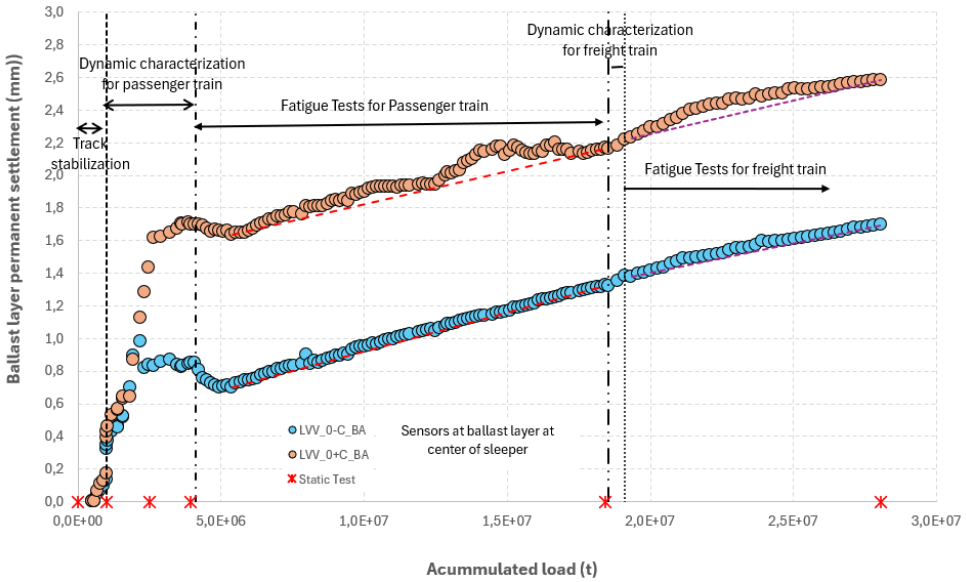

Figure 114.- Ballast layer permanent settlement recorded at accumulated load

Figure 115 shows the permanent settlement for the ballast layer as a function of the accumulated "Dynamic load index" [Σ(DAF·Q)] determined for the railway track section.

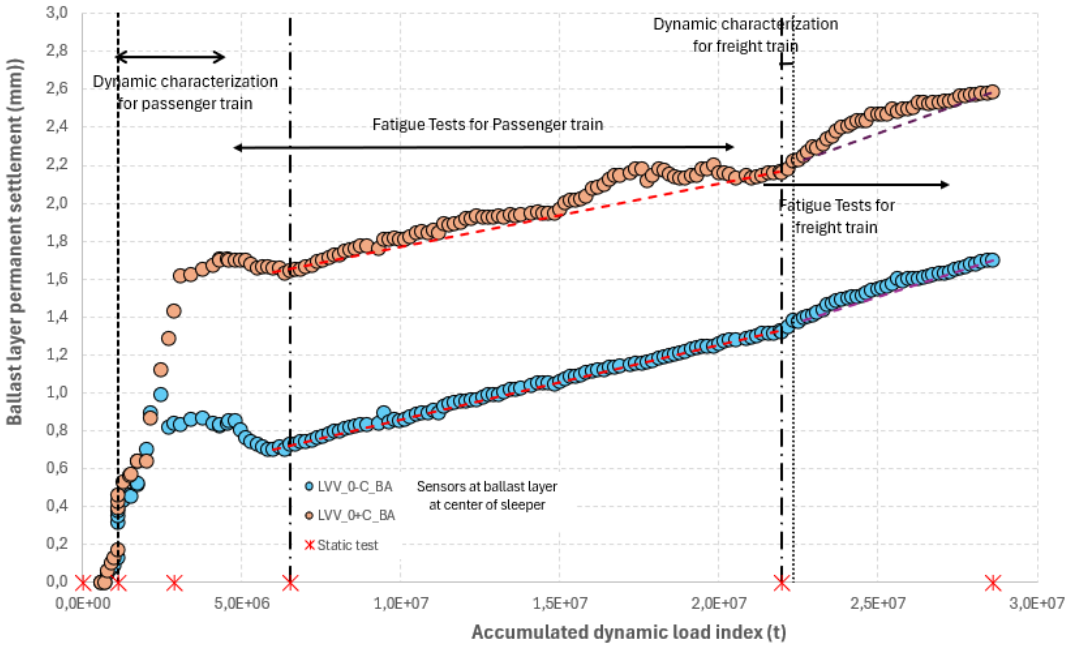

Figure 115.- Ballast layer permanent settlement recorded at accumulated dynamic load index

The analysis of the figure reveals the following facts:

- The ballast layer exhibits progressive permanent settlement under repeated loading, without a sign of apparent stabilisation.
- During the initial phase, a rapid increase in settlement occurs within the first 200,000 accumulated axles, corresponding to track stabilisation, with a value of 0.17 mm.
- During the dynamic loading tests associated with passenger train passages, the LVDT located at 0− recorded a settlement increase of 0.68 mm, whereas the sensor at 0+ measured a much larger settlement of 1.52 mm.
- In the passenger train fatigue tests, settlement increases were more consistent between both sensors, ranging from 0.46 to 0.47 mm.
- During the freight train fatigue test characterisation, the settlement increase of the ballast layer ranged between 0.32 and 0.35 mm.
- So, the total permanent settlement measured in the ballast layer during all the testing programme was between 1.7 and 2.6 mm.

Table 25 summarises the reference values considered for both passenger and freight trains, which serve as the basis for defining the trend curves describing the ballast layer settlement (red and purple dotted lines at previous figures) during fatigue tests.

Table 25.- Reference values for calculating ballast settlement gradients (fatigue tests)

Fatigue Tests for Passenger Train

Ballast Settlement (mm)		Axles (No.)	Load (t)	Dynamic load index (t)
LVV_0-C_BA	LVV_0+C_BA			
0.699	1.634	352,485	5,106,937	6,003,526
1.325	2.164	1,272,485	18,427,387	21,902,630

	Sensor	mm/axle	mm/t	mm/t
Ratio	LVV_0-C_BA	$6.80 \cdot 10^{-7}$	$4.70 \cdot 10^{-8}$	$3.93 \cdot 10^{-8}$
	LVV_0+C_BA	$5.77 \cdot 10^{-7}$	$3.98 \cdot 10^{-8}$	$3.34 \cdot 10^{-8}$

Fatigue Tests for Freight Train

Ballast Settlement (mm)		Axles (No.)	Load (t)	Dynamic load index (t)
LVV_0-C_BA	LVV_0+C_BA			
1.378	2.229	1,322,395	19,572,497	22,646,102
1.696	2.582	1,692,373	28,061,086	28,598,134

	Sensor	mm/axle	mm/t	mm/t
Ratio	LVV_0-C_BA	$8.57 \cdot 10^{-7}$	$3.74 \cdot 10^{-8}$	$5.33 \cdot 10^{-8}$
	LVV_0+C_BA	$9.56 \cdot 10^{-7}$	$4.17 \cdot 10^{-8}$	$5.94 \cdot 10^{-8}$

As indicated by the data in the table, the calculated gradients are consistently low. The settlement per million axles ranged from 0.58 to 0.68 mm for passenger trains and from 0.86 to 0.96 mm for freight trains. Expressed in terms of settlement per million tonnes, the values ranged between 0.04 and 0.05 mm for passenger traffic and are approximately 0.04 mm for freight traffic.

6.4.3 PERMANENT SETTLEMENT AT LECA EMBANKMENT

The following figures illustrate the permanent settlement recorded in the LECA embankment in relation to the cumulative number of axles (Figure 116), the cumulative applied load (Figure 117), and the cumulative "Dynamic load index" [Σ(DAF·Q)] determined for the railway track section (Figure 118). All graphs also include selected measurements obtained from sensors installed on adjacent sleepers (+1 and –2), to illustrate the overall settlement trend.

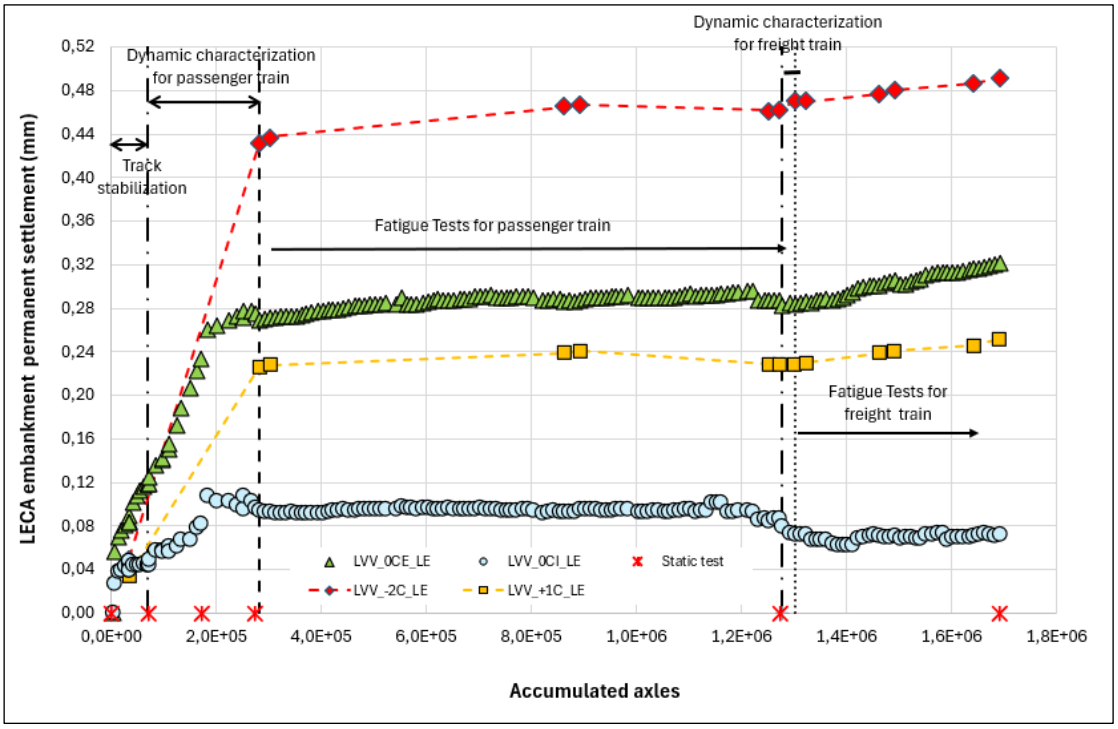

Figure 116.- LECA embankment permanent settlement recorded at accumulated axles

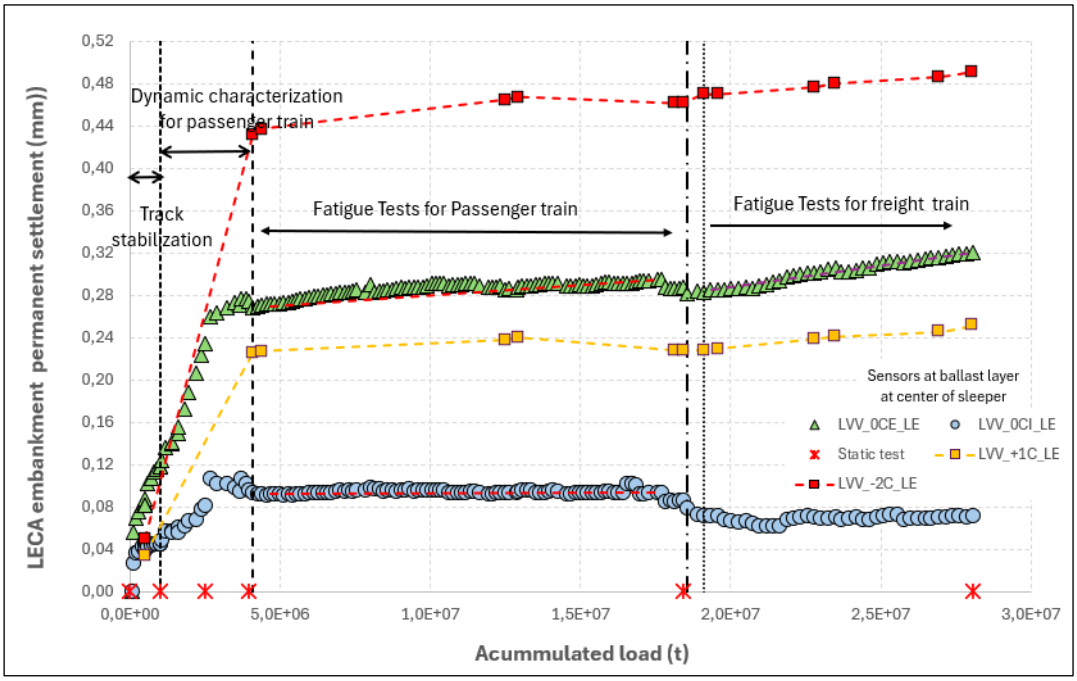

Figure 117.- LECA embankment permanent settlement recorded at accumulated load

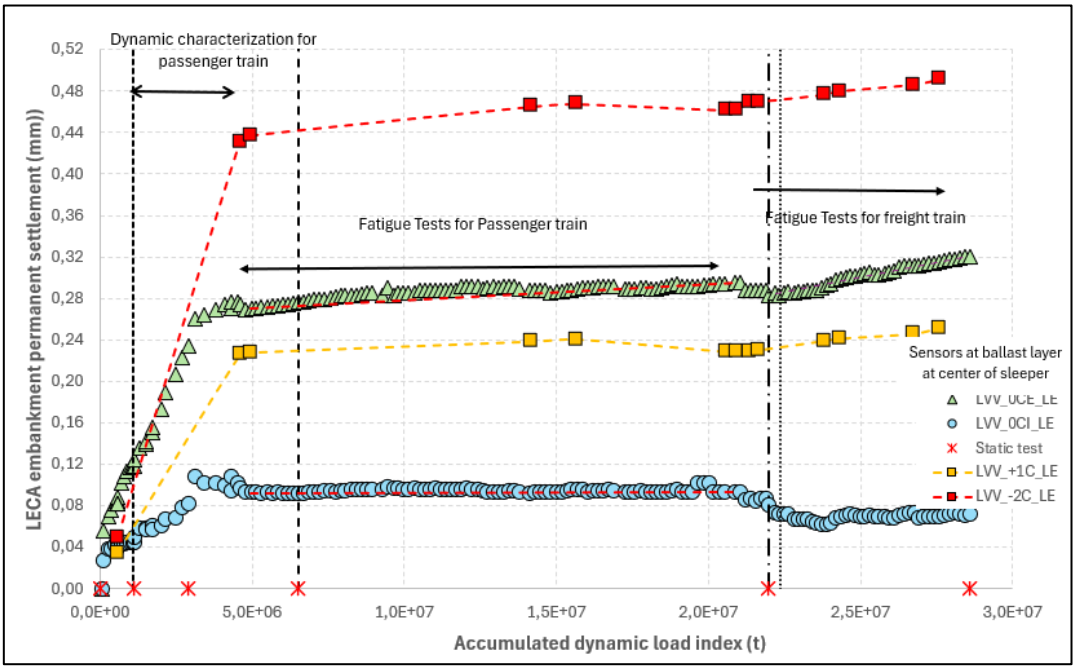

Figure 118.- LECA embankment permanent settlement recorded at accumulated dynamic load index

The analysis of the figures that present the permanent settlements recorded in the LECA embankment throughout the entire testing programme makes it possible to highlight the following facts:

- During the track stabilisation phase, settlements of 0.05 mm and 0.12 mm were measured by the inner and outer rail LVDTs, respectively.
- During the dynamic characterisation tests associated with passenger train passages, an additional increase in settlement was observed, ranging from 0.05 mm (inner rail measurement) to 0.15 mm (outer rail measurement).
- The data recorded during the passenger train fatigue tests indicate a negligible increase in permanent settlement at the inner rail, with a value of approximately 0.02 mm measured at the outer rail.
- During the freight train fatigue tests, a divergence was observed in the behaviour of the sensors installed on the central sleeper. While the sensor located towards the outer rail recorded an increase in settlement, the sensor near the inner rail exhibited the opposite trend.
- To verify the overall settlement trend of the LECA embankment, measurements from sensors installed on adjacent sleepers (+1 and –2) were included in all graphs. These data (yellow squares and red diamonds) indicate a progressive increase in LECA embankment settlement with the number of freight train passages.

Table 26 summarises the reference values considered for both passenger and freight trains, which serve as the basis for defining the trend curves describing LECA embankment layer settlement (red and purple dotted lines at previous figures) during fatigue tests. The table also presents data from the sensors installed on sleepers +1 and –2, which are used as reference points for evaluating performance during the freight train fatigue tests, together with the sensor located on the central sleeper along the inner rail.

Table 26.- Reference values for calculating LECA embankment settlement gradients (fatigue tests)

Fatigue Tests for Passenger Train

LECA Settlement (mm)		Axles (No.)	Load (t)	Dynamic load index (t)
LVV_0CE_LE	LVV_0CI_LE			
0.0927	0.270	292,485	4,238,212	4,966,291
0.0935	0.295	1,222,469	17,703,218	21,038,449

	Sensor	mm/axle	mm/t	mm/t
Ratio	LVV_0CE_LE	$8.28 \cdot 10^{-10}$	$5.72 \cdot 10^{-11}$	$4.79 \cdot 10^{-11}$
	LVV_0CI_LE	$2.68 \cdot 10^{-8}$	$1.85 \cdot 10^{-9}$	$1.55 \cdot 10^{-9}$

Fatigue Tests for Freight Train

LECA Settlement (mm)		Axles (No.)	Load (t)	Dynamic load index (t)
LVV_0CE_LE	LVV_0CI_LE			
--	0.285	1,292,403	18,884,376	22,199,315
--	0.321	1,692,373	28,061,086	28,598,134

Ratio	Sensor	mm/axle	mm/t	mm/t
	LVV_0CE_LE	--	--	--
	LVV_0CI_LE	$8.98 \cdot 10^{-8}$	$3.91 \cdot 10^{-9}$	$5.61 \cdot 10^{-9}$

Fatigue Tests for Freight Train

LECA Settlement (mm)		Axles (No.)	Load (t)	Dynamic load index (t)
LVV_+1C_LE	LVV_-2C_LE			
0.230	0.470	1,322,395	19,572,497	22,646,102
0.252	0.492	1,692,373	28,061,086	28,598,134

Ratio	Sensor	mm/axle	mm/t	mm/t
	LVV_+1C_LE	$5.85 \cdot 10^{-8}$	$2.55 \cdot 10^{-9}$	$3.64 \cdot 10^{-9}$
	LVV_-2C_LE	$5.79 \cdot 10^{-8}$	$2.52 \cdot 10^{-9}$	$3.60 \cdot 10^{-9}$

As indicated by the table, the calculated gradients are consistently low. The settlement per million axles ranged from 0.83 μm to 27 μm for passenger trains, and is about 58 μm for freight trains. Expressed in terms of settlement per million tonnes, the values ranged between 0.06 and 1.8 μm for passenger traffic and are approximately 3.9 μm for freight traffic.

These results indicate that the LECA embankment experiences minimal settlement compared to the ballast layer, as expected due to the depth at which the LECA embankment was built.

6.4.4 EVOLUTION OF TOTAL DISPLACEMENT OF THE TRACK SECTION

This section presents the evolution of the total railway track section displacement recorded by the laser system, at the outer rail, during fatigue tests induced by the passage of passenger and freight trains. To this end, Figure 119 shows several of the values recorded by the laser system located on the sleeper 0+ (LSV_0+E_PC-MA) as a function of the number of accumulated axles. The records from which these were obtained are similar to the ones shown in Figure 76.

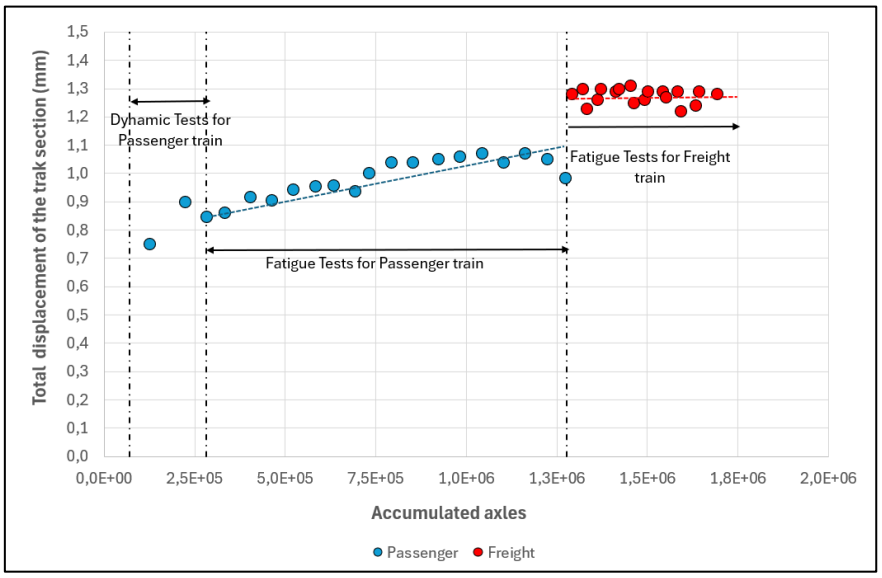

Figure 119.- Total displacement of the track section during fatigue test at accumulated axles

Based on the recorded displacements during the fatigue tests, the track section exhibits a stable and controlled response under both passenger and freight loading. During the passenger train phase, the total displacement increases gradually from approximately 0.85 mm to 1.10 mm, suggesting a possible progressive and predictable settlement under moderate cyclic loading. After switching to freight trains, the displacement shifts to a higher level (ranging between 1.22 mm and 1.33 mm) but remains nearly constant, indicating the possibility that the structure accommodates the higher axle loads without entering a regime of accelerated degradation. Overall, the observed behaviour implies that the track system may retain adequate stiffness and structural integrity throughout the entire accumulated load range.

6.4.5 EVOLUTION OF BALLAST LAYER DISPLACEMENT

This section presents the evolution of the ballast layer displacement recorded by the LVDT, at the centre of the sleeper, during fatigue tests induced by the passage of passenger and freight trains. To this end, Figure 123 shows several of the values recorded by the LVDT (LVV_0-C_BA) as a function of the number of accumulated axles. The records from which these were obtained are similar to the ones shown in Figure 88.

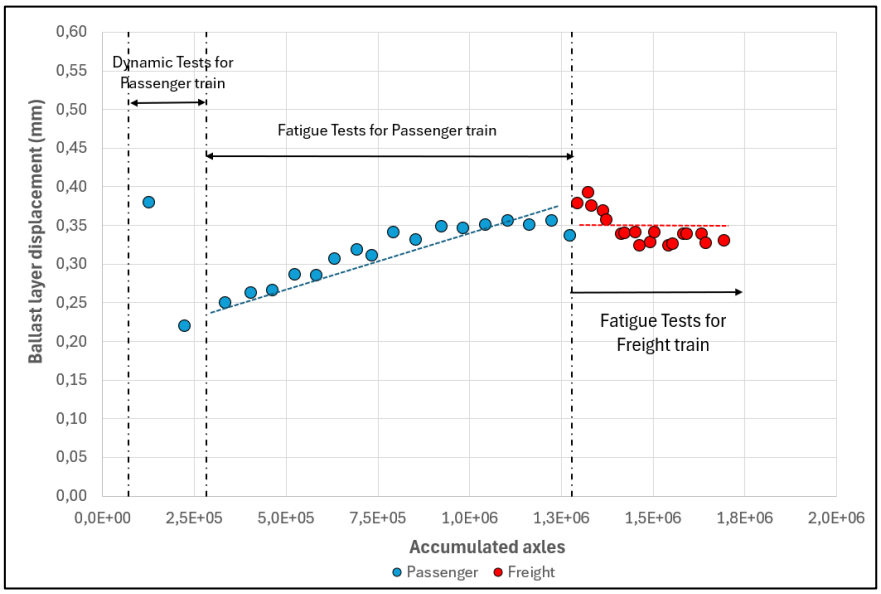

Figure 120.- Ballast layer displacement during fatigue test at accumulated axles

From the measured displacements within the ballast layer during the fatigue tests, the ballast layer exhibits a stable and well-controlled response under both passenger and freight traffic. During the passenger train loading phase, the ballast displacement increases progressively from approximately 0.24 mm to 0.38 mm, which may indicate a gradual and predictable densification of the ballast under repeated moderate axle loads. After the transition to freight trains, the displacement shifts to a slightly higher level, ranging between 0.32 mm and 0.40 mm, but remains essentially stable with low scatter, suggesting the possibility that the ballast layer accommodates the higher axle loads without entering a regime of accelerated settlement or structural degradation. Overall, the observed behaviour may imply that the ballast maintains adequate stiffness and internal stability throughout the entire accumulated loading sequence.

6.4.6 EVOLUTION OF LECA EMBANKMENT DISPLACEMENT

This section presents the evolution of the LECA embankment displacement recorded by the LVDT, at the centre of the sleeper, during fatigue tests induced by the passage of passenger and freight trains. To this end, Figure 121 shows several of the values recorded by the LVDT (LVV_0CE_LE) as a function of the number of accumulated axles. The records from which these were obtained are similar to the ones shown in Figure 95.

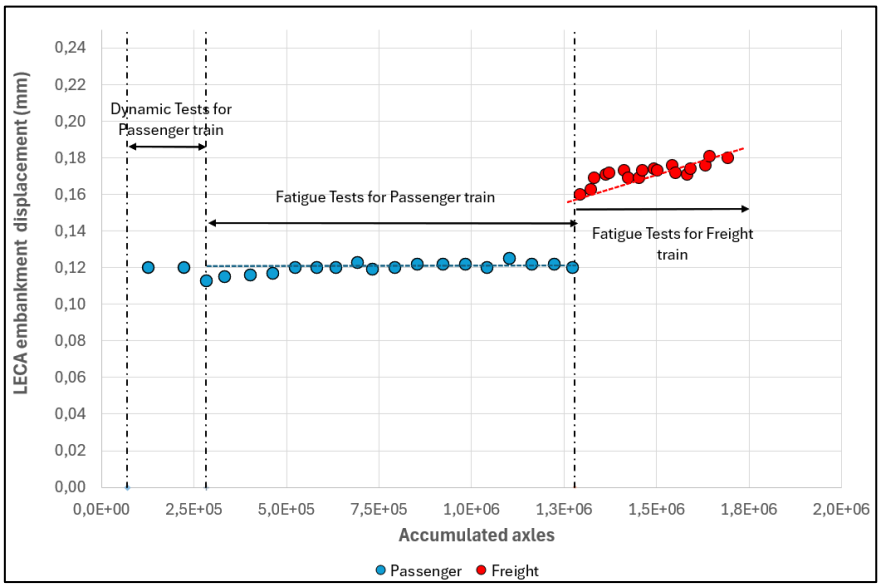

Figure 121.- LECA embankment displacement during fatigue test at accumulated axles

The recorded displacements in the LECA embankment layer exhibit a highly stable mechanical response throughout the fatigue loading sequence. During the passenger train phase, the displacement remains nearly constant, varying only between 0.11 mm and 0.13 mm, which may indicate that the embankment undergoes minimal additional compaction under moderate cyclic loading. After the transition to freight trains, the displacement increases slightly to a range between 0.16 mm and 0.18 mm, showing a mild upward trend that could be associated with the higher axle loads applied. However, the evolution remains smooth and limited in magnitude, suggesting the possibility that the LECA embankment retains sufficient stiffness and volumetric stability without signs of accelerated settlement or structural degradation under heavier traffic. Overall, the response suggests that the LECA embankment may behave as a resilient and deformation-tolerant component of the track system.

6.4.7 EVOLUTION OF THE SLEEPER VELOCITY

This section presents the evolution of the speed recorded on the sleeper, at the outer rail, during fatigue tests induced by the passage of passenger and freight trains. To this end, Figure 122 shows several of the values recorded by the geophone located on the sleeper as a function of the number of accumulated axles.

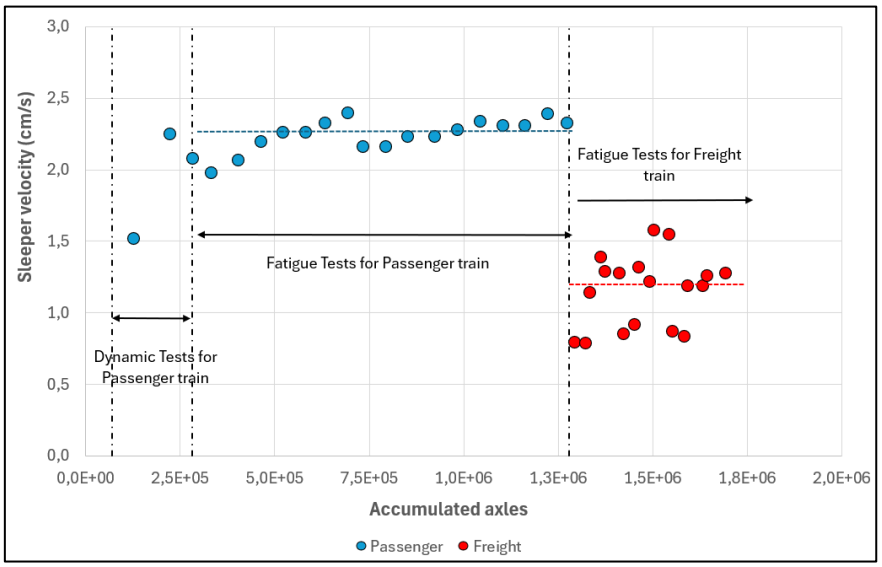

Figure 122.- Sleeper velocity recorded during fatigue test for passenger and freight trains

As shown in the previous graph, the sleeper velocity values recorded for passenger trains during fatigue tests (train passages at a speed of 300 km/h) ranged from 2.0 to 2.4 cm/s (with a representative value of 2.3 cm/s). In the case of freight trains, travelling at 120 km/h, a sleeper velocity between 0.8 and 1.55 cm/s was recorded by the sensor located on the outer rail. In this case, a representative value of 1.25 cm/s could be selected.

The sleeper velocity values recorded during the fatigue tests are similar to those obtained in the dynamic tests with passenger trains travelling at 300 km/h and freight trains at 120 km/h, as presented in section 6.3.2.

Thus, for passenger trains, representative sleeper velocities of 2.1 cm/s and 2.2 cm/s can be considered for the dynamic and fatigue tests, respectively. For freight trains, the corresponding values are 1.15 cm/s and 1.25 cm/s.

6.4.8 EVOLUTION OF THE SLEEPER ACCELERATION

This section presents the evolution of the acceleration recorded on the sleeper, at the outer rail, during fatigue tests induced by the passage of passenger and freight trains. To this end, Figure 123 shows several of the values recorded by the accelerometer located on the sleeper as a function of the number of accumulated axles.

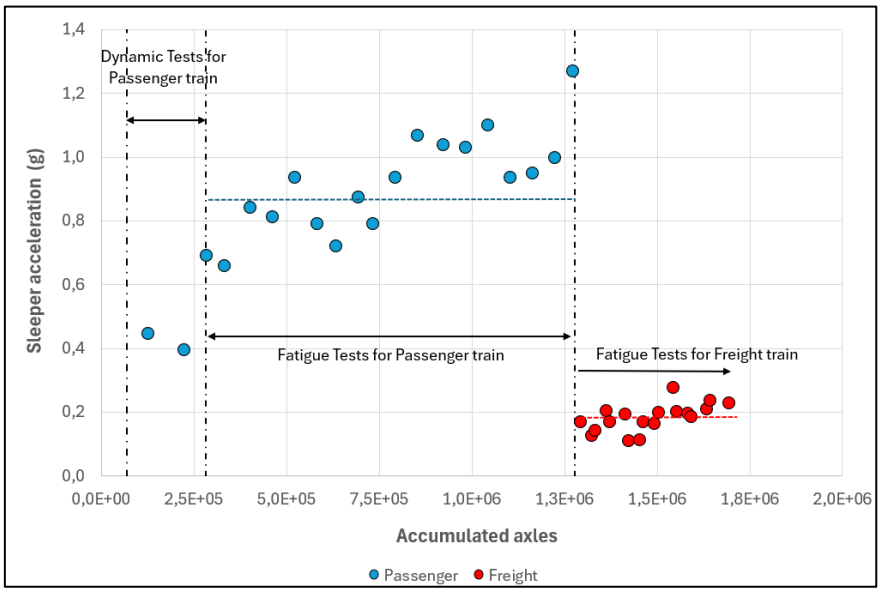

Figure 123.- Sleeper acceleration values recorded during fatigue test for passenger and freight trains

As shown in the previous figure, the acceleration values measured on the sleeper during the fatigue tests ranged from 0.66 to 1.27 g for passenger trains (trains travelling at 300 km/h), with a representative value of 0.87 g. In the case of freight trains, travelling at 120 km/h, the recorded accelerations vary between 0.17 and 0.28 g, with a representative value of 0.2 g. In this case, for both types of trains, the values tend to increase with the number of accumulated axles.

For the dynamic tests, representative acceleration values of 0.45 g for passenger trains and 0.21 g for freight trains can be considered, as shown in 6.3.11.

6.4.9 EVOLUTION OF THE BALLAST PARTICLE ACCELERATION

This section presents the evolution of the acceleration recorded by the ballast particle located at the ballast layer, at the outer rail, during fatigue tests induced by the passage of passenger and freight trains. To this end, Figure 124 shows several of the values recorded by the accelerometer located as a function of the number of accumulated axles.

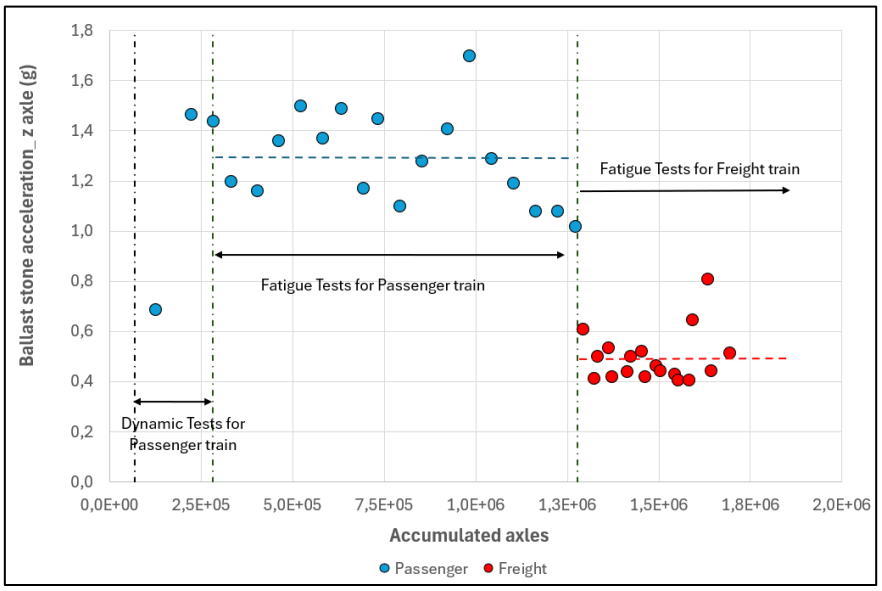

Figure 124.- Ballast acceleration values (at z axle) recorded during fatigue test for passenger and freight trains

As shown in the previous figure, the acceleration values measured on the ballast particle during the fatigue tests ranged from 1.0 to 1.7 g for passenger trains (trains travelling at 300 km/h), with a representative value of 1.28 g. In the case of freight trains, travelling at 120 km/h, the recorded accelerations vary between 0.4 and 0.8 g, with a representative value of 0.5 g. In this case, there is no significant increment in the acceleration values with the increase in the number of accumulated axles.

For the dynamic tests, representative acceleration values of 1.0 g for passenger trains and 0.5 g for freight trains as determined in 6.3.12. These values are in good agreement with those obtained at fatigue tests.

7. COMPARATIVE ANALYSIS OF RESULTS WITH OTHER SECTIONS TESTED AT CTB

7.1 GENERAL ASPECTS

The primary objective of this study was to assess the behaviour of a railway track section incorporating LECA material within the embankment. Due to the lack of prior experience with this type of material, the performance analysis was conducted by comparing the obtained results with results from tests performed at CTB, on railway track sections of Spanish high-speed lines, constructed using the materials and conditions specified by ADIF.

The comparison is performed based on the results presented in the preceding sections, together with the results obtained from the analysis of the railway section under passenger train traffic conditions.

7.2 STATIC TEST RESULTS

The main purpose of the static tests was to assess the stiffness of the railway track section. As detailed in 6.2, these tests were conducted at different stages of the process: immediately after the track construction was completed, once the track stabilisation was carried out, after the dynamic tests, and finally at the end of the fatigue tests.

Figure 125 illustrates the deflection of the rail from which the railway stiffness is determined in the static tests performed on the section built with LECA material (left) compared to standard values for a typical section of Spanish HSL (right), both after the track stabilisation.

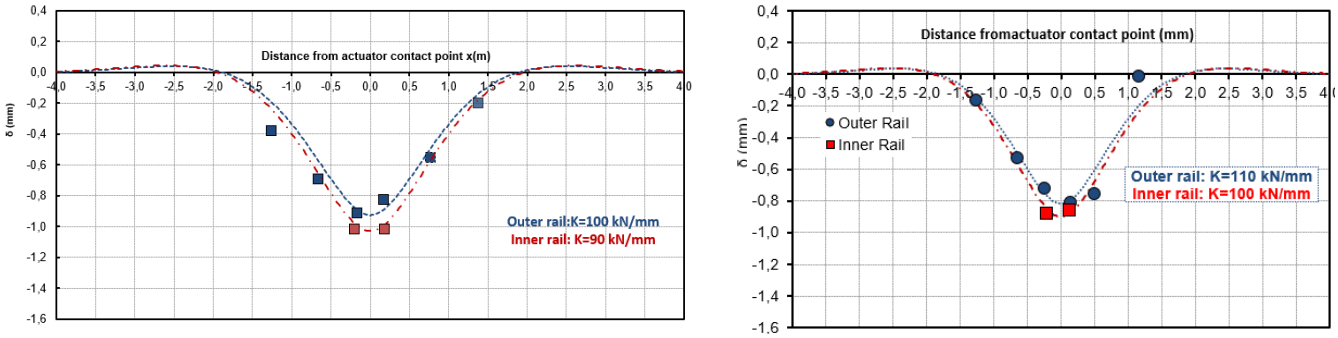

Figure 125.- Stiffness values obtained in LECA section (left) and HSL tested at CTB (right) after track stabilisation

The figure above demonstrates that the stiffness values in both cases were largely comparable, with a slight reduction observed in the section incorporating the LECA material. However, these values remain within a range that allows for direct comparison.

7.3 DYNAMIC TEST RESULTS

7.3.1 VERTICAL DISPLACEMENTS OF THE ENTIRE RAILWAY TRACK SECTION

The movement of the entire railway track section was recorded using laser systems installed on the rails and on reference points. These movements are referred to in the graphs as *rail deflection or total displacement*. Figure 126 displays the results obtained comparing both the embankment constructed with LECA material and a conventional high-speed rail section (HSL) tested at the CTB.

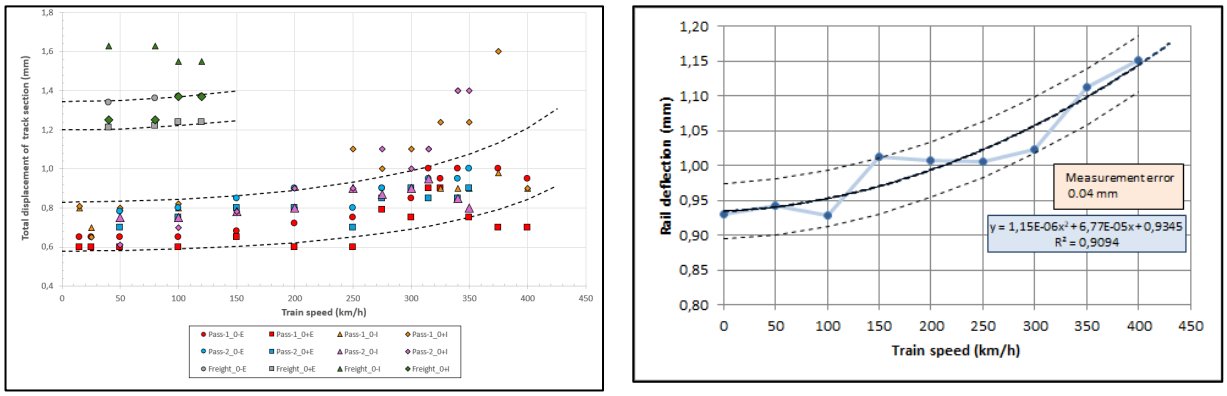

Figure 126.- Rail deflections recorded in LECA section (left) and HSL at CTB (right)

In both railway track sections, an increase in rail deflection is documented as the speed of the trains escalates. In the section constructed with LECA material, the representative vertical displacement values ranged from 0.6 mm to 1.2 mm. Conversely, the section featuring an embankment entirely comprised of earth material exhibited deflection values ranging from 0.90 mm to 1.15 mm. It can be concluded that the values in both types of sections were of similar magnitude.

On the other hand, the percentage contributions of vertical movements affecting each layer of the railway track section can be compared. To achieve this, the vertical displacements measured in the pad, ballast layer, sub-ballast layer with form layer, and those occurring in the embankment were considered. Table 27 presents the percentage of vertical movement, relative to the total vertical displacement measured using laser systems, for each layer. This data is provided for both the section constructed with LECA material and the conventional HSL.

Table 27.- Comparison of each layer contribution to the total vertical displacement for LECA and HSL section

Layer	Contribution to total settlement (%)	
	LECA section	*HSL section*
Pad	35	25

Layer	Contribution to total settlement (%)	
	LECA section	*HSL section*
Ballast layer	45	45
Sub-ballast and Form layer	4	20
Embankment	16 [(a)]	10
Total	100	100
Note (a): In the LECA section, "Embankment" includes LECA material		

As can be seen in the table above, the contribution of each layer to the total settlement of the railway section is similar. The largest proportion of settlement comes from the ballast layer and the under-sleeper pad. The biggest difference is in the contribution from the form and the sub-ballast layer. This may be due to the fact that the compaction carried out on these two layers in the LECA section was very intense.

7.3.2 CRITICAL SPEED

The tests conducted at the CTB enabled the determination of the critical speed of the section under study. In addition, the instrumentation work carried out by Laboratorio de Geotecnia-CEDEX on in-service high-speed lines provided independent estimates of this parameter.

The values obtained for the section constructed with LECA material, together with those corresponding to a representative Spanish high-speed line section, are presented beneath the DAF curves in Figure 127.

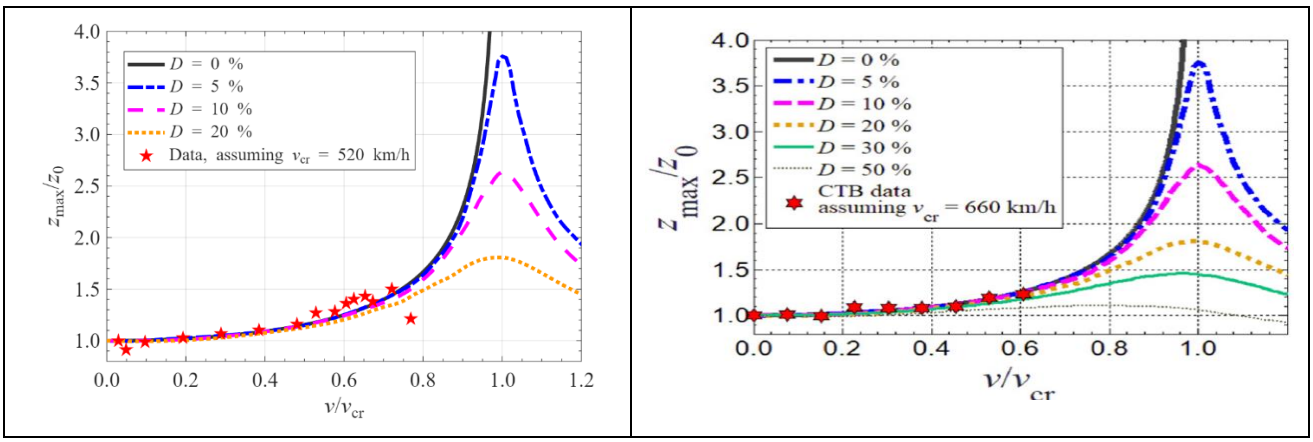

Figure 127.- Critical speed at LECA section (left) and HSL at CTB (right)

In both cases, the experimental data show a satisfactory agreement with the fitted curves. The resulting critical speed is approximately 520 km/h for the section constructed with LECA-type

material, whereas for the representative Spanish high-speed section, the corresponding value is about 660 km/h, in the tests performed in CTB, while it is around 600 km/h in the tests performed on in-service high-speed lines.

Since the LECA layer exhibits a shear-wave velocity (around 285 m/s – see Section 5.2.3) clearly higher than ballast layers in high-speed railway lines (see the report published by CEDEX in 2021[9]), from Kausel et al. (2020)[10] it is concluded that the previous difference (520 vs 660 km/h) is mainly due to the mechanical condition of the ballast layer.

7.3.3 VERTICAL VELOCITIES IN SLEEPERS

Geophones installed on sleepers were used to measure the velocities induced in the sleepers by passing trains. Figure 128 displays results collected from the section with LECA material on the left, and those determined from a section of HSL on the right.

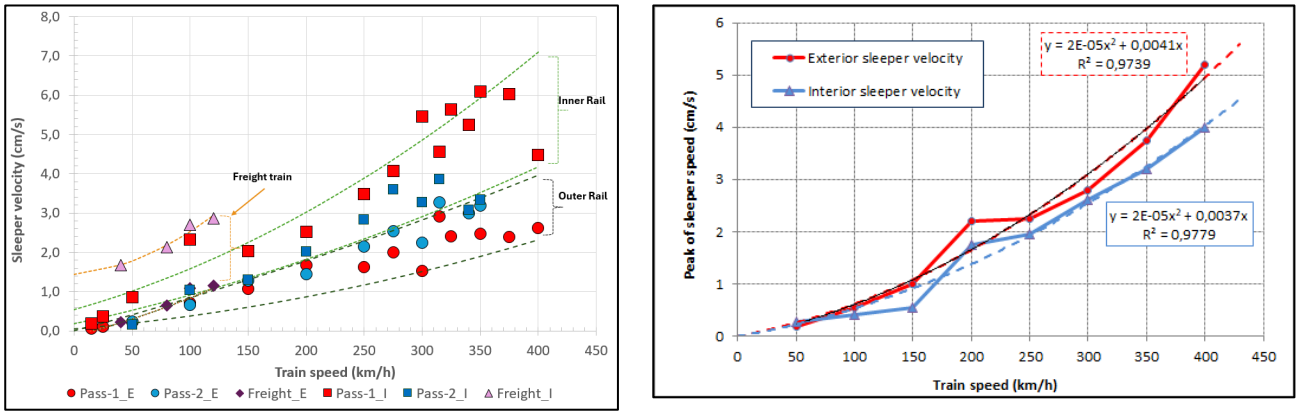

Figure 128.- Sleeper velocity recorded for LECA section (left) and HSL at CTB (right)

As shown in the graphs, both sections exhibit a clear increase in the vertical velocity of the sleeper with increasing train speed.

The results obtained in the HSL section fall just in the middle of the values determined in the LECA section, where there is a slightly wider dispersion: the maximum recorded values ranged between 0.5 and 6.0 cm/s, while in the HSL section, the range is only between 4 and 5 cm/s.

It should also be noted that, in both sections, the measured sleeper velocities differ depending on whether the inner or outer rail is considered, indicating a certain degree of transverse asymmetry in the dynamic response.

[9] Report published by CEDEX in 2021, entitled "Determinación de la velocidad de propagación de ondas S en el balasto del Cajón Ferroviario del CEDEX mediante el análisis espectral de ondas superficiales (campañas 2008, 2019 Y 2020)". Informe Parcial nº8 de la serie "Proyectos internos del Laboratorio de Geotecnia (Trienio 2019-2021) - Trabajos internos realizados en el Cajón Ferroviario del CEDEX". Informes oficiales del CEDEX. Clave CEDEX: 80-919-1-002. Año 2021.

[10] Kausel, E., Estaire, J. & Crespo-Chacón, I. 2020. Proof of critical speed of high-speed rail underlain by stratified media. Proc. R. Soc. A 476: 20200083. http://dx.doi.org/10.1098/rspa.2020.0083

These results show that there is a very similar behaviour of both sections relative to the velocity of sleeper vibration.

7.3.4 VERTICAL ACCELERATIONS IN SLEEPERS

Accelerometers mounted on sleepers were used to measure sleeper acceleration induced by passing trains. Figure 129 displays records collected from the section with LECA material on the left, and those recorded from a section of HSL on the right.

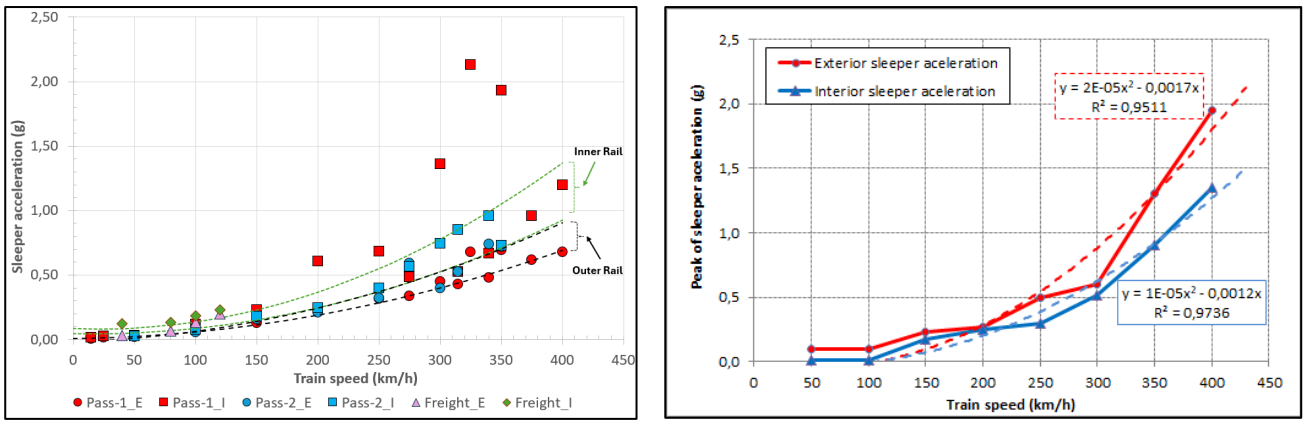

Figure 129.- Sleeper acceleration recorded for LECA section (left) and HSL at CTB (right)

The graphs above clearly illustrate that the acceleration values measured in both sections were quite similar. In the section containing LECA material, the acceleration values ranged from 0 to 1.5 g, while in the section with earth material, they ranged from 0 to 1.9 g. Additionally, in both sections, there is a noticeable increase in recorded acceleration as the train velocity increases. Therefore, it can be concluded that the behaviour with respect to this parameter is quite similar in both sections.

7.4 FATIGUE TEST RESULTS

This section presents a comparison between the results obtained from fatigue tests (simulating passenger train loading on the LECA section) in terms of permanent settlements within the ballast layer, and the fatigue criteria established for high-speed railway sections tested at the CTB.

The study by Estaire et al. (2026)[11] compiles settlement laws for ballast beds derived from experimental testing at the CTB, encompassing a range of representative track section configurations.

Figure 130 (left) summarises the different track section typologies for which the fatigue law of the ballast layer has been established. A distinction is made according to the type of sub-ballast

[11] Estaire, J. Cámara, J.L., and Santana, M. Settlement laws of bed layers of a ballast track as determined in CEDEX Track Box. 12th International Conference on Bearing Capacity of Roads, Railways, and Airfields; 12th BCRRA 26 (to be published in June 2026).

employed, namely granular sub-ballast (with thicknesses of 20–30 cm) and bituminous sub-ballast (ranging from 8 to 16 cm in thickness). In addition, the modelling speed, the overall stiffness of the track system, and the number of applied axle loads are also indicated.

Figure 130 (right) presents, for each of the modelled tests, the ballast layer settlement normalised per million axles, together with the corresponding applied axle load. It also includes the parameters *a* and *b* used to characterise the relationship between settlement (δ) and the number of load cycles (*N*).

Test	Track characteristics			Train characteristics		Number of cycles
	Track system	Sub-ballast	Stiffness K (kN/mm)	Speed (km/h)	Axle load (kN)	
1	A	Granular:30 cm	81	300-360	119-178	2,0 x 106
2	A	Bituminous:12 cm	122	300	85-138	1,0 x 106
			121		170	1,0 x 106
			128		170	1,0 x 106
			119		170	0,3 x 105
3	A	Bituminous:8 cm	106-110	300	170-210	4 tests 1,0 x 106
4	A	Bituminous:16 cm	104-109	300	170-210	4 tests 1,0 x 106
5	A	Bituminous:12 cm	120-129	120	225	2 tests 1,0 x 106
			121		250	2 tests 1,0 x 106
6	A	Bituminous8 cm	113-127	120	225	2 tests 1,0 x 106
			124-128		250	2 tests 1,0 x 106
7	B	Bituminous12 cm	78	120	225	2,0 x 106
8	B	Bituminous12 cm	79	120	225	1,0 x 106
9	A	Granular: 20 cm	64	320	165	1,3 x 106
10	A	Granular: 20 cm	90	320	165	1,0 x 106

Track system A: Sleeper: GIF AI-99 // Pad: 100 kN/mm
Track system B: Sleeper: B90.2 // Pad:450 kN/mm // Under sleeper pad: G04 (5LN1010)

Test	Settlement for 10^6 axels (mm)	Train speed (km/h)	Axle load (kN)	Track stiffness (kN/mm)	Parameter "a"	Parameter "b"
1	1,52	300	170	81	0,085	0,180
2	0.31	300	85-138 (112)[1]	121	0.029	0.166
	0.58	300	170	122	0.063	0.162
	0.56	300	170	128	0.042	0.188
	---	300	170	119	0.057	0.145
3	0.78	300	170-210 (190)[1]	106	0.053	0.194
	0.68	300	170-210 (190)[1]	110	0.068	0.167
	0.71	300	170-210 (190)[1]	109	0.107	0.139
	0.70	300	170-210 (190)[1]	108	0.088	0.150
4	0.80	300	170-210 (190)[1]	108	0.078	0.168
	0.55	300	170-210 (190)[1]	104	0.064	0.155
	0.65	300	170-210 (190)[1]	106	0.082	0.150
	0.41	300	170-210 (190)[1]	109	0.050	0.153
5	0.81	120	225	129	0.115	0.142
	0.86	120	225	120	0.127	0.139
	0.71	120	250	121	0.110	0.135
	0.62	120	250	121	0.075	0.153
6	0.75	120	225	113	0.099	0.144
	0.85	120	225	127	0.061	0.190
	0.95	120	250	128	0.125	0.146
	0.77	120	250	124	0.072	0.172
7	1.10	120	225	78	0.082	0.189
8	1.14	120	225	79	0.230 (2)	0.116 (2)
9	1.76	320	166	64	0.120	0.193
10	0.95	320	166	90	0.075	0.185

Notes: (1)Values in brackets represent an average load; (2)Out of range value

Figure 130.- Summary of tests evaluated to determine ballast settlement laws (left) and characteristics of each model (right)

The slope of the settlement law obtained for each of the tested models for the high-speed section evaluated at the CTB ranges from 8.08×10^{-8} to 1.10×10^{-7}, with a representative value of 3×10^{-7} for the section with granular sub-ballast. In contrast, for the LECA section, the corresponding values are slightly higher, ranging from 5.77×10^{-7} to 6.80×10^{-7}.

Figure 131 illustrates the settlement trends obtained for the ballast layer in the LECA section, shown in red, alongside the corresponding trends from previous CTB tests on high-speed sections with granular sub-ballast (Tests 9 and 10), marked with black lines. As shown, the LECA section exhibits a slightly steeper gradient.

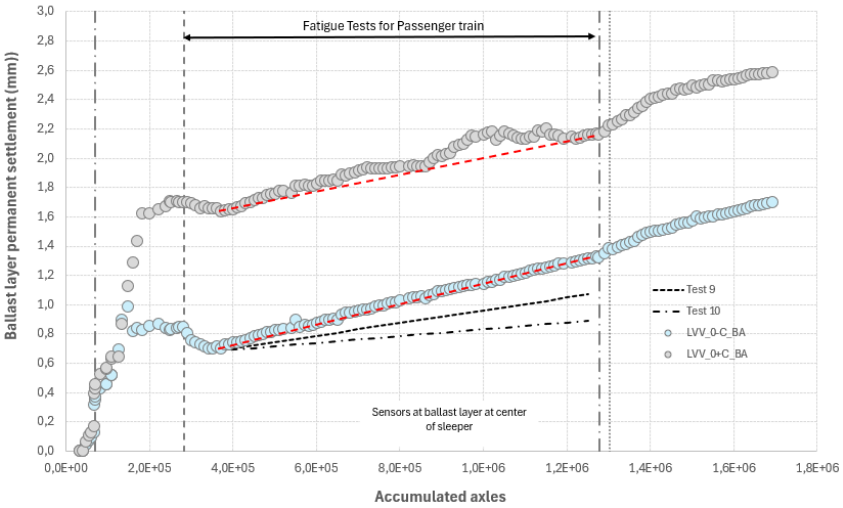

Figure 131.- Fatigue Test Evolution in the Ballast Layer: Passenger Train on the LECA Section (Red) and CTB Tests 9 and 10 (Black)

8. SUMMARY AND CONCLUSIONS

8.1 SUMMARY

Below is a summary of the most relevant points of this report:

- This work is part of the European GEOLAB Project (No. 101006512), whose main objective was to enhance the resilience of critical infrastructures. CEDEX participated in this project through the unique infrastructure, CEDEX Track Box (CTB).

- Within this framework, CEDEX developed the PEDLER project, which focuses on analysing the behaviour of a railway section whose embankment incorporates lightweight expanded clay (LECA).

- The most relevant characteristics of the PEDLER project are:

    - Section constructed with:

        - 1.7 m thickness of earth embankment,
        - 1.1 m thickness of LECA embankment,
        - 0.3 m of form layer,
        - 0.3 m of granular sub-ballast,
        - 0.35 m of ballast,
        - Sleeper, rail and fastening system.

    - Analysis of the behaviour of the track section through dynamic and fatigue tests.

    - Modelling of train passages corresponding to Siemens S-103 passenger trains and Type 7 freight trains, defined in Eurocode 1.

- Some of the construction characteristics of the section are as follows:

    - LECA embankment: it was constructed in 15 cm layers, with light watering applied to improve compaction, which was carried out using a vibrating plate. The entire embankment was also wrapped in a non-woven geotextile. The resistance to penetration (q_d) obtained from the PANDA tests was 6 MPa. The modulus of deformation (E_{vd}) determined from the plate load tests was 28 MPa, while the shear wave velocity measured using the SASW method was around 285 m/s.

    - Form layer: it was constructed using granular material with a dry density of 2.25 Mg/m³ and an optimum moisture content of 4.7%. The resistance to penetration was 9.5 MPa and the modulus of deformation was 12 MPa.

    - Sub-ballast layer: it was constructed with granular material. To comply with ADIF specifications, heavier compaction equipment was used than that employed in the underlying layers. A resistance to penetration of 28 MPa and a modulus of deformation of 47 MPa were obtained.

- Ballast layer: the material was sourced from a quarry approved by ADIF for high-speed railway lines. PANDA tests yielded a representative penetration resistance of 18 MPa.

- The section was extensively instrumented, both on its surface and within the embankment. Vertical displacements were measured using laser systems, LVDTs and potentiometers. Velocity was recorded using geophones, accelerations using accelerometers, and pressures using pressure cells. The report describes each of the instrumentation systems used and defines the nomenclature adopted to identify their location within the section.

- The testing programme carried out on the section included: static tests to determine the stiffness of the track structure, dynamic tests to characterise its behaviour under train passages at different speeds (50 to 400 km/h), and fatigue tests to assess its performance after a large number of train passage axles (one million for passenger trains and 400,000 for freight trains).

- Railway stiffness was measured for both the inner and outer rails at different stages of the tests (values are given in Table 13). After the stabilisation of the section (which marked the start of testing), the stiffness was 90 kN/mm for the inner rail and 100 kN/mm for the outer rail. Following the dynamic tests, these values changed to 100 kN/mm and 95 kN/mm, respectively. After the fatigue tests with passenger trains, the stiffness values were 75 kN/mm and 85 kN/mm, and after the fatigue tests with freight trains, 80 kN/mm and 85 kN/mm for the inner and outer rails, respectively.

    - The most relevant characteristics of the **dynamic** tests are:

    - 25 tests were performed by modelling a passenger train passing at speeds from 15 to 400 km/h. For the modelling of freight trains, four tests were conducted at speeds of 40, 80, 100, and 120 km/h.

    - The analysis and verification of the results are based on dynamic amplification curves (DAF). In addition, using the total displacement values of the section, the critical speed of the test section has been determined to be 520 ± 30 km/h. All graphs include the band representing the expected displacement trend based on the critical velocity, and in all cases, the recorded data show good agreement with this theoretical prediction.

    - The total displacements of the section (measured with a laser system) increase with train speed, with those caused by freight trains being larger in magnitude due to their higher axle loads. The recorded displacements show good agreement with the model when using the critical speed. The measured values range from 0.65 to 1.00 mm for passenger trains and from 1.20 to 1.27 mm for freight trains.

    - Calculations of dynamic stiffness indicate that stiffness decreases with increasing train speed, dropping from 103 to 70 kN/mm for passenger trains and from 77 to 74 kN/mm for freight trains. Furthermore, this trend is consistent with the theoretical predictions based on the critical speed.

- The vertical displacements of the under-rail pad were measured using potentiometers. The results indicate that these displacements increase with train speed and are larger for the freight train simulations. For passenger trains, the displacements range from 0.20 to 0.27 mm, while for freight trains they range from 0.27 to 0.37 mm. These movements correspond to pad deformations of 1.5–3.4% for passenger trains and 3.9–5.4% for freight trains.

- Vertical displacements of the ballast layer were measured using LVDTs. The recorded displacements increase with train speed and are slightly higher for the freight train simulations. At speeds up to 250 km/h, the ballast layer measurements exhibit greater variability. For passenger trains, the displacements range from 0.22 to 0.35 mm, while for freight trains they range from 0.30 to 0.38 mm. In all cases, these movements correspond to a variation in ballast layer thickness of less than 0.1%.

- Vertical displacements of the sub-ballast layer were measured using LVDTs. These displacements increase with train speed. For passenger trains, the displacements are below 0.03 mm, corresponding to a layer deformation of less than 0.005%. For freight trains, the displacements are 0.02 mm, corresponding to less than 0.004% deformation. These minimal movements are likely due to the high compaction of the layer.

- Vertical displacements of the ballast layer were measured using LVDTs. The displacements increase with train speed. For passenger trains, the measured values range from 0.06 to 0.12 mm, while for freight trains, they range from 0.12 to 0.17 mm. In both cases, the resulting layer deformations are considered negligible (<0.02%).

- Analysis of the vertical displacements of the entire railway section under passenger train traffic shows that the largest movements occur in the ballast layer, accounting for 45% of the total. This is followed by the rail pad with 35%, the LECA embankment with 16%, and the combined form and sub-ballast layers with 4%. Finally, the earth embankment contributes less than 0.4% of the total displacement.

- The sleeper velocity and acceleration were measured using geophones and accelerometers, respectively. Sleeper velocity increased with train speed, ranging from 0.06 to 3.86 cm/s for passenger trains and from 0.22 to 2.87 cm/s for freight trains. Sleeper acceleration varied between 0.006 and 0.96 g for passenger trains and between 0.03 and 0.23 g for freight trains. Abnormally high values were observed for train passages at speeds between 300 and 350 km/h.

- The instrumented ballast particle recorded an increase vertical acceleration (z-axis) with increasing train speed. Accelerations range from 0.02 to 1.85 g for passenger trains and from 0.16 to 0.75 g for freight trains.

- During the static and dynamic tests, the pressures at the different interfaces of the embankment were recorded. The static tests show good agreement between the measured

average values and those predicted by stress distribution theory. The largest discrepancies occur at the sleeper–ballast interface due to the unique granulometric characteristics of the ballast. This agreement with theory is generally maintained in the dynamic tests. Furthermore, the evolution of pressure with train speed was observed to be fairly stable, with the largest variations occurring at speeds above 250 km/h.

- The most relevant characteristics of the **fatigue tests** are:

  - Permanent settlements have been recorded in both the ballast layer and the LECA embankment. In each case, the results are presented as a function of the cumulative number of axles, the cumulative tonnage, and the cumulative dynamic load index.

  - The permanent settlement of the ballast layer increases with the number of simulated train passages, for both passenger and freight trains. The observed trends indicate increases of 0.6–0.7 mm per million axles for passenger trains and 0.8–0.9 mm per million axles for freight trains.

  - The permanent settlement recorded in the LECA embankment increases with the number of simulated train passages. For passenger trains, settlements range from 0.84 µm to 0.03 mm, while for freight trains they range from 0.06 to 0.09 mm. They are significantly lower than those registered at the ballast layer.

  - The evolution of the total track section displacement shows a stable response, with small, gradual settlements under passenger loading and slightly higher but still steady displacements under freight trains, without signs of progressive degradation.

  - The evolution of the ballast layer displacement shows a gradual increase in displacement under passenger loading and slightly higher but stable values under freight trains, indicating a controlled and non-progressive settlement.

  - The evolution of the LECA embankment displacement exhibits very small and nearly constant displacements under passenger trains and only a slight increase under freight loading, suggesting a highly stable and resilient behaviour.

  - The sleeper velocity induced by train passages was recorded. In terms of velocity, passenger trains generated sleeper velocities ranging from 2.0 to 2.4 cm/s, while freight trains produced a representative value of 1.25 cm/s. These values are consistent with those obtained during the dynamic tests (2.2 cm/s and 1.2 cm/s for passenger and freight trains, respectively).

  - Sleeper accelerations produced by passenger trains increase with the number of accumulated train passages, ranging from 0.66 to 1.27 g. In the case of freight trains, the increase is smaller, with values ranging from 0.17 to 0.28 g. These values fall within the range of those recorded during the dynamic tests (0.45 g for passenger trains and 0.21 g for freight trains).

- The evolution of the vertical acceleration recorded by the instrumented ballast particle shows no clear trend with the increase in the number of simulated train passages. The recorded values range from 1.0 to 1.7 g for passenger trains and from 0.4 to 0.8 g for freight trains. These values fall within the range observed during the dynamic tests (1.0 g and 0.6 g for passenger and freight trains, respectively).

- Some of the parameters presented in this report have been compared with data obtained from CTB tests carried out on high-speed railway sections consisting entirely of earth embankments, with the following conclusions:

  - The stiffness obtained from the static tests is similar in both sections, with representative values of approximately 100 kN/mm.

  - The critical speed of the LECA section has been estimated at 520±30 km/h, compared with 630 km/h for the conventional high-speed railway section. Both values can be considered similar.

  - The sleeper velocity recorded in the LECA section is around 4.5 cm/s, while the values measured in the conventional high-speed railway section range from 2.5 to 6 cm/s. These values are therefore comparable.

  - Sleeper acceleration ranges from 0 to 1.5 g in the LECA section and from 0 to 1.9 g in the conventional section. These values are therefore comparable.

  - The trend in permanent deformation of the ballast layer in the LECA section, as derived from fatigue tests, is slightly higher than that recorded for the high-speed section, with values on the order of 6.3×10^{-7} (LECA) compared to 3×10^{-7} (HSL).

8.2 CONCLUSIONS

Overall, the experimental results obtained in the CEDEX Track Box indicate that the railway track section incorporating a LECA embankment exhibited a satisfactory global mechanical response within the range of loads, train types and speeds considered in the present study.

After the stabilisation stage, the static stiffness of the section reached values within the range commonly observed in other railway track sections tested at the CTB, while the estimated critical speed is at least 1.7 times the current maximum commercial operating speed. From a global dynamic point of view, the behaviour of the section was therefore considered adequate for the loading conditions analysed.

The vertical response of the railway track section was governed mainly by the ballast layer and the under-rail pad, which together accounted for most of the total vertical displacement. By contrast, the contribution of the LECA embankment was clearly smaller, and its deformation remained very limited within the tested range. The contribution of the sub-ballast and form layers was also minor, which is consistent with their high degree of compaction during construction.

With regard to the fatigue programme, the results suggest that the long-term evolution of the section was controlled primarily by the permanent settlement of the ballast layer. In contrast, the LECA embankment showed no evidence of significant degradation under the applied loading programme, and its measured settlements remained low throughout the test campaign.

The pressure measurements and the general trend of the displacement, velocity and acceleration records were also consistent with the expected behaviour of the section and, in general terms, compatible with the theoretical interpretation adopted in the report. Although some local scatter and a limited number of non-representative measurements were identified, these did not alter the overall trends derived from the test results.

These conclusions should nevertheless be interpreted taking into account the limitations inherent to the experimental programme, particularly the use of compaction control procedures not yet fully standardised for LECA materials and the known difficulties associated with some measurements in granular interfaces. Within these limitations, however, the results support the technical interest of LECA as an alternative embankment material in railway applications where reducing self-weight may be advantageous.

In summary, the results obtained in this study indicate that the tested LECA railway section provided an overall response that can be considered technically favourable within the investigated range, with the main source of deformability concentrated in the upper track layers rather than in the LECA embankment itself.

Madrid, a fecha de firma electrónica.

Los autores del informe:

María Santana Ruiz de Arbulo

Licenciada en Geología
Coordinadora de programa técnico-científico

Firmado por SANTANA RUIZ DE ARBULO MARIA - DNI ***8088** el día 14/04/2026 con un

Inés Crespo Chacón
Licenciada en Física
Técnica superior

Firmado por CRESPO CHACON INES - ***4762** el día 14/04/2026 con un certificado emitido por AC FNMT Usuarios

José Estaire Gepp

Dr. Ingeniero de Caminos, Canales y Puertos
Jefe de Área de Infraestrcutura Tecnológica

Firmado por ESTAIRE GEPP JOSE - DNI ***1934** el día 14/04/2026 con un certificado emitido por AC Sector Público

Examinado y conforme:

José Estaire Gepp

Dr. Ingeniero de Caminos, Canales y Puertos

Director del Laboratorio de Geotecnia

Firmado por ESTAIRE GEPP JOSE - DNI ***1934** el día 14/04/2026 con un certificado emitido por AC Sector Público

ACKNOWLEDGEMENTS

The work described in this report was carried out by the Area de Infraestructura Tecnológica of the Laboratorio de Geotecnia del CEDEX. In addition to the signatories of the report, the following individuals have also played a fundamental and highly valuable role in its development:

- Juan Luis Cámara,
- Sagrario Merino,
- Ángel Tijera,
- Natalia Montero,
- Fernando Pesquera,
- Miguel Martínez and
- Marcos Asperilla.

Their contributions were essential to the successful execution of the tasks involved.

CEDEX